

Multipion Final States from π^-p Interactions at 3.2 and 4.2 GeV/c*

SUH URK CHUNG,† ORIN I. DAHL, JANOS KIRZ, AND DONALD H. MILLER

Lawrence Radiation Laboratory, University of California, Berkeley, California

(Received 31 July 1967)

We have analyzed approximately 30 000 four-prong events at π^- beam momenta of 3.2 and 4.2 GeV/c, obtained with the 72-in. hydrogen bubble chamber at the Lawrence Radiation Laboratory. We present all the effective-mass distributions obtainable from the final states $p\pi^+\pi^-\pi^-$, $p\pi^+\pi^0\pi^-\pi^-$, and $n\pi^+\pi^+\pi^-\pi^-$, as well as the cross sections of these final states. In addition, we present the results of our study of the quasi-three-body final states $N^{*++}(1238)\pi^-\pi^-$, $p\pi^-\rho^0$, $p\pi^-\omega$, and $p\pi^-\eta$. We have given particular emphasis to the production and decay of the A_1 , A_2 , and B enhancements; the A_1 and B enhancements observed in our data are consistent with the interpretations as kinematic enhancements, although the possibility exists that what we observe at our energies is an admixture of resonant states and kinematic enhancements. On the other hand, the A_2 enhancement can be interpreted only as a genuine resonant state. From the study of the decay angular correlations in the A_2 region as well as the control regions, we have determined that the lowest possible quantum numbers of the A_2 are $J^P=2^+$.

I. INTRODUCTION

DURING the past few years, many people have investigated the multipion final states from π^-p interactions at incident beam momenta ranging from 1.5 to 10 GeV/c.¹ This report consists of an analysis of approximately 30 000 four-prong events leading to multipion production from π^-p interactions at 3.2 and 4.2 GeV/c.

Previous investigations in πp interactions have shown abundant production of resonant states such as the isobars [especially the $N^*(1238)$] and the meson resonances ρ , ω , and η . More recently, many investigators have observed enhancements in the spectrum of a pion and one of the meson resonances cited above. Thus, the A_1 and A_2 enhancements have been observed in the spectrum of π and ρ ,² and the B enhancement in the spectrum of π and ω .³

Our main objective in this report is to describe in detail the production and decay mechanisms of these enhancements, as well as the competing channels which contribute to their background. For the A_1 and B enhancements, we show that the competing channels dominate and the enhancements as observed *in our data* may be interpreted as kinematic effects in the competing channels themselves. On the other hand, the A_2 enhancement is shown to be consistent with the interpretation as a genuine meson resonance. From the study of the internal correlations for the A_2 as well as the control regions, its spin-parity (J^P) assignment is shown to be consistent only with $J^P=2^+$.

In Secs. II and III, we discuss briefly the experimen-

tal procedures and the results of cross-section measurements. A more detailed account of experimental details is given in Appendix D.

In Sec. IV, we discuss the final state $p\pi^+\pi^-\pi^-$ in which the ρ^0 and the doubly charged isobar $N^{*++}(1238)$ are produced copiously. Results concerning the A_1 and A_2 enhancements are presented here, while the matrix elements used in their spin and parity analysis are given in Appendix A.

In Sec. V, we discuss the final state $p\pi^+\pi^0\pi^-\pi^-$, in which ω and η production is observed. Results concerning the B enhancement are presented in this section. Properties of the ω Dalitz plot are derived in Appendix B, while in Appendix C the expected angular correlations in the $B \rightarrow \pi\omega$ decay are given for various spin-parity assignments.

II. EXPERIMENTAL PROCEDURE

This experiment was carried out in the 72-in. hydrogen bubble chamber (at the Lawrence Radiation Laboratory) exposed to a π^- beam from the bevatron. A total of 37 000 four-prong events were measured and processed through the standard data-reduction system of the Alvarez Group at the Lawrence Radiation Laboratory.⁴ The pictures were taken at two distinct beam momenta; the lower momentum was determined to be 3.21 ± 0.026 GeV/c and the higher momentum to be 4.16 ± 0.015 GeV/c.

About 42% of the total sample came from the higher beam-momentum data where all four-prong events were scanned for and measured (the 4.2-GeV/c sample). Of the remaining 58% of the sample, at 3.2-GeV/c beam momentum, about 33% consists of events measured only when an outgoing proton could be identified on the scanning table on the basis of ionization density; we call this the 3.2-GeV/c selected sample. In the remaining 25% of the total sample all four-prong events were scanned for and measured; we call this the 3.2-GeV/c normal sample.

* See A. H. Rosenfeld and W. E. Humphrey, *Ann. Rev. Nucl. Sci.* **13**, 103 (1963).

* Work done under auspices of the U. S. Atomic Energy Commission. Based on Suh Urk Chung's Ph.D. thesis (UCRL-16881, 1966).

† Present address: Physics Department, Brookhaven National Laboratory, Upton, N. Y.

¹ See Refs. 8-17. See, in addition, T. G. Schumann, (Ph.D. thesis, Lawrence Radiation Laboratory Report No. UCRL-11942, 1965 (unpublished). For a comprehensive list of references on π^+p interactions in the same energy range, see F. E. James and H. L. Kraybill, *Phys. Rev.* **142**, 896 (1966).

² For the A_1 and A_2 enhancements, see Refs. 25-35 and Ref. 54.

³ For the B enhancement, see Refs. 59, 60, 64, 73, and 75.

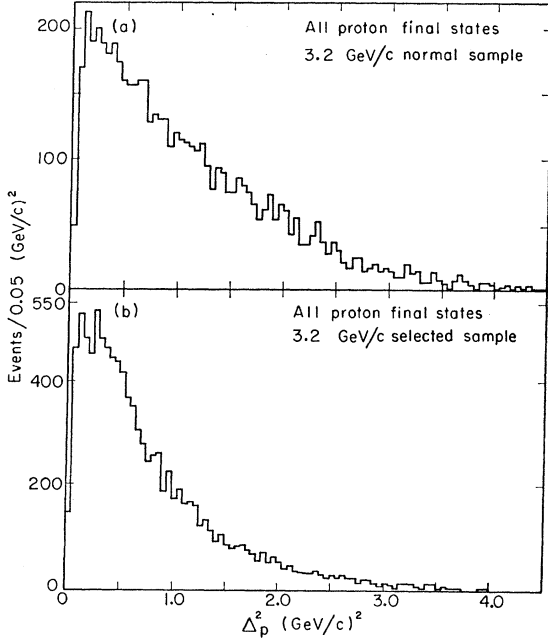


FIG. 1. Distributions in the square of four-momentum transfer to the proton for final states $p3\pi$, $p4\pi$, and $p3\pi\text{MM}$: (a) 3.2-GeV/c normal, and (b) 3.2-GeV/c selected samples.

We note that the distribution for the selected sample in the four-momentum transfer squared to the proton (Δ_p^2) is more peaked in the lower region than that for the normal sample (see Fig. 1). For this reason, only the 3.2-GeV/c normal and 4.2-GeV/c samples have been used for histograms and scatter plots involving Δ_p^2 or $\Delta_{p\pi^{\pm 2}}$. Since resonances of interest are produced more often in peripheral collisions than in other types of interactions, the selected sample should be richer in these resonances.

Types of reactions that have been tried are as follows:

$$\pi^- p \rightarrow p\pi^+\pi^-\pi^- \quad (1a)$$

$$\rightarrow p\pi^+\pi^0\pi^-\pi^- \quad (1b)$$

$$\rightarrow n\pi^+\pi^+\pi^-\pi^- \quad (1c)$$

$$\rightarrow p\pi^+\pi^-\pi^-(k\pi^0), \quad k \geq 2 \quad (1d)$$

$$\rightarrow \pi^+\pi^+\pi^-\pi^-n(k\pi^0), \quad k \geq 1. \quad (1e)$$

For convenience, we shall denote the final states in

TABLE I. Number of events used in the analysis.

Final states	3.2-GeV/c Normal	3.2-GeV/c Selected	4.2-GeV/c	Total
$p\pi^+\pi^-\pi^-$	2333	3985	2986	9304
$p\pi^+\pi^0\pi^-\pi^-$	2336	3772	3471	9579
$n\pi^+\pi^+\pi^-\pi^-$	1114	449	1803	3366
$p\pi^+\pi^-\pi^-(k\pi^0), k \geq 2$	665	1379	1954	3998
$n\pi^+\pi^+\pi^-\pi^-(k\pi^0), k \geq 1$	1040	165	2236	3441
Total	7488	9750	12 450	29 688

TABLE II. Partial cross sections.

Reactions	Cross sections (mb)	
	3.2 GeV/c	4.2 GeV/c
$\pi^- p \rightarrow p\pi^+\pi^-\pi^-$	1.91 ± 0.08	1.92 ± 0.10
$\rightarrow p\pi^+\pi^0\pi^-\pi^-$	1.86 ± 0.08	2.18 ± 0.11
$\rightarrow n\pi^+\pi^+\pi^-\pi^-$	0.89 ± 0.04	1.16 ± 0.06
$\rightarrow p\pi^+\pi^-\pi^-(k\pi^0), k \geq 2$	1.46 ± 0.07	2.75 ± 0.14
$\rightarrow n\pi^+\pi^+\pi^-\pi^-(k\pi^0), k \geq 1$		
Total	6.13 ± 0.24	8.01 ± 0.39

reactions (1a) through (1e) by $p3\pi$, $p4\pi$, $n4\pi$, $p3\pi\text{MM}$, and $4\pi\text{MM}$, respectively, where MM stands for the unobserved neutral system (as well as its effective mass).

For fitted events [reactions (1a), (1b), and (1c)], only those with a confidence level greater than 0.5% were accepted.⁵ Events were tried for hypotheses (1d) and (1e) only if they failed to fit reactions (1a), (1b), and (1c). All ambiguous events that could be resolved on the basis of ionization density were looked at by physicists and trained scanners, and the hypotheses inconsistent with the observations were eliminated.

In addition, a small fraction of $p4\pi$ events (less than 3%) which were ambiguous with $p3\pi$ events was dropped from the $p4\pi$ sample; it was judged from effective-mass plots that 80% of this sample contained $p3\pi$ events. Moreover, if the measured missing mass for any $p4\pi$ event was too far removed from the π^0 mass and the confidence level was low, that event was dropped from the sample (less than 4%). In a similar fashion, a small fraction (6%) of events was deleted from the $n4\pi$ sample. A more detailed account of the event separation among different hypotheses, as well as other related topics, is given in Appendix D.

The total number of events used in the analysis for each reaction category is given in Table I. As expected,

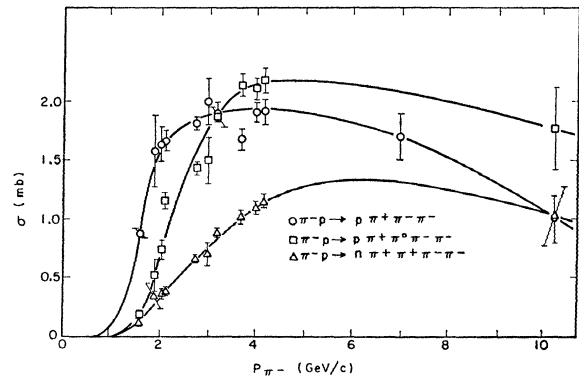


FIG. 2. Summary of cross sections for multipion production at various π^- beam momenta, taken from the results given in Refs. 8 through 17. The curves drawn are freehand fits to the data.

⁵ The χ^2 from which the confidence level is calculated has been adjusted separately for each constraint class, so that the distribution in the resulting confidence level is as isotropic as possible (see Appendix D3).

the 3.2-GeV/c selected sample shows a drastically reduced number of events for the final states with no proton ($n4\pi$ and $4\pi MM$); the events fitted to these final states represent cases in which the low-momentum π^+ track (or steeply dipping track) was misidentified as an outgoing proton during visual examination of ionization.

III. CROSS-SECTION MEASUREMENTS

Table II shows partial cross sections at the two beam momenta studied (3.2 and 4.2 GeV/c). The cross sections were obtained by normalizing the total number of interactions to the precise measurements of the π^-p total cross sections given by Citron *et al.*⁶

In a special cross-section scan, the entire quantity of film used for this experiment was rescanned to find the number of two-prong, four-prong, and strange-particle-production events. For two-prong events, we corrected for the loss of events due to small-angle scatterings.⁷ Other corrections were made for scanning efficiency, failing events, and the possible contamination in each channel due to misassigned hypotheses. A more detailed account on cross-section measurements is given in Appendix D4.

Figure 2 shows partial cross sections reported to date for reactions (1a), (1b), and (1c) at various beam momenta.⁸⁻¹⁷ The curves drawn are freehand fits to the data. According to these curves, the cross sections for $p3\pi$ and $p4\pi$ final states reach their maxima in the region of π^- beam momentum from 3.5 to 5.0 GeV/c, whereas the maximum for $n4\pi$ final states seems to lie above this interval.

⁶ A. Citron, W. Galbraith, T. F. Kycia, B. A. Leontić, R. H. Phillips, and A. Rousset, *Phys. Rev. Letters* **13**, 205 (1964); A. N. Diddens, E. W. Jenkins, T. F. Kycia, and K. F. Riley, *ibid.* **10**, 262 (1963).

⁷ L. D. Jacobs, (Ph.D. thesis), Lawrence Radiation Laboratory Report No. UCRL-16877, 1966 (unpublished).

⁸ Saclay-Orsay-Bari-Bologna Collaboration, *Nuovo Cimento* **29**, 515 (1963) (π^-p at 1.59 GeV/c).

⁹ R. Christian, A. R. Erwin, H. R. Fechter, F. E. Schwamb, S. H. Vegors, and W. D. Walker, *Phys. Rev.* **143**, 1105 (1966) (π^-p at 1.89 GeV/c).

¹⁰ D. D. Carmony, F. Grard, R. T. Van de Walle, and Nguyen-Huu Xuong, in *Proceedings of the 1962 Annual International Conference on High-Energy Nuclear Physics at CERN*, edited by J. Prentki (CERN, Geneva, 1962), p. 44, (π^-p at 2.03 GeV/c).

¹¹ P. H. Satterblom, W. D. Walker, and A. R. Erwin, *Phys. Rev.* **134**, B207 (1964) (π^-p at 2.1 GeV/c).

¹² J. Alitti, J. P. Baton, A. Berthelot, B. Deler, W. J. Fickinger, M. Neveu-René, V. Alles-Borelli, R. Gessaroli, A. Romano, and P. Waloschek, *Nuovo Cimento* **35**, 1 (1965) (π^-p at 2.75 GeV/c).

¹³ V. Hagopian, Ph.D. thesis, University of Pennsylvania, 1964 (unpublished) (π^-p at 3.0 GeV/c).

¹⁴ W. D. C. Moebs, III, Ph.D. thesis, University of Michigan, 1965 (unpublished) (π^-p at 3.7 GeV/c).

¹⁵ Aachen-Birmingham-Bonn-Hamburg-London (I. C.)-München Collaboration, *Nuovo Cimento* **31**, 485 (1964) (π^-p at 4.0 GeV/c).

¹⁶ N. M. Cason, *Phys. Rev.* **148**, 1282 (1966) (π^-p at 7.0 GeV/c).

¹⁷ N. N. Biswas, I. Derado, N. Schmitz, and W. D. Shephard, *Phys. Rev.* **134**, B901 (1964) (π^-p at 10.25 GeV/c).

IV. $p\pi^+\pi^-\pi^-$ FINAL STATE

A. Effective-Mass Distributions

In this section we present general features of the $p3\pi$ final state. In Figs. 3 and 4, all the effective-mass distributions are shown separately for 3.2- and 4.2-GeV/c data. The histograms at 3.2 GeV/c (Fig. 3) include both the normal and selected samples. Both these samples exhibit rather similar effective-mass distributions, except for somewhat stronger production of resonances such as $N^*(1238)$, A_1 , and A_2 for the selected sample.

The most striking feature of this final state is that both $N^{*++}(1238)$ and ρ^0 resonances are copiously produced. The curves in Figs. 3 and 4 were obtained by adding nonresonant phase space (42%), phase space modified by a Breit-Wigner form for $N^{*++}(1238)$ (34%), and the same for ρ^0 (24%).¹⁸ The amount assumed for each resonance is somewhat arbitrary¹⁹; the curves are meant to show only to what extent gross features of this final state can be explained in terms of phase-space curves modified by the two noninterfering resonances.

The effective mass of the $\pi^+\pi^-\pi^-$ system ($M_{\pi^+\pi^-\pi^-}$) shows clear deviation from phase space at the mass of the A_2 and a broad enhancement in the region of the A_1 [see Figs. 3(g) and 4(g)]. The distribution in $M_{p\pi^-}$ [Figs. 3(b) and 4(b)] shows evidence for $N^{*0}(1238)$, $N^{*0}(1518)$, and $N^{*0}(1688)$ productions.

Note that the $M_{\pi^+\pi^-}$ distributions [Figs. 3(c) and 4(c)] do not show evidence for $f^0(1253)$, in contrast with the results from π^+p interactions in this energy range²⁰; it has been shown that the f^0 production from π^+p interactions takes place mainly through the channel $N^{*++}(1238)f^0$. The equivalent channel for π^-p interactions would be the channel $N^{*0}(1238)f^0$, the cross section of which should be only $\frac{1}{3}$ that of the reaction $\pi^+p \rightarrow N^{*++}(1238)f^0$. In addition, f^0 cannot be produced in conjunction with higher-mass isobars such as $N^*(1688)$, since the reactions of this type are below the threshold at our energies.

For the partial cross-section evaluation at 3.2 GeV/c, we use the normal sample alone; the cross section for ρ^0 production is determined to be 0.48 ± 0.07 mb, and for N^{*++} production, it is 0.59 ± 0.07 mb. At 4.2 GeV/c,

¹⁸ The mass and width assumed for $N^{*++}(1238)$ and ρ^0 are as follows: $M(N^*)=1.236$ GeV, $\Gamma(N^*)=0.12$ GeV; $M(\rho^0)=0.769$ GeV, $\Gamma(\rho^0)=0.112$ GeV. The phase-space curves on the $M_{p\pi^+}$ ($M_{\pi^+\pi^-}$) histograms are obtained by including only the effect of $\rho^0(N^{*++})$ resonance and by normalizing to the events outside the N^{*++} region, where the N^{*++} region is chosen to be the interval 1.0 to 1.46 GeV, and the ρ^0 region the interval 0.60 to 0.92 GeV. The phase-space curves on the $M_{\pi^+\pi^-\pi^-}$ (or $M_{\pi^-\rho^0}$) histograms are normalized to the portion of the histograms with $M_{\pi^+\pi^-\pi^-}$ (or $M_{\pi^-\rho^0}$) above 1.45 GeV.

¹⁹ In particular, these values are not the ones used to calculate the production cross sections of N^{*++} and ρ^0 . See the following section for the cross sections.

²⁰ See, for instance, Aachen-Berlin-Birmingham-Bonn-Hamburg-London (I. C.)-München Collaboration, *Phys. Rev.* **138**, B897 (1965); B. C. Shen, Ph.D. thesis, Lawrence Radiation Laboratory Report No. UCRL-16170, 1965 (unpublished).

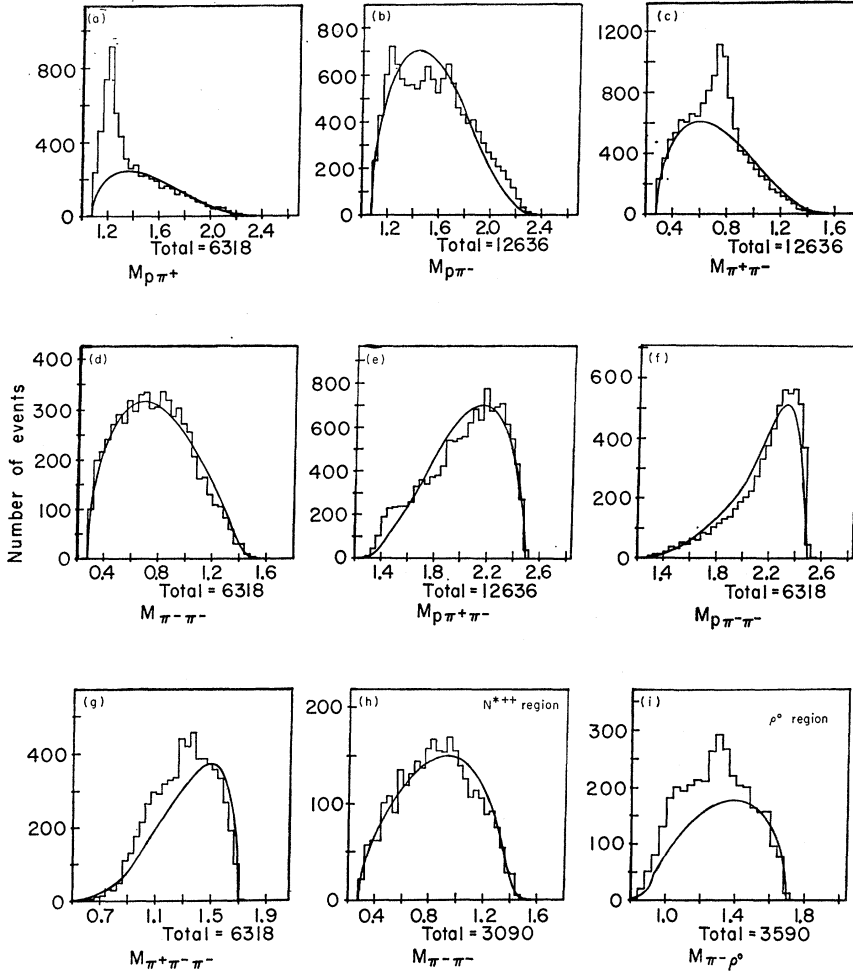


FIG. 3. (a-g) All effective-mass distributions for the $p3\pi$ final state at 3.2 GeV/c. (h) The $M_{\pi^-\pi^-}$ distributions for events at 3.2 GeV/c with $M_{p\pi^+}$ in the N^{*++} region (1.12 to 1.32 GeV). (i) The $M_{\pi^+\pi^-\pi^-}$ distributions for events at 3.2 GeV/c with $M_{p\pi^+}$ in the ρ^0 region (0.66 to 0.84 GeV). The horizontal scales are in GeV, and the vertical scales are for the number of combinations per 40 MeV. In each histogram, the total number of combinations is shown after the heading "Total." The curves represent 42% phase space, 32% N^{*++} (1238), and 24% ρ^0 except on (a) and (c), where the N^{*++} and ρ^0 contributions are left out in turn. On (g) and (i) the curves are normalized to the region above 1.45 GeV (see Ref. 18).

we find the cross sections 0.52 ± 0.07 and 0.59 ± 0.07 mb for ρ^0 and N^{*++} productions, respectively.

The respective production cross sections for the A_1 and A_2 are 140 and 150 μb at 3.2 GeV/c, and 160 and 175 μb at 4.2 GeV/c. The errors in these values are large because of the proximity of the resonances and the uncertainty in estimating the background. The errors range from 25 to 35%.

In the following sections we discuss in detail the channels $N^{*++}\pi^-\pi^-$ and $p\pi^-\rho^0$ in turn.

B. Reaction $\pi^-p \rightarrow N^{*++}\pi^-\pi^-$

In order to investigate the production mechanism of the 3-3 isobar, we present in Fig. 5(a) the Chew-Low plot of four-momentum transfer to the $p\pi^+$ system ($\Delta_{p\pi^+}^2$) against $M_{p\pi^+}$. The fact that the isobar is produced predominantly in the region of low $\Delta_{p\pi^+}^2$ suggests the one-pion-exchange process represented in Fig. 6. This feature is emphasized further in Figs. 7(a), 7(b) and 8(a), 8(b), where we show the $\Delta_{p\pi^+}^2$ distribution²¹ in the

²¹ As pointed out in Sec. II, when plotting the histograms and

isobar region (1.12 to 1.32 GeV) and the $M_{p\pi^+}$ distribution for $\Delta_{p\pi^+}^2 < 0.5$ (GeV/c)² at each beam momentum separately.

Before we study the final state $N^{*++}\pi^-\pi^-$, we first look for possible contamination in the N^{*++} sample. As is shown in Sec. IVC, one of the important channels of the $p3\pi$ final state is that of double resonance formation, $N^{*0}(1238)\rho^0$, $N^{*0}(1518)\rho^0$, and $N^{*0}(1688)\rho^0$. Figure 5(b) is a scatter plot of $M_{p\pi^-}$ versus $M_{\pi^+\pi^-}$ for events in the N^{*++} region [and with $\Delta_{p\pi^+}^2 < 0.5$ (GeV/c)²], where we used only the combinations $M_{p\pi_1^-}$ and $M_{\pi^+\pi_2^-}$ satisfying the condition $\Delta_{p\pi_1^-}^2 \leq \Delta_{p\pi_2^-}^2$. There is clear evidence that the $N^{*0}\rho^0$ channel is present; the $N^{*0}(1238)$ channel especially appears to be an important one. The projections onto the $M_{\pi^+\pi^-}$ and $M_{p\pi^-}$ axes shown in Figs. 7(d), (e) and 8(d), (e) demonstrate further the presence of ρ^0 and N^{*0} resonances.

It is rather difficult, however, to estimate quantitatively the amount of ρ^0 formation in the N^{*++} sample; the distribution of $M_{\pi^+\pi_2^-}$ with $\Delta_{p\pi_1^-}^2 > \Delta_{p\pi_2^-}^2$ tends to

scatter plots which involve Δ_{p^2} or $\Delta_{p\pi^+}^2$, we have eliminated the 3.2-GeV/c selected sample.

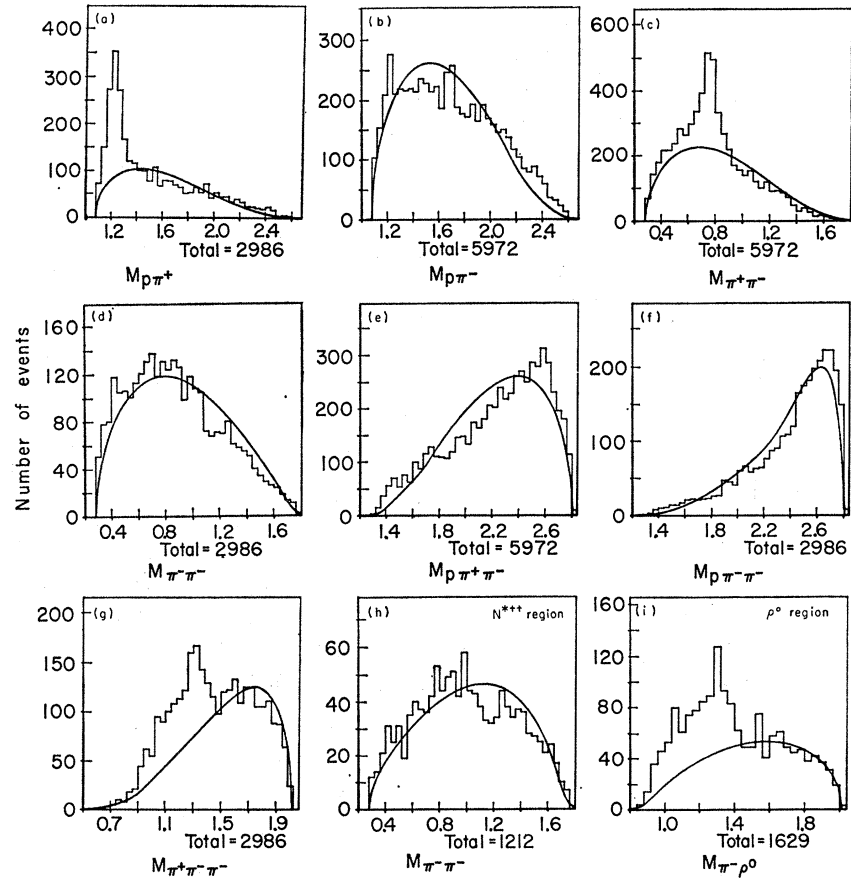


FIG. 4. Same effective-mass distributions as in Fig. 3 for the 4.2-GeV/ c data.

be peaked below the ρ^0 region, and it is not clear how one should estimate the background. Nevertheless, we believe that there is a fair amount of contamination from the $N^{*0}\rho^0$ channel. Furthermore, kinematics and decay angles of the $N^{*++}\pi^-\pi^-$ channel are such that some of the N^{*++} events “spill over” to $N^{*0}\rho^0$ final states, especially in the $N^{*0}(1238)$ region.

With this possible contamination in mind, we next turn to the description of decay correlations at $\pi^-\pi^-$ and N^{*++} vertices (see Fig. 6). For this purpose, we define two coordinate systems as follows: In the $\pi^-\pi^-$ ($p\pi^+$) rest frame, the z axis is parallel to the beam (target) momentum and the y axis is parallel to the normal to the production plane. Polar and azimuthal angles in these systems are denoted by $\theta(\pi^-\pi^-)$, $\phi(\pi^-\pi^-)$, $\theta(p\pi^+)$, and $\phi(p\pi^+)$, where the symbols in parentheses indicate the rest frames in which they are evaluated. Note that the azimuthal angles thus defined are just the Treiman-Yang angles.

Figure 9 gives the distributions in $\cos\theta$ and ϕ for events in the N^{*++} region (and with low $\Delta_{p\pi^+}^2$) and also the same distributions for those events with the further selection that $M_{\pi^+\pi_1^-}$ ($\Delta_{p\pi_2}^2 \leq \Delta_{p\pi_1}^2$) lie outside the ρ^0 region (0.66 to 0.84 GeV).

We see that the Treiman-Yang angles are relatively isotropic, supporting our belief that the one-pion-

exchange mechanism is the dominant one. Note that the distributions in $\cos\theta(p\pi^+)$ become more symmetric outside the ρ^0 band²² [see Figs. 9(c) and 9(g)] and approach the well-known $(1+3\cos^2\theta)$ distribution for the isobar decay. The solid curves in these figures are fitted by the least-squares method to the Legendre polynomials,

$$\frac{d\sigma}{d\cos\theta} = \sum_{l=0}^n a_l P_l(\cos\theta). \quad (2)$$

The coefficients a_0 , a_1 , and a_2 , normalized to the total number of events at each momentum, are as follows:

Momentum (GeV/ c)	a_0	a_1	a_2
3.2	166.0 ± 4.1	105.9 ± 7.8	111.0 ± 9.5
4.2	66.0 ± 2.6	48.2 ± 5.0	62.6 ± 6.0

The behavior of $\cos\theta(\pi^-\pi^-)$ and $\phi(\pi^-\pi^-)$ as a function of $M_{\pi^-\pi^-}$ is shown in Figs. 5(c) and 5(d). Here the distribution in $\cos\theta(\pi^-\pi^-)$ is relatively isotropic (s wave) at the low-mass region of $M_{\pi^-\pi^-}$; higher partial waves appear gradually as $M_{\pi^-\pi^-}$ increases. The distribution in $\phi(\pi^-\pi^-)$, on the other hand, remains relatively

²² A similar conclusion has been drawn in Ref. 15: see their section on the 3-3 isobar channel.

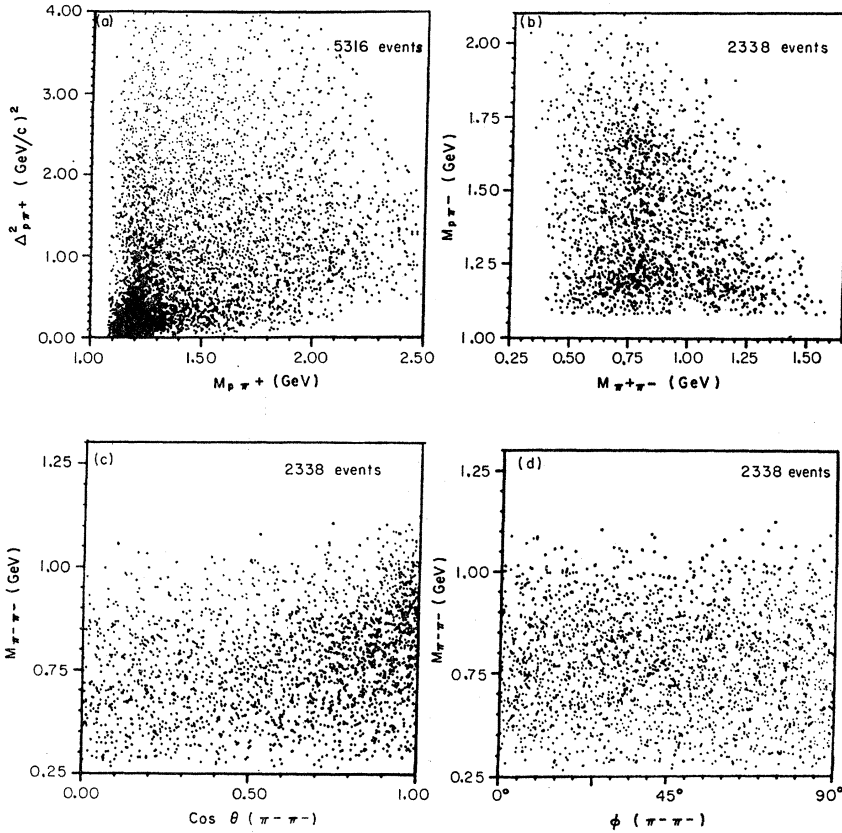


FIG. 5. Scatter plots relating to the final state $N^{*++}\pi^-\pi^-$ at 3.2 and 4.2 GeV/c: (a) Δ_{pp+}^2 versus M_{pp+} for all events (see Ref. 22); (b) $M_{p\pi^-}$ versus $M_{\pi^+\pi^-}$ ($\Delta_{pp+}^2 \leq \Delta_{pp+}^2$); (c) $M_{\pi^-\pi^-}$ versus $\cos\theta(\pi^-\pi^-)$; and (d) $M_{\pi^-\pi^-}$ versus $\phi(\pi^-\pi^-)$. In (b), (c), and (d) we have taken events with M_{pp+} in the N^{*++} region 1.12 to 1.32 GeV and with $\Delta_{pp+}^2 < 0.5$ (GeV/c)². See Sec. IVB for the definition of angles $\theta(\pi^-\pi^-)$ and $\phi(\pi^-\pi^-)$.

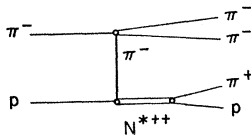


FIG. 6. One-pion-exchange diagram for the process $\pi^- p \rightarrow N^{*++}\pi^-\pi^-$.

isotropic throughout the entire range of $M_{\pi^-\pi^-}$. The $\cos\theta(\pi^-\pi^-)$ for four different regions of $M_{\pi^-\pi^-}$ are shown in Fig. 10 for two beam momenta separately. Results of a least-squares fit to the data are shown in Table III.

The $M_{\pi^-\pi^-}$ plots for the N^{*++} region with $\Delta_{pp+}^2 < 0.5$ (GeV/c)² are given in Figs. 7(c) and 8(c); we see no evidence of a $\pi\pi$ resonance ($I=2$). Several authors²³ have used $M_{\pi^-\pi^-}$ distributions to calculate the total

cross section for the reaction $\pi^-\pi^- \rightarrow \pi^-\pi^-$. However, in view of the contamination in our data from the $N^*\rho^0$ channel and of the uncertainty in using semi-empirical formulas, we do not present our result here at this time; we merely point out that our results are in fair agreement with those obtained by others.

Finally, the $M_{\pi^-\rho^0}$ distributions (with ρ^0 selected as described above) are shown in Figs. 7f and 8f; there is little evidence that the A_2 production contaminates this channel.

C. Reaction $\pi^- p \rightarrow p \pi^- \rho^0$

In order to study this reaction, we cut off the N^{*++} region [M_{pp+} in the interval 1.12 to 1.32 GeV and

TABLE III. Least-squares fits to the $\cos\theta(\pi^-\pi^-)$ distribution.^a

$M_{\pi^-\pi^-}$ (GeV)	a_0	a_2	a_4	a_6	n^b	χ^2	C.L. (%)
3.2 GeV/c							
0.28-0.56	33.55±1.30				9	4.54	87.6
0.56-0.84	65.69±1.81	48.17±4.42			8	7.08	52.6
0.84-1.12	53.54±1.63	82.47±4.63	36.17±5.47		7	1.51	98.2
1.12-1.60	11.67±0.76	26.50±2.45	19.71±3.28	14.77±2.97	6	11.28	7.9
4.2 GeV/c							
0.28-0.56	10.67±0.73				9	10.28	32.7
0.56-0.84	21.66±1.04	11.0 ±2.44			8	2.39	96.6
0.84-1.12	20.07±1.00	32.39±2.90	17.70±3.18		7	5.32	62.3
1.12-1.60	12.31±0.78	31.85±2.67	23.26±3.45	9.60±3.16	6	4.95	55.1

^a Fitted to the Legendre-polynomial series [see Eq. (2)]. (Coefficients are normalized to the total number of events.)

^b n is number of degrees of freedom.

²³ N. Schmitz, Nuovo Cimento **31**, 255 (1964); see also Refs. 12 and 14.

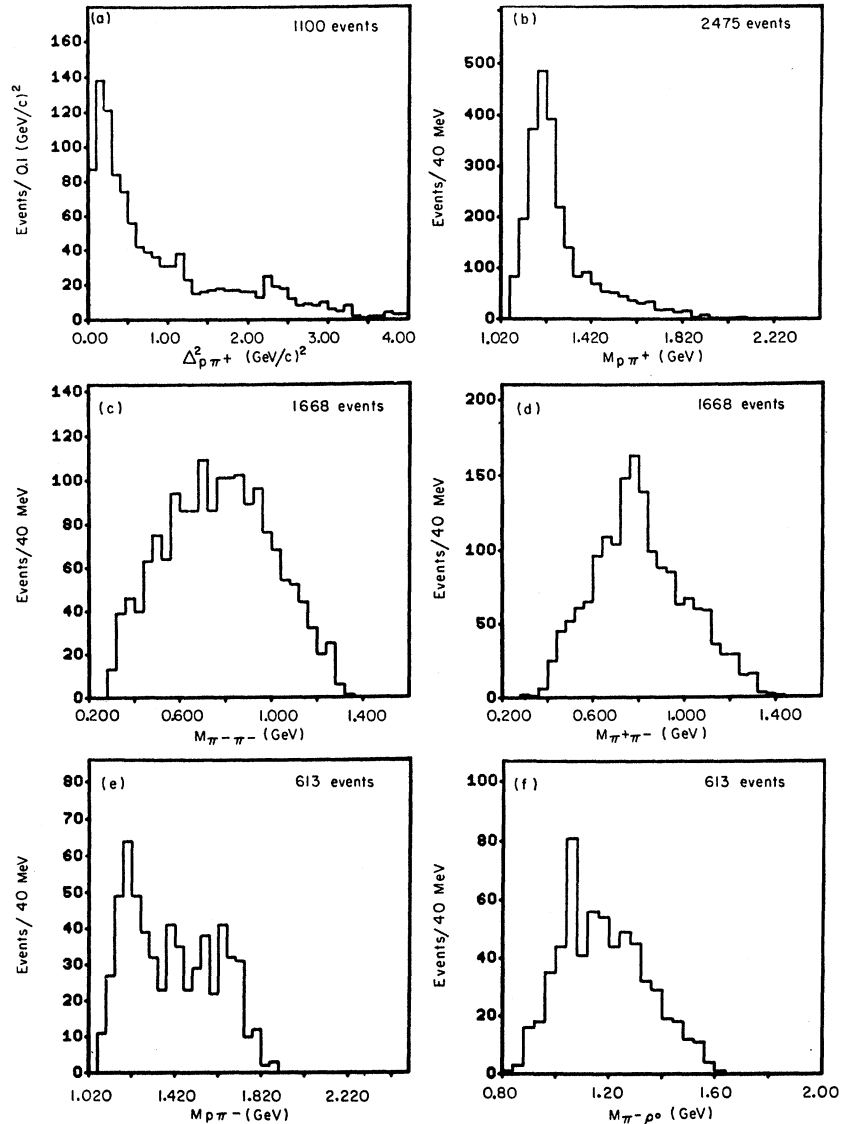


FIG. 7. Various distributions relating to the final state $N^{*++}\pi^-\pi^-$ at 3.2 GeV/c: (a) Histogram of $\Delta_{p\pi^+}^2$ for events (see Ref. 21) with $M_{p\pi^+}$ in the N^{*++} region 1.12 to 1.32 GeV. (b) The $M_{p\pi^+}$ distribution with $\Delta_{p\pi^+}^2 < 0.5$ (GeV/c)². (c) and (d) The $M_{\pi_1^-\pi_2^-}$ and $M_{\pi^+\pi_1^-\pi_2^-}$ distributions ($\Delta_{p\pi_1^-}^2 \leq \Delta_{p\pi_2^-}^2$) for events with $M_{p\pi^+}$ in the interval 1.12 to 1.32 GeV and with $\Delta_{p\pi^+}^2 < 0.5$ (GeV/c)²; (e) and (f) the histograms of $M_{p\pi^-}$ and $M_{\pi^+\pi_1^-\pi_2^-}$ ($\Delta_{p\pi_1^-}^2 \leq \Delta_{p\pi_2^-}^2$) with the further requirement that $M_{\pi^+\pi_2^-}$ lie in the ρ^0 interval 0.66 to 0.84 GeV.

$\Delta_{p\pi^+}^2 < 1.5$ (GeV/c)²].²⁴ This cutoff does not substantially affect the analysis presented here, except for certain angular distributions; these are shown separately for the N^{*++} region.

It is in this channel that we observe the well-established enhancements—the A_2 meson,^{25–34} and the A_1

²⁴ We have eliminated these events [$1.12 \text{ GeV} < M_{p\pi^+} < 1.32 \text{ GeV}$ if $\Delta_{p\pi^+}^2 < 1.5$ (GeV/c)²] to reduce the N^* contamination in Figs. 11–28 [except Figs. 18(i) through 18(l)].

²⁵ G. Goldhaber, J. L. Brown, S. Goldhaber, J. A. Kadyk, B. C. Shen, and G. H. Trilling, Phys. Rev. Letters **12**, 336 (1964).

²⁶ S. U. Chung, O. I. Dahl, L. M. Hardy, R. I. Hess, G. R. Kalbfleisch, J. Kirz, D. H. Miller, and G. A. Smith, Phys. Rev. Letters **12**, 621 (1964).

²⁷ Aachen-Berlin-Birmingham-Bonn-Hamburg-London (I. C.)-München Collaboration, Phys. Letters **10**, 226 (1964).

²⁸ M. Deuschmann, R. Schulte, H. Weber, W. Woischnig, C. Grote, J. Klugow, S. Nowak, S. Brandt, V. T. Cocconi, O. Czyzewski, P. F. Dalpiaz, G. Kellner, and D. R. O. Morrison, Phys. Letters **12**, 356 (1964).

²⁹ R. L. Lander, Maris Abolins, D. D. Carmony, T. Hendricks, Nguyen-Huu Xuong, and P. M. Yager, Phys. Rev. Letters **13**, 346 (1964).

enhancement,³⁵ which is not so well understood. Figure 11(a) shows the Chew-Low plot of Δ_p^2 versus $M_{\pi^-\rho^0}$,

³⁰ J. Alitti, J. P. Baton, B. Deler, M. Neveu-René, J. Crussard, J. Ginestet, A. H. Tran, R. Gessaroli, and A. Romano, Phys. Letters **15**, 69 (1965).

³¹ A. Bettini, M. Cresti, A. Grigoletto, S. Limentani, A. Loria, L. Peruzzo, and R. Santangelo, Nuovo Cimento **38**, 1495 (1965).

³² V. E. Barnes, W. B. Fowler, K. W. Lai, S. Orenstein, D. Radojčić, M. S. Webster, A. H. Bachman, P. Baumel, and R. M. Lea, Phys. Rev. Letters **16**, 41 (1966).

³³ M. Deuschmann, R. Steinberg, H. Weber, W. Woischnig, V. Belyakow, C. Grote, J. Klugow, S. Nowak, S. Brandt, V. T. Cocconi, O. Czyzewski, P. F. Dalpiaz, E. Flaminio, H. Hromadnik, G. Kellner, and D. R. O. Morrison, Phys. Letters **20**, 82 (1966).

³⁴ G. Benson, L. Lovell, E. Marquit, B. Roe, D. Sinclair, and J. Vander Velde, Phys. Rev. Letters **16**, 1177 (1966).

³⁵ In addition to Refs. 25–34, see also J. F. Allard, D. Drijard, J. Hennessy, R. Huson, A. Lloret, P. Musset, J. J. Veillet, H. H. Bingham, M. Dickinson, R. Diebold, W. Koch, D. W. G. Leith, M. Nikolić, B. Ronne, G. Bellini, E. Fiorini, P. Negri, M. Rollier, J. Crussard, J. Ginestet, A. H. Tran, M. Di Corato, W. B. Fretter, H. J. Lubatti, and W. Michael, Phys. Letters **12**, 143 (1964); *ibid.* **19**, 431 (1965); G. Bozóki, E. Fenyves, E. Gombosi, and E. Nagy, *ibid.* **18**, 206 (1965).

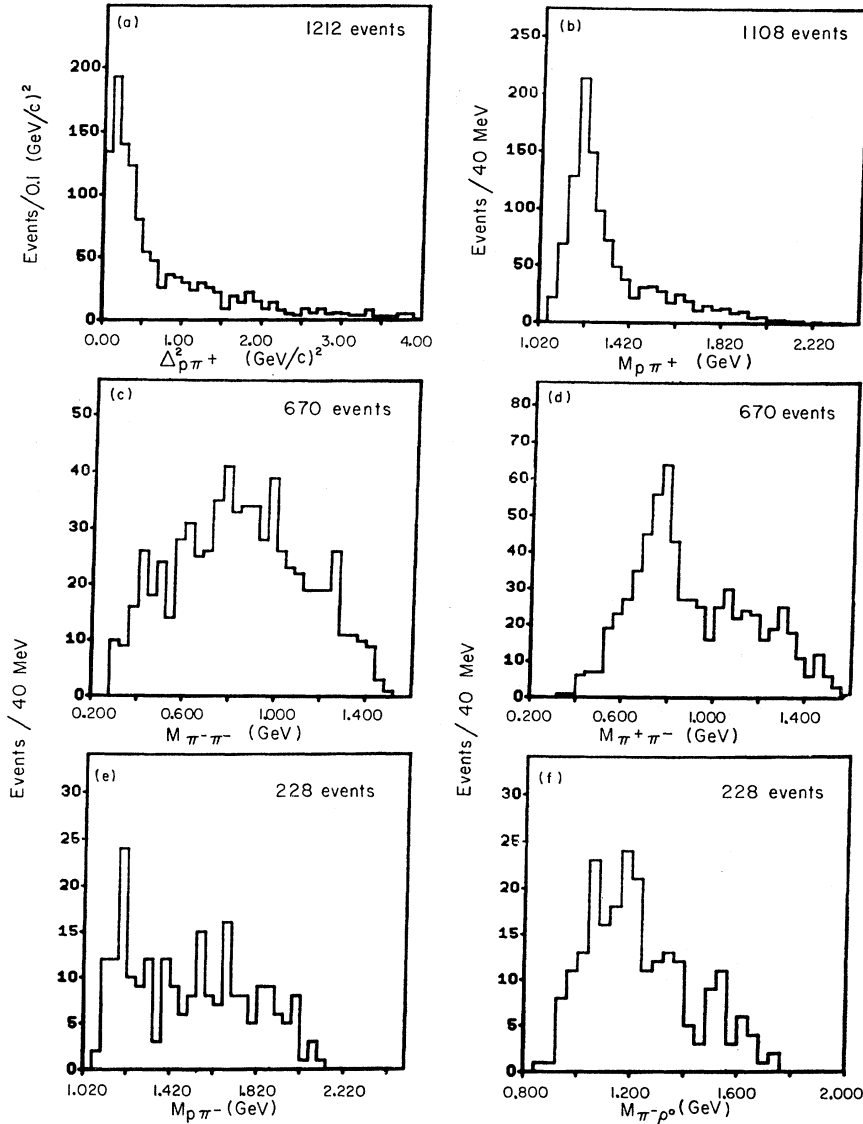


FIG. 8. Same distributions as in Fig. 7, but for the 4.2-GeV/c data.

where we have taken those events with $M_{\pi^+\pi^-}$ in the ρ^0 interval (0.66 to 0.84 GeV); since these enhancements appear to be primarily associated with the low Δ_{p^2} , it appears likely that peripheral processes are responsible for their production [see Fig. 12(a)]. The histogram projected onto the $M_{\pi^-\rho^0}$ axis [Fig. 11(b)] shows a prominent peak at the A_2 mass and a broad enhancement in the region of the A_1 . Broken lines in Fig. 11(b) show the distribution of $M_{\pi^-\pi^+\pi^-}$ for events with $M_{\pi^+\pi^-}$ outside the ρ^0 interval; there is no evidence that either the A_1 or the A_2 decays directly into a 3π channel without the intermediate ρ^0 formation.

According to our data, the mass and width of the A_2 meson are 1310 ± 20 and 80 ± 20 MeV. As for the A_1 , the mass and width of 1090 and 125 MeV are consistent with our data; their precise values are rather difficult to determine, as the A_1 does not appear as a sharp peak.

In this connection, note that a recent world compilation by Ferbel³⁶ of the $M_{\pi^+\pi^-\pi^0}$ distribution from $\pi^\pm p$ interactions shows a similar trend; the A_1 enhancement does not appear as a sharp peak.

In this channel, another important process occurs, namely that of double-resonance formation $N^{*0}\rho^0$, as is illustrated in Figs. 11(c) and 11(d). We see from these figures that $N^{*0}(1238)$, $N^{*0}(1518)$, and $N^{*0}(1688)$ are copiously produced. Again, they are produced primarily at low $\Delta_{p\pi^2}$, which suggests the one-pion-exchange (OPE) mechanism for the process [see Fig. 12(b)].

In Figs. 11(c) and 11(d), only one combination of $p\pi^-$ (or $\pi^+\pi^-$) has been chosen for each event. For single- ρ^0 events (only one combination of $M_{\pi^+\pi^-}$ in the ρ^0 interval), we naturally choose the combination $p\pi_2^-$

³⁶ T. Ferbel, Phys. Letters **21**, 111 (1966).

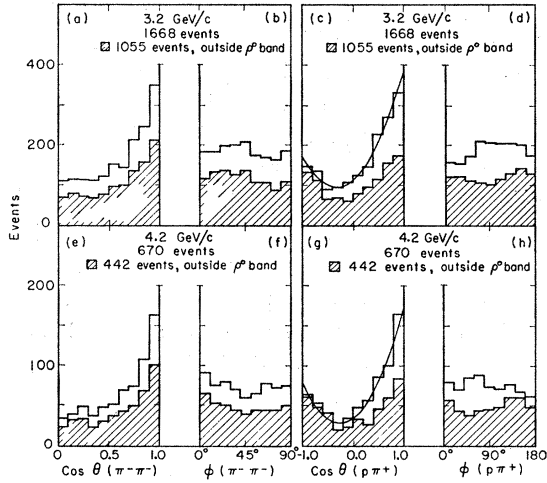


FIG. 9. Angular correlations for the OPE process leading to the final state $N^{*++}\pi^-\pi^-$: (a)–(d) angular distributions at the meson and isobar vertices for N^{*++} events at 3.2 GeV/c [$1.12 \text{ GeV} \leq M_{p\pi^+} \leq 1.32 \text{ GeV}$ and $\Delta_{p\pi^+} < 0.5 \text{ (GeV/c)}^2$]; (e)–(h) same angular distributions for events at 4.2 GeV/c. The shaded histograms are for those N^{*++} events with $M_{\pi^+\pi^-}$ ($\Delta_{p\pi^+} \leq \Delta_{p\pi^+}$) outside the ρ^0 interval 0.66 to 0.84 GeV. The curves drawn in (c) and (g) are least-squares fits to the data. See Sec. IVB for the definition of the angles used in these figures.

(or $\pi^+\pi_1^-$) if $M_{\pi^+\pi_1^-}$ is in the ρ^0 interval. As for the double- ρ^0 events (both combinations of $M_{\pi^+\pi^-}$ in the ρ^0 interval), the following method has been used to choose

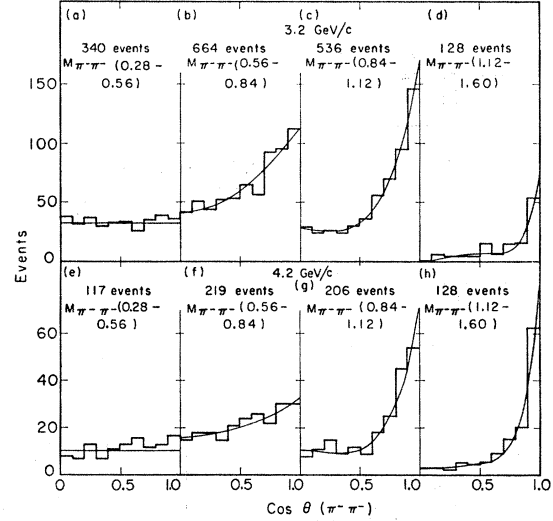


FIG. 10. $\text{Cos}\theta(\pi^-\pi^-)$ distributions as functions of $M_{\pi^+\pi^-}$ for N^{*++} events [$1.12 \text{ GeV} \leq M_{p\pi^+} \leq 1.32 \text{ GeV}$ and $\Delta_{p\pi^+} < 0.5 \text{ (GeV/c)}^2$]: (a)–(d) events at 3.2 GeV/c; (e)–(h) events at 4.2 GeV/c. The curves are least-squares fits to the data (see Table III).

the one combination: We first take a somewhat narrower ρ^0 interval (0.70 to 0.80 GeV), and if, for an event, $M_{\pi^+\pi_1^-}$ falls in the narrower ρ^0 interval and $M_{\pi^+\pi_2^-}$ in the wider one, the combination $p\pi_2^-$ (or $\pi^+\pi_1^-$) is chosen. If, however, both combinations of $M_{\pi^+\pi^-}$ fall in the

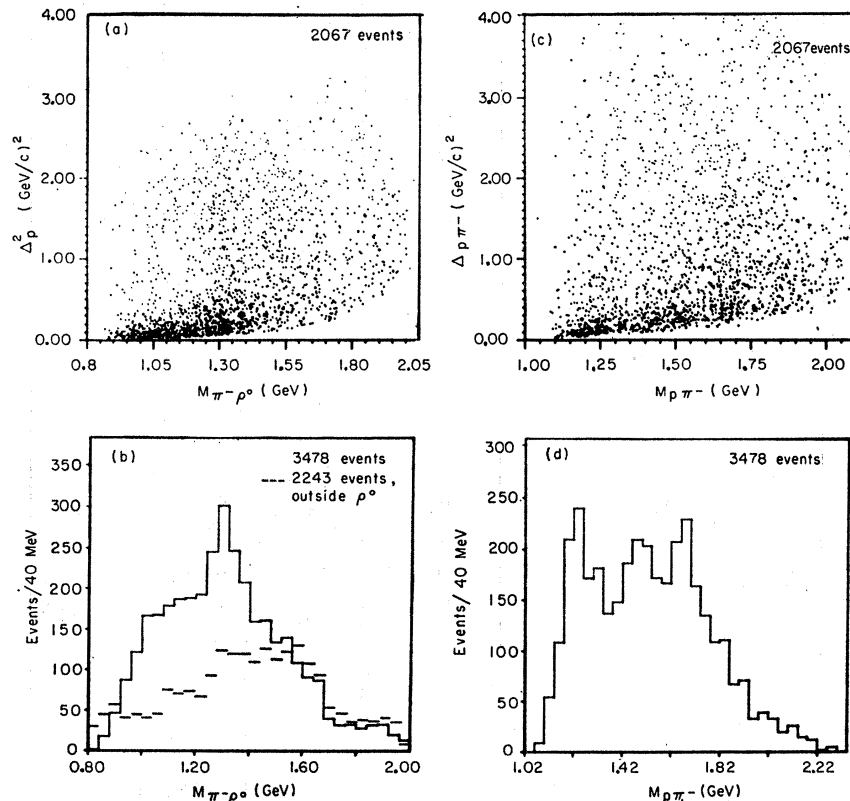


FIG. 11. (a) Scatter plot of Δ_{p^2} versus $M_{\pi^+\rho^0}$, and (b) the projection onto the $M_{\pi^+\rho^0}$ axis for ρ^0 events ($0.66 \text{ GeV} \leq M_{\pi^+\pi^-} \leq 0.84 \text{ GeV}$) at both momenta. (Ref. 21) (c) scatter plot of $\Delta_{p\pi^+}^2$ versus $M_{p\pi^-}$ and (d) projection onto the $M_{p\pi^-}$ axis for the same events (see Ref. 37). No N^{*++} events are included in these figures (see Ref. 24).

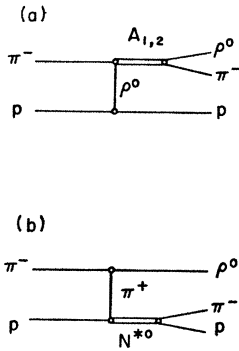


FIG. 12. (a) The ρ^0 -exchange and (b) the π^+ -exchange diagrams for the process $\pi^-p \rightarrow p\pi^-\rho^0$.

narrower ρ^0 interval, we choose that combination of $p\pi_2^-$ (or $\pi^+\pi_1^-$) for which $\Delta_{p\pi_2^-}$ is less than $\Delta_{p\pi_1^-}$. This is done in an effort to isolate the peripheral process of Fig. 12(b) as much as possible.³⁷

An additional purpose in devising this method has been to somehow circumvent the effect of interference due to double- ρ^0 events so that, for instance, a meaningful comparison can be made between the virtual process at the lower vertex of Fig. 12(b) and the physical process $\pi^-p \rightarrow \pi^-p$. We emphasize, however, that the analysis which follows does not differ appreciably from other methods that can be devised; for instance, one

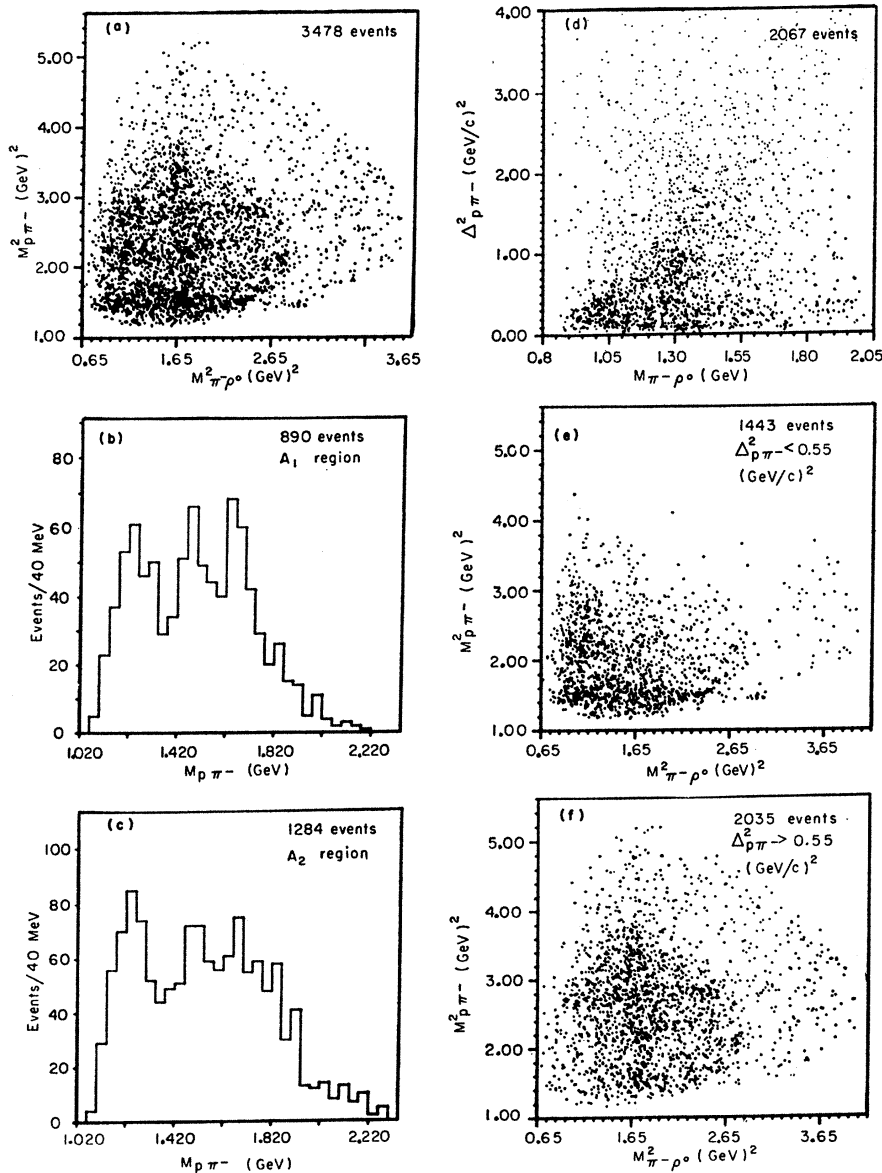


FIG. 13. Correlations between the $p\pi^-$ and the $\pi^-\rho^0$ systems for ρ^0 events at both momenta (see Refs. 22, 24, and 37): (a) Dalitz plot of $M_{p\pi^-}^2$ versus $M_{\pi^-\rho^0}^2$; (b,c) the $M_{p\pi^-}$ spectra in the A_1 region ($1.0 \text{ GeV} \leq M_{\pi^-\rho^0} \leq 1.20 \text{ GeV}$) and in the A_2 region ($1.20 \text{ GeV} \leq M_{\pi^-\rho^0} \leq 1.42 \text{ GeV}$); (d) scatter plot of $\Delta_{p\pi^-}^2$ versus $M_{\pi^-\rho^0}$; (e) and (f) Dalitz plot of $M_{p\pi^-}^2$ versus $M_{\pi^-\rho^0}^2$ with $\Delta_{p\pi^-}^2 < \text{and } > 0.55$ (GeV/c^2), respectively.

³⁷ We have used the method described above to select one combination of $p\pi^-$ (or $\pi^+\pi^-$), whenever necessary, to plot Figs. 11–22.

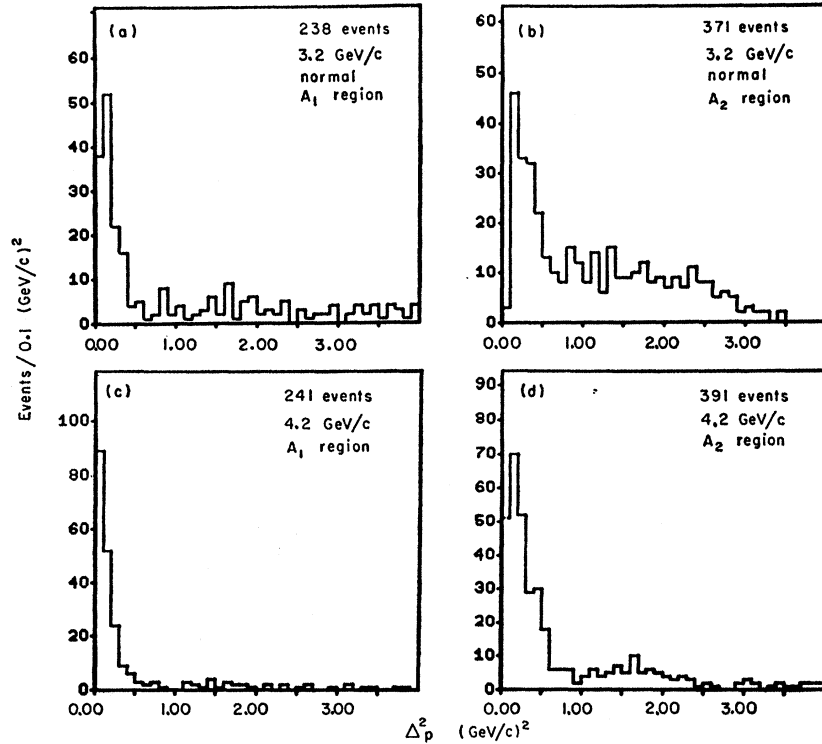


FIG. 14. The Δ_p^2 distributions for ρ^0 events (see Refs. 21 and 24): (a) the A_1 region ($1.0 \text{ GeV} \leq M_{\pi^-\rho^0} \leq 1.2 \text{ GeV}$) and (b) the A_2 region ($1.2 \text{ GeV} \leq M_{\pi^-\rho^0} \leq 1.42 \text{ GeV}$) at $3.2 \text{ GeV}/c$; (c) and (d) the A_1 and A_2 regions at $4.2 \text{ GeV}/c$.

could have simply chosen that combination of $\pi^+\pi^-$ which is closer to the ρ^0 mass.

1. Differences between the A_1 and A_2 Enhancements

A number of authors³⁸⁻⁴¹ have observed that the A_1 and A_2 enhancements have different production mechanisms; the production of the A_2 meson seemed to be consistent with that of a genuine resonant state, whereas the A_1 enhancement seemed to be associated with the OPE process leading to the final state $p\pi^-\rho^0$, which would be clearly inconsistent with the A_1 's being a resonant state.

We first show the Dalitz plot of $M_{p\pi^-}^2$ against $M_{\pi^-\rho^0}^2$ in Fig. 13(a); this plot illustrates the extent to which the A_1 and A_2 interfere with the three neutral isobars. The projections onto the $M_{p\pi^-}$ axis for the A_1 and A_2 regions separately show that isobars are more prominent in the A_1 than in the A_2 region [see Figs. 13(b) and 13(c)]. A further difference is seen when $\Delta_{p\pi^-}^2$ is plotted against $M_{\pi^-\rho^0}$ [Fig. 13(d)]; the A_1 enhancement is concentrated in the region of low $\Delta_{p\pi^-}^2$, while the A_2 clearly is not. In fact, the Dalitz plot for $\Delta_{p\pi^-}^2 < 0.55 \text{ (GeV}/c)^2$ [Fig. 13(e)] shows the entire A_1 but almost

none of the A_2 , while the same plot for $\Delta_{p\pi^-}^2 > 0.55 \text{ (GeV}/c)^2$ [Fig. 13(f)] shows very little evidence for the A_1 . These figures clearly demonstrate that the A_1 enhancement is primarily associated with the channel $N^*0\rho^0$, which is produced through a peripheral process (presumably an OPE process). For completeness, we show distributions of Δ_p^2 and $\Delta_{p\pi^-}^2$ for the A_1 and A_2 regions separately at two different beam momenta (Figs. 14 and 15).

If the A_1 enhancement is produced in association with the channel $N^*0\rho^0$ through an OPE process [see Fig. 12(b)], the decay angular distribution of ρ^0 with respect to the incident beam direction, $\cos\theta(\pi^+\pi^-)$, should show the characteristic $\cos^2\theta$ distribution, while for the A_2 , this would not necessarily be true.⁴² Distributions in $\cos\theta(\pi^+\pi^-)$ for four different regions of $M_{\pi^-\rho^0}$ (below A_1 , A_1 , A_2 , above A_2 regions) are shown in Fig. 16. We see a strong $\cos^2\theta$ distribution for the A_1 region but not for the A_2 region. We note that about 50% of events in the A_2 region are estimated to be the background events. If these background events are subtracted out, we may have a drastically different distribution for the A_2 . The corresponding Treiman-Yang angle for the A_1 region is relatively isotropic, which is consistent with an OPE process. The same distribution for the A_2 shows a significantly anisotropic distribution.

³⁸ L. Seidlitz, O. I. Dahl, and D. H. Miller, Phys. Rev. Letters **15**, 217 (1965).

³⁹ B. C. Shen, G. Goldhaber, S. Goldhaber, and J. A. Kadyk, Phys. Rev. Letters **15**, 731 (1965).

⁴⁰ See also Refs. 20, 32, and 34.

⁴¹ For a detailed analysis on the A_1 as well as $K^{**}(1320)$ enhancements, see G. Goldhaber and S. Goldhaber, Lawrence Radiation Laboratory Report No. UCRL-16744, 1966 (unpublished).

⁴² If the A_2 were a meson with $J^P = 1^+(l=0)$ and produced in a peripheral process through exchange of the vacuum trajectory, one should observe a $\cos^2\theta$ distribution for the A_2 ; see Ref. 41.

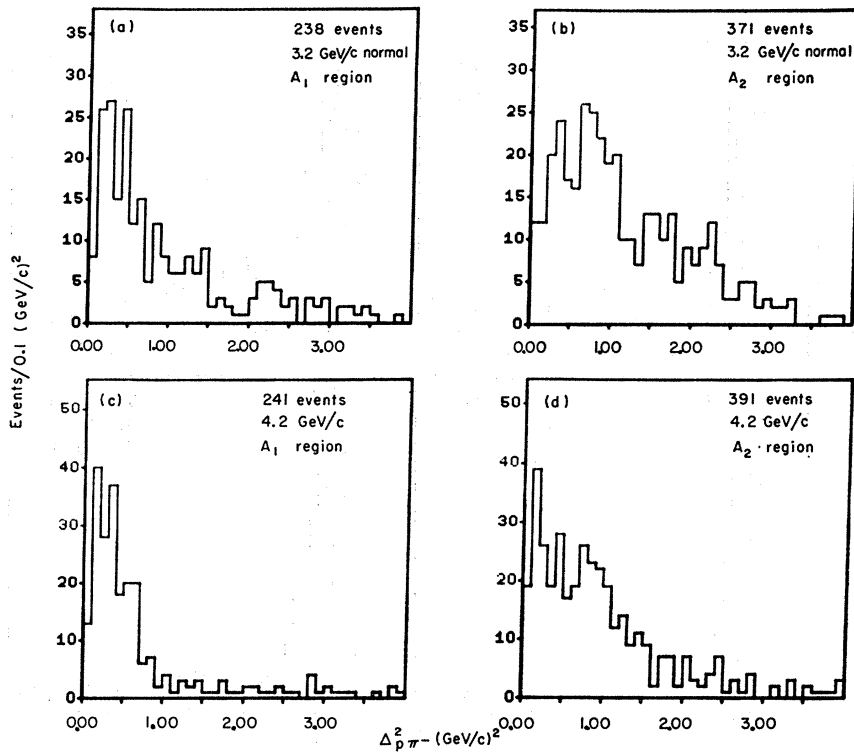


FIG. 15. The $\Delta_{p\pi^2}$ distributions for ρ^0 events (see Refs. 21, 24, and 37): (a) the A_1 region ($1.0 \text{ GeV} \leq M_{\pi^-\rho^0} \leq 1.2 \text{ GeV}$); (b) the A_2 region ($1.2 \text{ GeV} \leq M_{\pi^-\rho^0} \leq 1.42 \text{ GeV}$) at $3.2 \text{ GeV}/c$; (c) and (d) the A_1 and A_2 regions at $4.2 \text{ GeV}/c$.

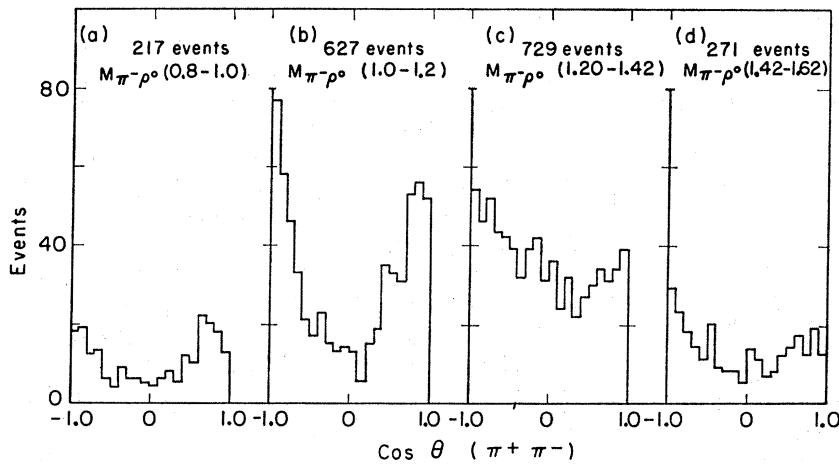


FIG. 16. (a)-(d) $\text{Cos}\theta(\pi^+\pi^-)$ distributions for various $M_{\pi^-\rho^0}$ intervals, where we have taken the ρ^0 events at both momenta with $\Delta_{p^2} < 0.65 \text{ (GeV}/c)^2$ (see Refs. 24 and 37).

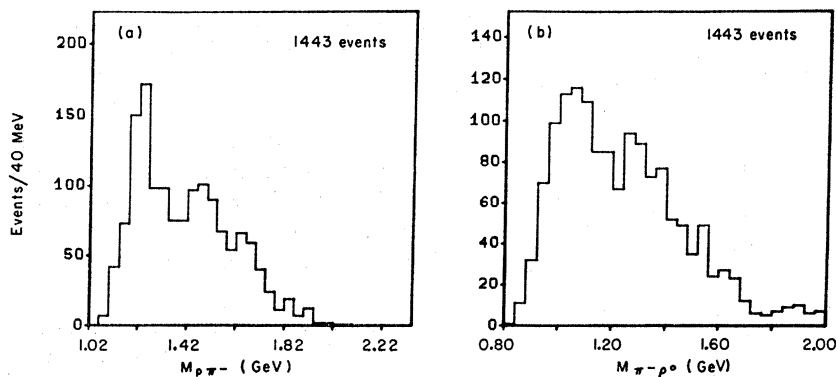


FIG. 17. (a) The $M_{\pi^-\rho^0}$ and (b) $M_{\pi^-\rho^0}$ spectra for ρ^0 events at both momenta with $\Delta_{p\pi^2} \leq 0.55 \text{ (GeV}/c)^2$ (see Refs. 24 and 37).

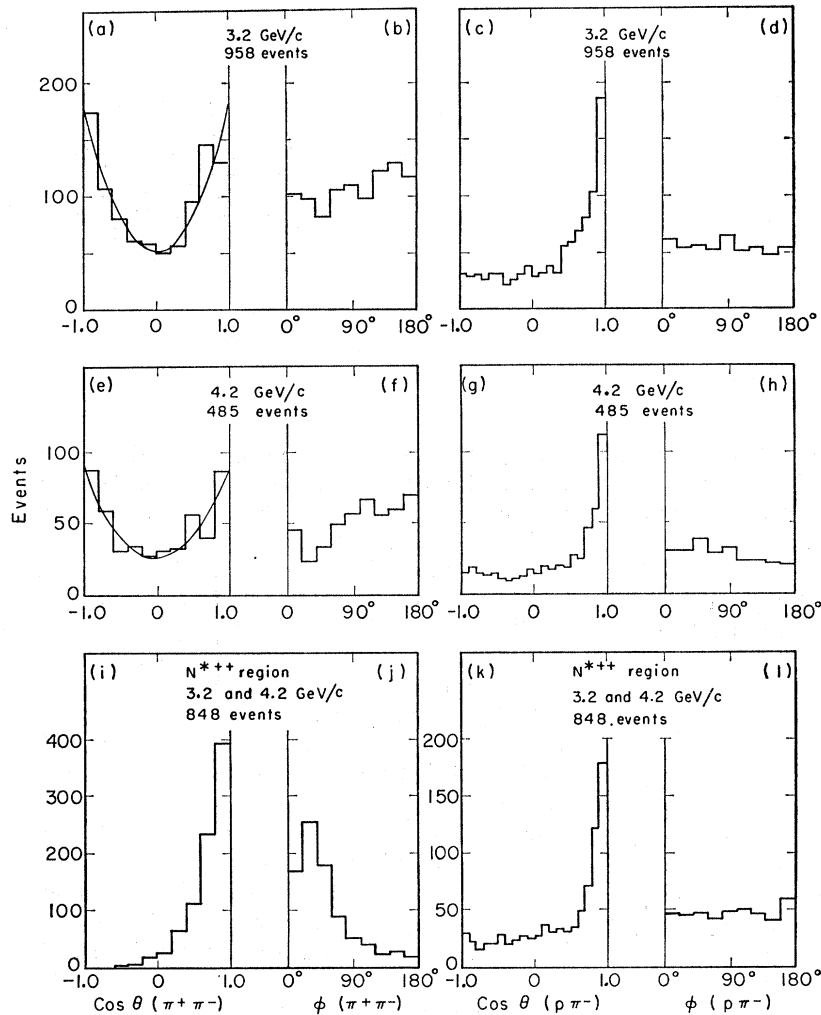


FIG. 18. Angular correlations at the meson and isobar vertices [see Fig. 12(b)] for ρ^0 events with $\Delta_{p\pi^-2} < 0.55$ $(\text{GeV}/c)^2$ (see Refs. 24 and 37): (a)–(d) 3.2-GeV/c data, (e)–(h) 4.2-GeV/c data, and (i)–(l) the N^{*++} region [$1.12 \leq M_{p\pi^+} \leq 1.32$ GeV and $\Delta_{p\pi^+2} < 1.5$ $(\text{GeV}/c)^2$] at both momenta. See Sec. IVC2 for the definition of angles used in these figures. The curves drawn in (a) and (e) are the least-squares fits to the data.

2. Interpretation of the A_1 as Kinematic Enhancement

Since the A_1 is predominantly associated with the final state $N^{*0}\rho^0$, is the A_1 merely a kinematic reflection of this final state and not a resonant state at all? Shen *et al.*³⁹ showed that this interpretation was indeed consistent with their $\pi^\pm p$ data at 3.7 GeV/c; a strong diffractive process at the $\pi^\pm p$ vertex caused an enhancement near the A_1 mass in the $M_{\pi^\pm p}$ distribution, in conformity with a theoretical model proposed by Deck⁴³ and developed further by Maor and O'Halloran.⁴⁴ We find that the A_1 in our data can be explained in substantially the same way, although we cannot rule out the possibility that the A_1 resonance is produced on top of the strong background due to the Deck mechanism.

In order to study the angular distributions for the $N^{*0}\rho^0$ channel, we first make a cut on $\Delta_{p\pi^-2}$ at 0.55 $(\text{GeV}/c)^2$. This cut has been chosen to reduce the background in the $N^{*0}\rho^0$ final state and at the same time to

hold the A_2 contamination at a minimum. The histogram of $M_{\pi^-\rho^0}$ for $\Delta_{p\pi^-2} < 0.55$ $(\text{GeV}/c)^2$ together with that of $M_{p\pi^-}$ is shown in Fig. 17; the A_2 peak is seen to be drastically reduced, as was pointed out in Sec. IVC1.

We present in Fig. 18 decay angular correlations at ρ^0 and N^{*0} vertices for two different beam momenta. Relevant angles are defined as follows: $\theta(\pi^+\pi^-)$ and $\phi(\pi^+\pi^-)$ are polar and azimuthal angles of π^- in a coordinate system defined in the $\pi^+\pi^-$ rest frame with the z axis along the incident beam momentum and the y axis along the normal to the production plane. Similarly, $\theta(p\pi^-)$ and $\phi(p\pi^-)$ are polar and azimuthal angles of the outgoing proton in the $p\pi^-$ rest frame, with the z axis along the incoming proton direction and the y axis along the production normal.

Again, the $\cos^2\theta$ distributions in $\cos\theta(\pi^+\pi^-)$ are consistent with an OPE process. However, the forward-backward asymmetry seen in the data of Shen *et al.*³⁹ does not show up in our data. This is to a large extent caused by the N^{*++} cutoff [see Fig. 18(i)]; decay angular correlations and reaction kinematics are such

⁴³ R. T. Deck, Phys. Rev. Letters **13**, 169 (1964).

⁴⁴ U. Maor and T. A. O'Halloran, Jr., Phys. Letters **15**, 281 (1965).

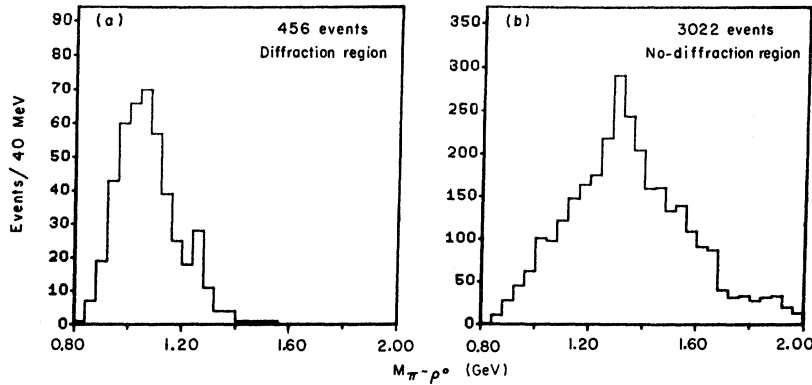


FIG. 19. The $M_{\pi^-\rho^0}$ distributions for ρ^0 events at both momenta (see Ref. 24); (a) in the diffraction region and (b) outside the diffraction region. The diffraction region contains ρ^0 events with $\Delta_{p\pi^-}^2 < 0.55$ $(\text{GeV}/c)^2$ and $\cos\theta(p\pi^-) > 0.8$ (see Ref. 37).

that the region near $\cos\theta(\pi^+\pi^-) \approx +1$ tends to be depleted by the N^{*++} cut. The distributions in $\phi(\pi^+\pi^-)$ are consistent with isotropy, if we take into account the effect of the N^{*++} cut [see Fig. 18(j)].

For completeness, we have fitted the $\cos\theta(\pi^+\pi^-)$ distributions [see Figs. 18(a) and 18(e)] to the Legendre polynomial series [Eq. (2)] by the least-squares method:

Momentum (GeV/c)	a_0	a_1	a_2
3.2	94.0 ± 3.1	-1.50 ± 5.98	85.5 ± 7.4
4.2	46.7 ± 2.2	-0.57 ± 4.17	41.7 ± 5.4

The coefficients a_0 , a_1 , and a_2 given above are normalized to the total number of events at each momentum.

As for the angular correlations at the $p\pi^-$ vertex, the most prominent feature is the strong diffraction peak in the $\cos\theta(p\pi^-)$ distribution. The corresponding Treiman-Yang angle $\phi(p\pi^-)$ is uniformly distributed, again consistent with the OPE process. Note that the angular distributions at the $p\pi^-$ vertex are not affected by the N^{*++} cutoff [see Figs. 18(k) and 18(l)].

In order to demonstrate the relationship between the diffraction region [$\cos\theta(p\pi^-) \approx +1$] in the $\cos\theta(p\pi^-)$ distribution and the A_1 enhancement, we show in Fig. 19(a) the $M_{\pi^-\rho^0}$ plot for only those events with $\cos\theta(p\pi^-)$

> 0.8 ; here the events are confined entirely to the A_1 region with a prominent peak near the A_1 mass. This demonstrates clearly that the events in the diffraction region and those in the A_1 peak come from the same events. Figure 19(b) shows that if this diffraction region is cut off, there is no evidence for the A_1 enhancement at all in the resulting $M_{\pi^-\rho^0}$ distribution.

If we can now show that the diffraction peak we observe in the $\cos\theta(p\pi^-)$ distribution is inherent in the virtual process $\pi^-p \rightarrow \pi^-p$ (at the $p\pi^-$ vertex) and not a reflection of a genuine resonant state A_1 , we will have established that the A_1 is a kinematic enhancement in our data.

For this purpose, we first show how the distributions in $\cos\theta(p\pi^-)$ and $\phi(p\pi^-)$ vary as a function of $M_{p\pi^-}$ (see Fig. 20). We see that most of the diffraction effect comes from high-mass isobar regions. The distribution in $\phi(p\pi^-)$ is essentially isotropic throughout the entire region of $M_{p\pi^-}$.

Figure 21 gives the $\cos\theta(p\pi^-)$ distributions for five different $M_{p\pi^-}$ intervals. With increasing $M_{p\pi^-}$, the peak at $\cos\theta(p\pi^-) \approx +1$ becomes more prominent and the slope is approximately exponential, which is characteristic of a diffraction scattering.

We now compare these distributions with the experimentally measured differential cross sections for the

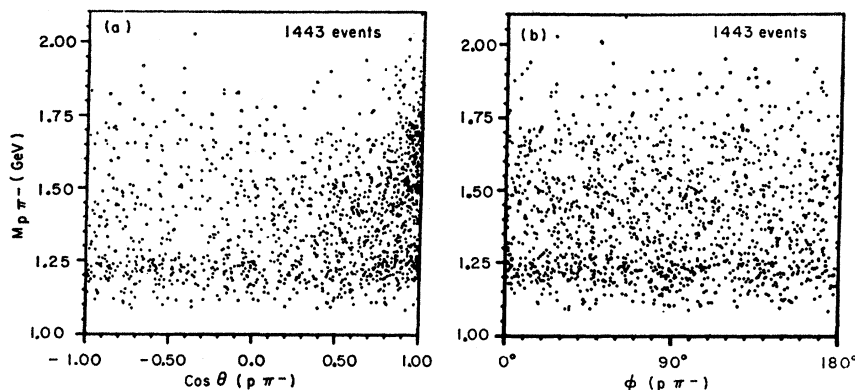


FIG. 20. Scatter plots of (a) $M_{p\pi^-}$ versus $\cos\theta(p\pi^-)$, and (b) $M_{p\pi^-}$ versus $\phi(p\pi^-)$ for ρ^0 events at both momenta with $\Delta_{p\pi^-}^2 < 0.55$ $(\text{GeV}/c)^2$ (see Refs. 24 and 37).

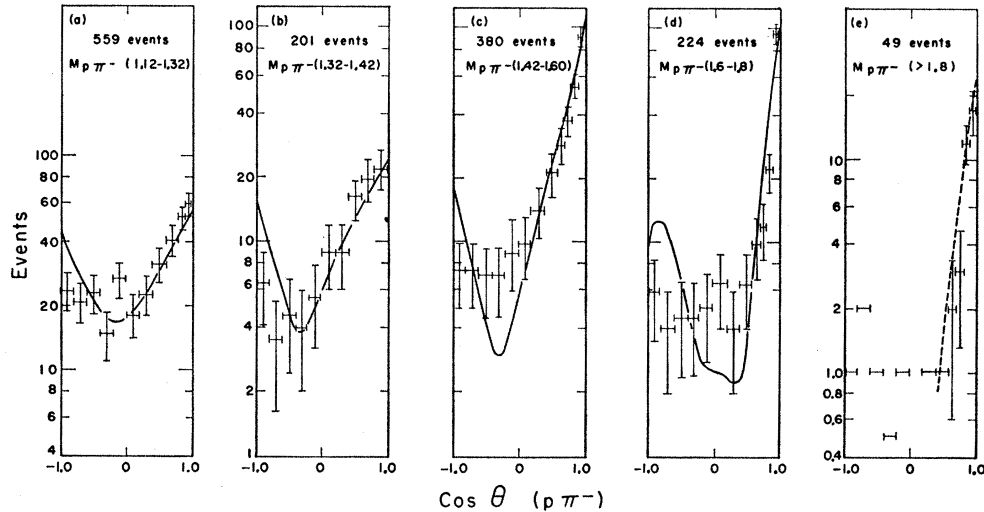


FIG. 21. $\cos\theta(p\pi^-)$ distributions for several $M_{p\pi^-}$ intervals, where we have taken the ρ^0 events at both momenta with $\Delta_{p\pi^-}^2 < 0.55$ (GeV/c^2) (see Refs. 24 and 37); the horizontal bars represent the number of events normalized to each bin size, and the vertical bars are the errors in these numbers. See Sec IVC2 for the explanation of the curves in these figures. Because of small statistics in (e), we have indicated only the slope in the diffraction region by a dotted line.

π^-p elastic scattering,^{45,46} This comparison is meaningful if we assume that the exchanged pion is sufficiently close to the physical region and that it behaves like a physical pion. With this assumption, the differential cross sections are averaged over each $M_{p\pi^-}$ interval and the resulting curves are compared with the $\cos(p\pi^-)\theta$ distributions⁴⁷ (see Fig. 21). For Figs. 21(a) and 21(b), the curves are normalized to the total number of events in each figure; for the rest of the figures, the curves are normalized to the number of events in the $\cos\theta(p\pi^-)$ interval from 0.8 to 1.0.

We see that our experimental distributions are in fair agreement with the curves. Thus it seems plausible to conclude that the peak near $\cos\theta(p\pi^-) \approx +1$ results from the diffractive scattering at the $p\pi^-$ vertex and is not a reflection of a resonant state.

Although our data appear to be consistent with the hypothesis that the A_1 is a kinematic enhancement of the type proposed by Deck, this is by no means a conclusive proof. In fact, it is quite possible that a genuine resonant state is present superimposed on a background enhanced by the mechanism of the type described here.

Finally, we comment on other theoretical models proposed for the A_1 . Month has shown that a triangle singularity can yield a three-pion peak at the A_1 mass.⁴⁸ According to this model, we expect to see a cluster of events at the low $M_{\pi^+\pi^-}$ region in the A_1 Dalitz plot. However, it does not appear that this condition is met

for our A_1 events. The region of low $M_{\pi^+\pi^-}$ would correspond to the region $\cos\beta \approx +1$ where β is the angle between π^+ and π_1^- in the $(\pi^+\pi_2^-)$ rest frame [see Fig. 27(b)]; we see very little evidence for an enhancement in this region. Another kinematic origin for the A_1 enhancement has been proposed by Chang,⁴⁹ who has shown that the effect of Bose symmetrization can lead to the enhancement. However, the test he proposed cannot be applied in our data due to the ill-defined A_1 peak.

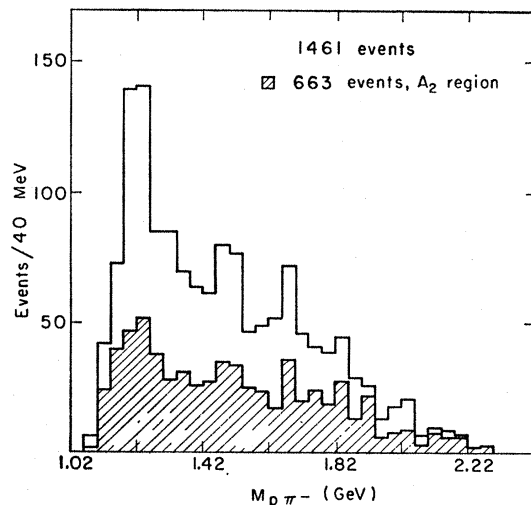


FIG. 22. The $M_{p\pi^-}$ spectrum for ρ^0 events (outside the diffraction region, see Fig. 19) at both momenta with $\Delta_{p\pi^-}^2 < 0.65$ (GeV/c^2) (see Refs. 24 and 37); the shaded histogram is for events in the A_2 region ($1.20 \text{ GeV} \leq M_{p\pi^-} \leq 1.42 \text{ GeV}$).

⁴⁵ J. A. Helland, C. D. Wood, T. J. Devlin, D. E. Hagge, M. J. Longo, B. J. Moyer, and V. Perez-Mendez, Phys. Rev. 134, B1079 (1964).

⁴⁶ C. D. Wood, T. J. Devlin, J. A. Helland, M. J. Longo, B. J. Moyer, and V. Perez-Mendez, Phys. Rev. Letters 6, 481 (1964).

⁴⁷ This is the same method as used by Shen *et al.*, Ref. 39.

⁴⁸ M. Month, Phys. Rev. Letters 18, 357 (1965).

⁴⁹ N. P. Chang, Phys. Rev. Letters 14, 806 (1965).

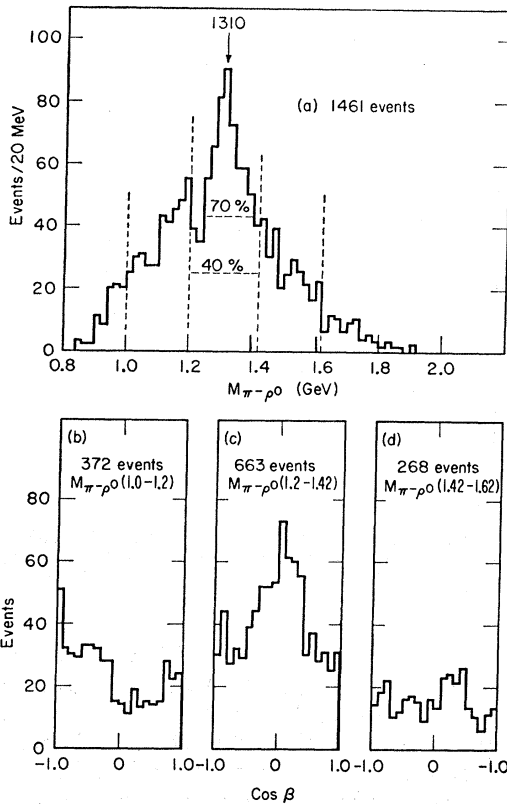


FIG. 23. (a) The $M_{\pi^-\rho^0}$ spectrum for ρ^0 events (outside the diffraction region, see Fig. 19) at both momenta with $\Delta p^2 < 0.65$ (GeV/c)² (see Ref. 24). The vertical dashed lines indicate the A_2 region as well as the control regions, and the horizontal dashed lines indicate background levels in the A_2 region. (b), (c), and (d) Distributions in $\cos\beta$ for the three $M_{\pi^-\rho^0}$ intervals indicated in (a). See Sec IVC3 for the definition of the angle β .

3. Spin and Parity of the A_1 and A_2 Enhancements

Before we present the results of our spin-parity analysis, we first comment on other quantum numbers for the A_2 . Many investigators⁵⁰ have shown that the isotopic spin for the A_2 is not consistent with $I=2$. Furthermore, the decay modes $\pi\eta$ or $K\bar{K}$ for the A_2 would be in contradiction with $I=2$. Since the $\pi\rho$ decay mode implies $G=-1$, we conclude that the A_2 meson has the quantum numbers $I^G=1^-$.

We shall apply the spin-parity analysis to the A_2 meson, as well as the A_1 enhancement, assuming the latter is a genuine resonant state. In addition, we shall investigate the production angular correlations for the A_1 and the A_2 in order to infer the possible quantum numbers as well as the production mechanisms.

Previous spin-parity analyses⁵¹ indicate that the

⁵⁰ M. A. Abolins, D. D. Carmony, R. L. Lander, N-H. Xuong, and P. M. Yager, in *Proceedings of the Second Topical Conference on Resonant Particles* (Ohio University Press, Athens, Ohio, 1965), p. 198; See also Refs. 34 and 38.

⁵¹ See Refs. 26, 29-32, and 34.

likely J^P assignments for the A_2 are 1^+ , 2^- , or 2^+ . The $K\bar{K}$ decay mode of the A_2 , however, limits the J^P assignment to 2^+ .⁵² Previous analyses did not take into account the large background associated with the A_2 peak (see, however, Ref. 34); assuming that the background does not interfere with the A_2 , we have subtracted the background effect by examining the control region.

Our basic approach to J^P analysis of the A_2 is to compare the distribution in $\cos\beta$ with that obtained by the theoretical calculation⁵³ for a given J^P , where β is the angle between π^+ and the "bachelor" π^- (not in ρ^0) evaluated in the ρ^0 rest frame. The matrix element assumed for each spin and parity is given in Appendix A.

In order to suppress the A_1 enhancement (and also the channel $N^{*0}\rho^0$), we have eliminated the diffraction region [see Fig. 19(a)], i.e., those events with $\Delta p^2 < 0.55$ (GeV/c)² and $\cos\theta(p\pi^-) > 0.8$. Furthermore, since the A_2 is produced at low Δp^2 , we limit our analysis to events with $\Delta p^2 < 0.65$ (GeV/c)² [see Fig. 23(a)]. We first show what the effect of N^{*0} 's are in this subsample (Fig. 22). Here $N^{*0}(1238)$ is strong, with some evidence for $N^{*0}(1518)$ and $N^*(1688)$. In the A_2 region itself, however, these isobars appear to be not so important (the shaded area in Fig. 22).

The distributions in $\cos\beta$ for the A_2 region as well as for control regions are shown in Figs. 23(b) through 23(d). Note that the distribution in the A_2 region is quite different from those of control regions.

In order to understand the background effect, we use

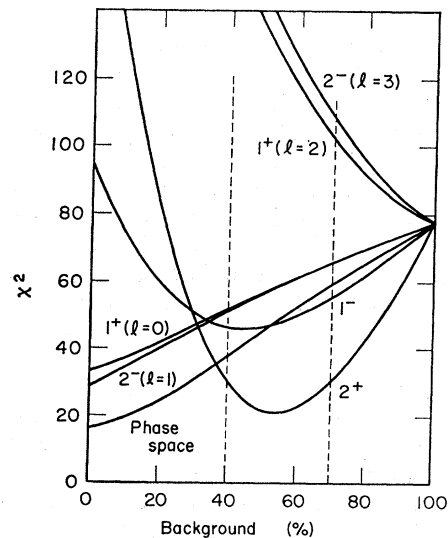
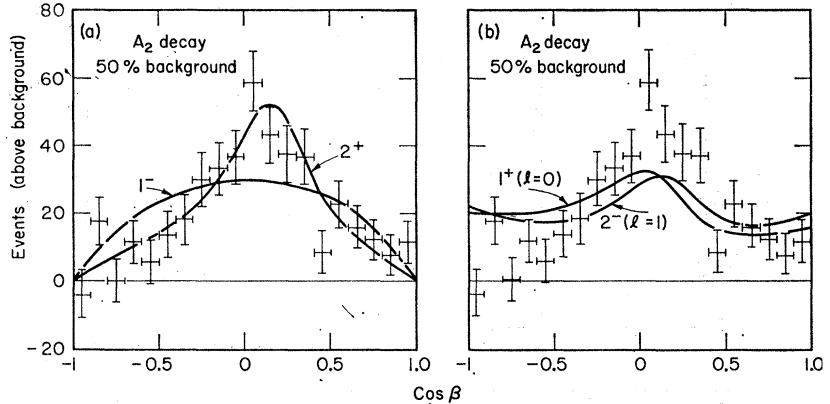


FIG. 24. Variations of χ^2 (19 degrees of freedom) for various J^P assignments for the A_2 as a function of the background level.

⁵² O. I. Dahl, L. M. Hardy, R. I. Hess, J. Kirz, and D. H. Miller, *Phys. Rev.* **163**, 1377 (1967); see also Ref. 26.

⁵³ We use a computer program written by R. Diebold, CERN/TC/PROG 64-25, which has been modified for our purpose.

FIG. 25. Comparison of the experimental $\cos\beta$ distributions in the A_2 region at the 50% background level with the theoretical curves for the $J^P = 1^-, 2^+, 1^+ (\ell=0)$ and $2^- (\ell=1)$.



the following method.⁵⁴ For a given amount of background, which is assumed to vary from 0 to 100%, we compare the theoretical distribution of a given J^P with the distribution composed of $\{n_i'\}$ ($i=1, 20$), where n_i' is obtained by

$$n_i' = n_i - \frac{\epsilon N}{N^{(1)} + \alpha N^{(2)}} [n_i^{(1)} + \alpha n_i^{(2)}]. \quad (3)$$

Here n_i is the number of events in the i th bin of the $\cos\beta$ distribution in the A_2 region [Fig. 23(c)], $n_i^{(1)}$ is the number of events in the i th bin for the region below the A_2 and $n_i^{(2)}$ above it [Figs. 23(b) and (d)], and N , $N^{(1)}$, and $N^{(2)}$ are total numbers of events in each category. The parameter ϵ varies from 0 to 1, corresponding to the amount of background level from 0 to 100%. The parameter α has been used to vary the relative amount of control regions. We have taken $\alpha=1$ for the spin-parity analysis on the A_2 . However, we have also tried other values of α (see below).

TABLE IV. Fits to various J^P hypotheses for the A_2 .^a

J^P	χ^2 ^b	Confidence level (%)
$\pi\rho$ phase space	44.89	≈ 0.07
1^-	46.25	≈ 0.04
2^+	21.56	30.7
0^-	316.08	0.0
$1^+ (\ell=0)$	56.22	0.0
$1^+ (\ell=2)$	135.04	0.0
$2^- (\ell=0)$	56.20	0.0
$2^- (\ell=3)$	145.19	0.0

^a 50% background level assumed.
^b 19 degrees of freedom.

⁵⁴ Criticism has been raised on the method we use to take into account the background [D. R. O. Morrison (private communication)]; the objection is that the peak in the $\cos\beta$ distribution due to the presence of ρ^0 shifts as the $M_{\pi^+\pi^-\pi^0}$ changes and that therefore the sum of the control regions does not adequately describe the background under the A_2 peak. However, this effect is not important as long as the background consists mostly of the 3π state and not much of the $\pi\rho$ state, which is the case experimentally with our data. In fact, a slightly different approach to the background problem, which takes into account the presence of the $\pi\rho$ background, gives practically identical results as the ones given here. See S. U. Chung, O. I. Dahl, L. M. Hardy, R. I. Hess, J. Kirz, and D. H. Miller, Phys. Rev. Letters 18, 100 (1967).

The resulting χ^2 (19 degrees of freedom) for each J^P assignment for the A_2 as a function of the amount of background is shown in Fig. 24. We observe that if the background is assumed to be zero, we obtain J^P assignments of either 1^+ ($\ell=0$) or 2^- ($\ell=1$) for the A_2 . We believe, however, that the amount of background is certainly not less than 40% and probably not more than 70% [see Fig. 23(a)]. Within this region (shown by dashed lines in Fig. 24), we find that there is only one unique J^P assignment consistent with the data—it is 2^+ . Assuming 50% background, we give in Fig. 25 the $\cos\beta$ distribution along with theoretical curves for a few J^P assignments. In Table IV, we list the value of χ^2 for each J^P assignment, along with the corresponding confidence level at 50% background.

We have also weighted $N^{(1)}$ and $N^{(2)}$ by different amounts ($\alpha=N^{(1)}/N^{(2)}$) so that equal numbers of events contribute to the background; the general structure of χ^2 did not change appreciably throughout the entire range of background level.

Therefore, with the assumption that the background

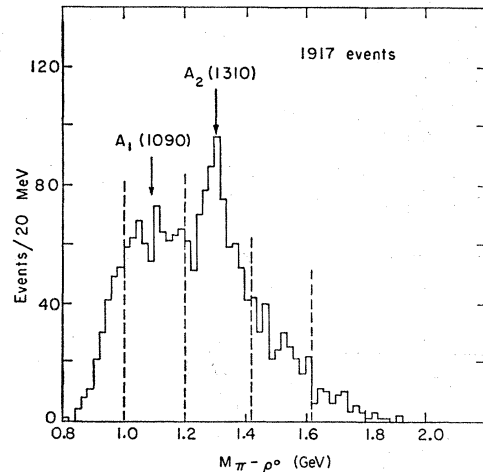


FIG. 26. The $M_{\pi-\rho^0}$ spectrum for ρ^0 events at both momenta with $\Delta_2^2 < 0.65$ (GeV/c)² (see Ref. 24). The dashed lines at $M_{\pi-\rho^0} = 1.0, 1.20, 1.42, 1.62$ GeV delineate the A_1 and A_2 regions as well as their control regions.

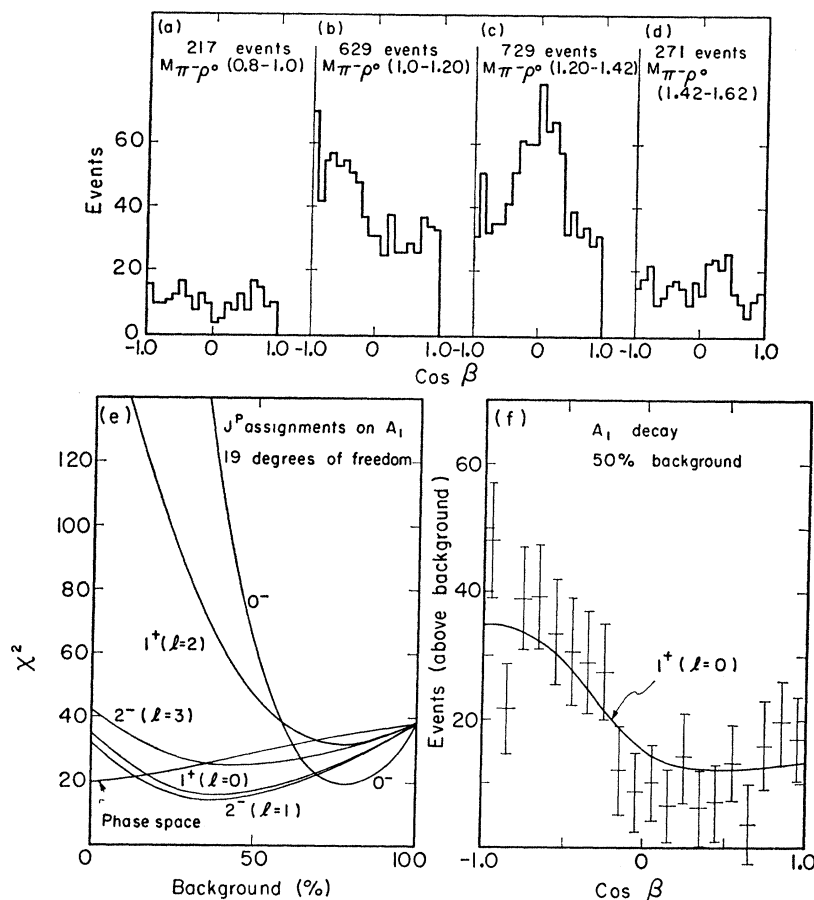


FIG. 27. (a)-(d) The distributions in $\cos \beta$ for the four $M\pi\rho^0$ intervals defined in Fig. 26. (e) Variations in χ^2 (19 degrees of freedom) for various J^P assignments for the A_1 as a function of the background level. (f) Comparison of the $\cos \beta$ distribution in the A_1 region at the 50% level with the theoretical curve of $J^P=1^+(\ell=0)$. See Sec. IVC3 for the definition of the angle β .

does not interfere with the A_2 meson, we conclude that its spin and parity are uniquely 2^+ , which is consistent with the observation of the $K\bar{K}$ decay mode.

We apply the same technique to the A_1 enhancement, assuming that it is a genuine resonant state. Again, we take only those events with $\Delta_p^2 < 0.65$ (GeV/c)² (Fig. 26). We select four regions of $M\pi\rho^0$ —namely, below the A_1 , in the A_1 and A_2 regions, and above the A_2 region; the distribution in $\cos \beta$ is given for each of these regions in Figs. 27(a) through (d).

Background has been taken into account as follows: Events in Figs. 27(a) and (c) are weighted differently

so that equal numbers of events contribute to the background [$\alpha = N^{(1)}/N^{(2)}$]; this particular choice of weight is somewhat arbitrary. However, the results are rather insensitive to any particular choice of weight. For instance, we could have taken events in the control regions with the same weight ($\alpha = 1$); the results do not change drastically.

Figure 27(e) shows the behavior of χ^2 for each J^P as a function of the background level. In the interval between 30 and 60% background, J^P assignments $1^+(\ell=0)$ or $2^-(\ell=1)$ seem quite consistent with the data. Figure 27(f) shows how the theoretical curve for $J^P=1^+(\ell=0)$ compares with the experimental distribution at 50% background level. The values of χ^2 for each J^P assignment at 50% background level are given in Table V.

We have also examined the production angular correlations for the A_1 and the A_2 . For this purpose, we chose to examine the distribution in $\cos z$, where z is the angle between the normal to the decay plane of A and the incident π^- momentum evaluated in the A rest frame. We present in Appendix A the theoretical distributions in $\cos z$ for various spin-parity assignments. We observe that for $J^P=0^-, 1^-, 2^+$, and 1^+ , the angular distributions are independent of the detailed

TABLE V. Fits to various J^P hypotheses for the A_1 .^a

J^P	χ^2 ^b	Confidence level (%)
$\pi\rho$ phase space	29.15	6.3
1^-	126.87	0.0
2^+	136.85	0.0
0^-	62.75	0.0
$1^+(\ell=0)$	16.70	61.0
$1^+(\ell=2)$	46.76	~ 0.04
$2^-(\ell=1)$	15.89	66.4
$2^-(\ell=3)$	25.20	15.4

^a 50% background level assumed.

^b 19 degrees of freedom.

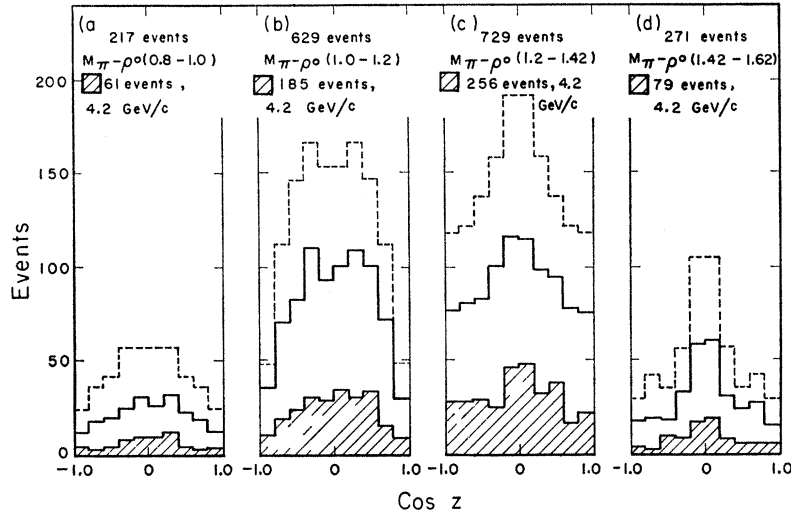


FIG. 28. The distributions in $\cos z$ for the four $M_{\pi^-\rho^0}$ intervals defined in Fig. 26. The solid-line histograms correspond to events at 3.2 and 4.2 GeV/c, and the shaded histograms correspond to events at 4.2 GeV/c alone; two points are plotted for the double- ρ^0 events and one point for the rest. The dashed-line histograms correspond to events at both momenta with two points plotted for each event. See Sec. IVC3 for the definition of the angle z .

internal structure of the three-pion system, whereas for 2^- this is generally not the case.

Figure 28 shows the distributions in $\cos z$ for the four different regions of $M_{\pi^-\rho^0}$ mentioned earlier. The solid

histograms were obtained by taking two points for double- ρ^0 events to take into account the interference effect,⁵⁵ and the shaded areas were obtained in the same way with events at 4.2 GeV/c alone. To take advantage

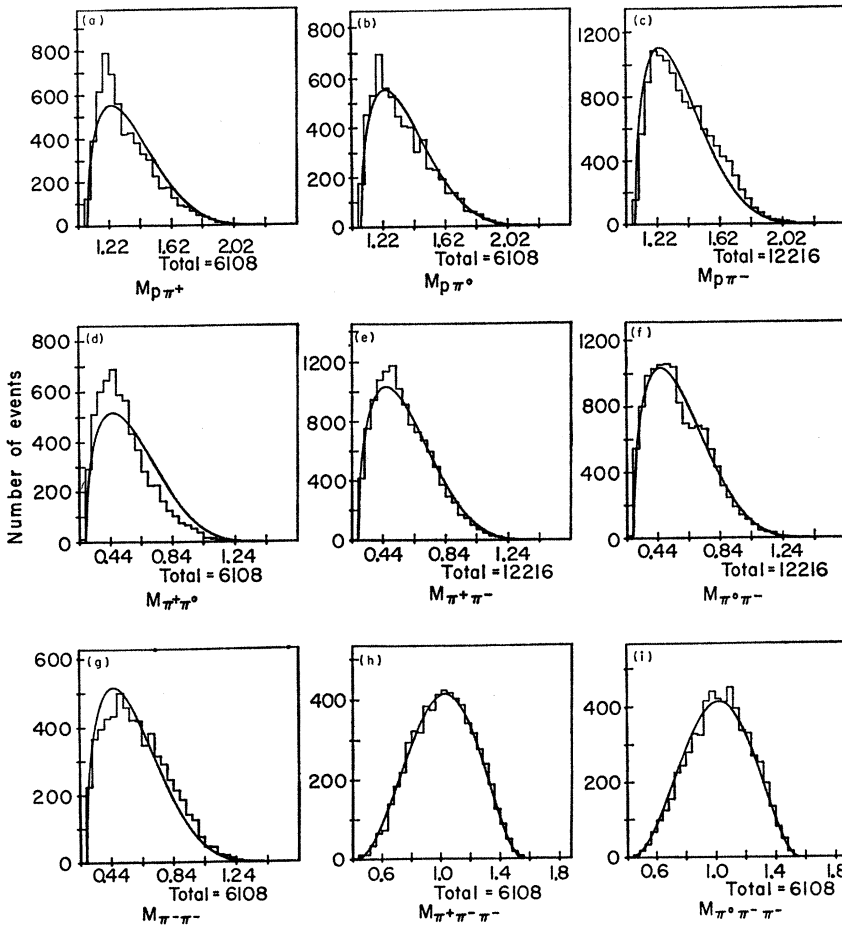


FIG. 29. Effective-mass distributions obtainable from the $p4\pi$ final state at 3.2 GeV/c. The horizontal scales are in GeV, and the vertical scales are for the number of combinations per 40 MeV. The total number of combinations for each histogram is shown after the heading "Total." The curves in each histogram are the phase-space curves normalized to the total number of combinations.

⁵⁵ For single- ρ^0 events, the normal to the decay plane of the A^- and its direction can be uniquely determined; we just form a cross product between the momentum of π^+ and that of the bachelor π^- . However, this procedure is not unique for double- ρ^0 events.

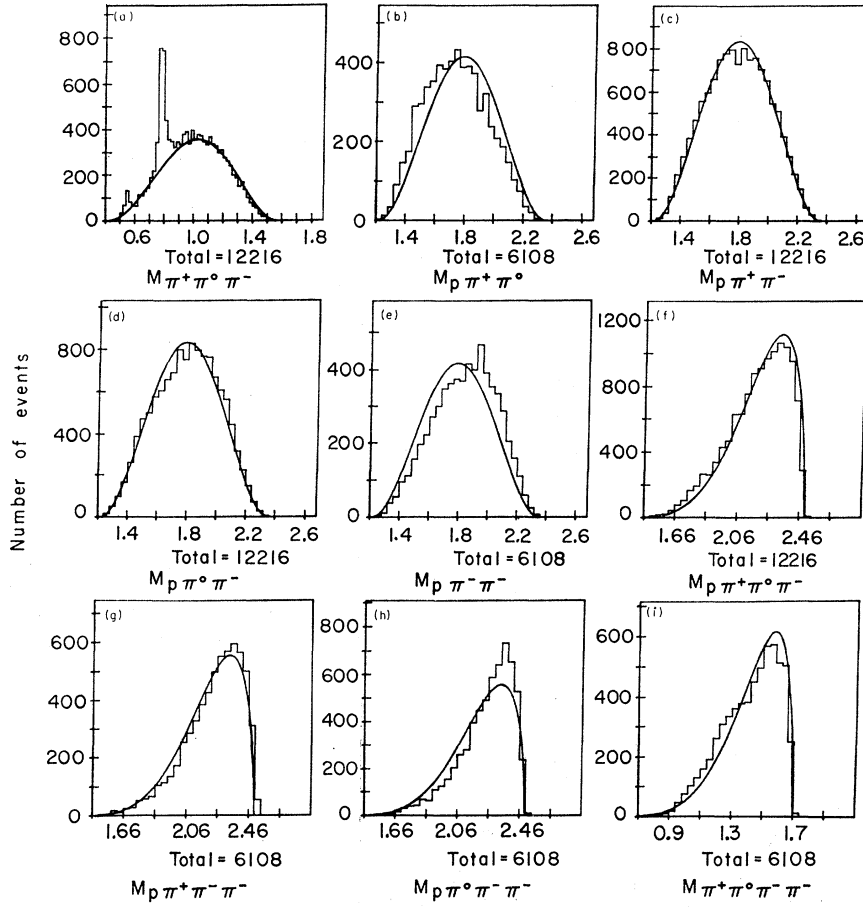


FIG. 30. Additional effective-mass distributions from the $p4\pi$ final state at 3.2 GeV/c. Scales are as on Fig. 29 except in (a) where the vertical scale corresponds to the number of combinations per 20 MeV, and the phase space is normalized to the portion of the histogram for $M_{\pi^+\pi^0\pi^-}$ above 0.9 GeV.

of the fact that for some values of J^P the distribution should be independent of the interference effect, we have taken two points for each event; the resulting histograms are shown as dotted lines in Fig. 28. Note that this particular method makes the resulting histograms symmetric with respect to $\cos z=0$.

In Fig. 28 there is an enhancement of events at the region $\cos z \approx 0$ for all four $M_{\pi^-\rho^0}$ regions. Taking the distributions at face value, we observe that the distribution in the A_1 region is consistent with a $\sin^2 z$ distribution. If J^P for the A_1 is assumed to be 1^+ and if it is produced via ρ^0 -exchange process, we may infer that $\rho_{11} \lesssim 0$, where $\rho_{mm'}$ is the density matrix for the A_1 (see Appendix A).

If the A_2 is produced via the ρ^0 -exchange process and absorptive effects are negligible, the angular distribution is predicted to be [see Eq. (A6), Appendix A]

$$I(z) \approx 1 - 3 \cos^2 z + 4 \cos^4 z, \quad (4)$$

which is peaked in the region $\cos z \approx \pm 1$. If the background in the A_2 region is taken into account, our experimental distributions are consistent with (4). However, due to the possible absorptive effects⁵⁶ and

⁵⁶ It is generally recognized that absorptive effects are not negligible; see, for instance, J. D. Jackson, Rev. Mod. Phys. **37**, 484 (1965).

the background contamination, it is difficult to make strong statements concerning the distribution in $\cos z$.

Finally, we observe that the dotted and solid histograms are consistent with each other within statistics. It is amusing to note that if the two histograms were significantly different for the A_1 region, we would have been able to distinguish between the two J^P assignments 1^+ and 2^- . As pointed out earlier, this is because for $J^P=2^-$, the angular distribution depends in general on the interference of double- ρ^0 events, whereas it is completely independent of the interference for $J^P=1^+$.

V. $p\pi^+\pi^0\pi^-\pi^-$ FINAL STATE

A. Effective-Mass Distributions

We present in Figs. 29–32 all the effective-mass plots for 3.2- and 4.2-GeV/c data separately. Again the 3.2-GeV/c data are for both the normal and selected samples. The effective-mass plots for the selected sample alone showed little difference from those of the normal sample. The curves drawn in each of these plots are simple phase-space curves.

The outstanding feature in this final state ($p\pi^+\pi^0\pi^-\pi^-$) is the production of ω and η mesons [see Figs. 30(a) and 32(a)]. Also, there is evidence for $N^{*++}(1238)$ production. For the production cross section for these reso-

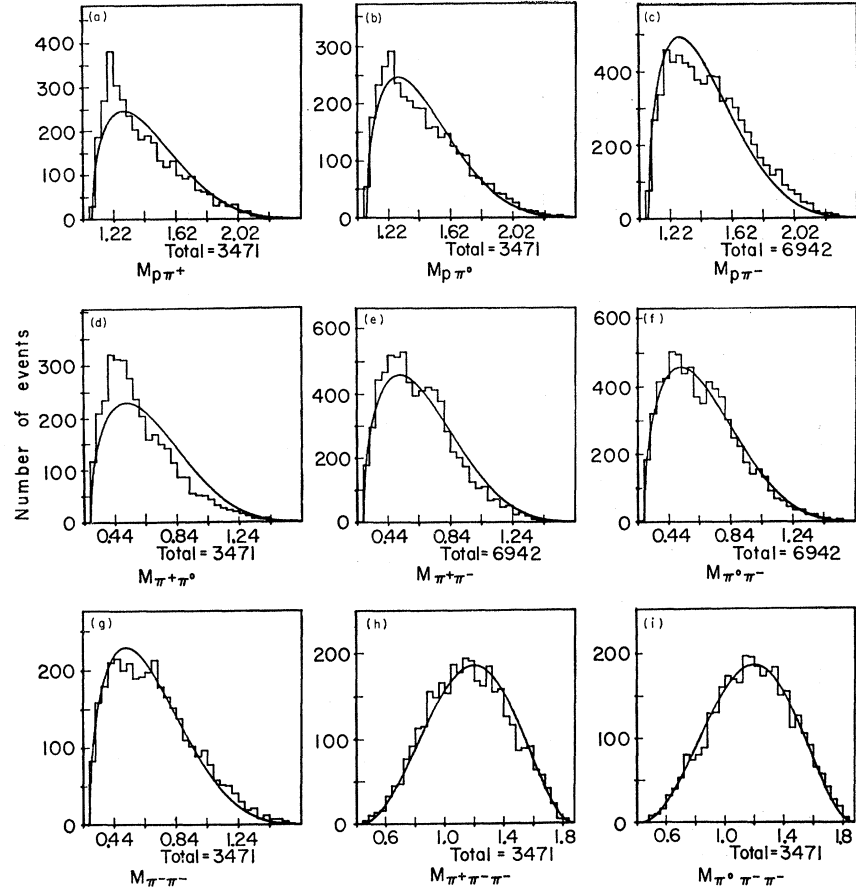


FIG. 31. Same effective-mass distributions as in Fig. 29 for events at 4.2 GeV/c.

nances at 3.2 GeV/c, we have again used the normal sample alone; the cross sections are determined to be 230 ± 30 , 31 ± 9 , and 320 ± 80 μb for ω , η , and N^{*++} productions, respectively.⁵⁷ At 4.2 GeV/c, the respective cross sections are 185 ± 25 , 21 ± 7 , and 335 ± 65 μb .⁵⁷

We show in Fig. 33 the effective-mass distributions for quasi-three-body final states when $M_{\pi^+\pi^-\pi^0}$ is limited to the ω region (0.76 to 0.80 GeV) or the η region (0.53 to 0.57 GeV). The phase-space curves are those of three-body final states normalized to the total number of combinations in each histogram.

In the $M_{\pi^-\omega}$ plots, we observe the B enhancement near 1220 MeV. Based on the combined data, we have obtained 1220 ± 20 MeV for the mass and 150 ± 20 MeV for the width. Rough estimates for its production cross sections are 108 ± 30 μb at 3.2 GeV/c and 67 ± 20 μb at 4.2 GeV/c. In the $M_{\pi^-\eta}$ plot at 3.2 GeV/c [Fig. 33(c)], we observe an enhancement near the A_2 mass; the $\pi\eta$ decay mode of the A_2 has also been observed in other experiments.^{27,30} However, the width appears to be too broad for the A_2 when compared with that of the $\pi^-\rho^0$ decay mode. In addition, there is little evidence for the A_2 decay at 4.2 GeV/c [see Fig. 33(g)], although our statistics are limited at this energy (66 events). We find

⁵⁷ The cross sections quoted here for ω and η productions do not include corrections for the other decay modes.

that its production cross sections are roughly 12 ± 7 μb at 3.2 GeV/c and 5 ± 5 μb at 4.2 GeV/c.

Schumann⁵⁸ reported an enhancement (mass ≈ 1.71 GeV and width < 50 MeV) in the $M_{p\pi^+\pi^0}$ distribution for π^-p data at 3.9 GeV/c. Our data, however, do not show any evidence for the enhancement [see Figs. 30(b) and 32(b)]. We note that our sample is 6 times as large as that of Schumann at 3.2 GeV/c, 3 times at 4.2 GeV/c.

In the $M_{p\pi^-}$ [Figs. 33(b) and 33(f)] there is evidence for the decay of $N^{*0}(1238)$, $N^{*0}(1518)$, and $N^{*0}(1688)$. The situation here appears to be analogous to that of the $p\pi^-\rho^0$ final state discussed earlier.

We discuss in detail the final states $p\pi^-\omega$ and $p\pi^-\eta$ in the following two sections.

B. Reaction $\pi^-p \rightarrow p\pi^-\omega$

In this section, we discuss in detail how the peak at 1220 MeV in $M_{\pi^-\omega}$, known as the B meson,⁵⁹ can be

⁵⁸ T. G. Schumann, Phys. Rev. Letters 15, 531 (1965).

⁵⁹ M. Abolins, R. L. Lander, W. A. W. Mehlhop, N-H. Xuong, and P. M. Yager, Phys. Rev. Letters 11, 381 (1963); S. U. Chung, O. I. Dahl, R. I. Hess, G. R. Kalbfleisch, J. Kirz, D. H. Miller, and G. A. Smith, in *Proceedings of the Sienna International Conference on Elementary Particles and High-Energy Physics, 1963*, edited by G. Bernardini and G. P. Puppi (Societa Italia di Fisica, Bologna, 1963), p. 201; for a review on the B enhancement as well as other multiparticle resonances, see G. Goldhaber, Lawrence Radiation Laboratory Report No. UCRL-11971, 1965 (unpublished).

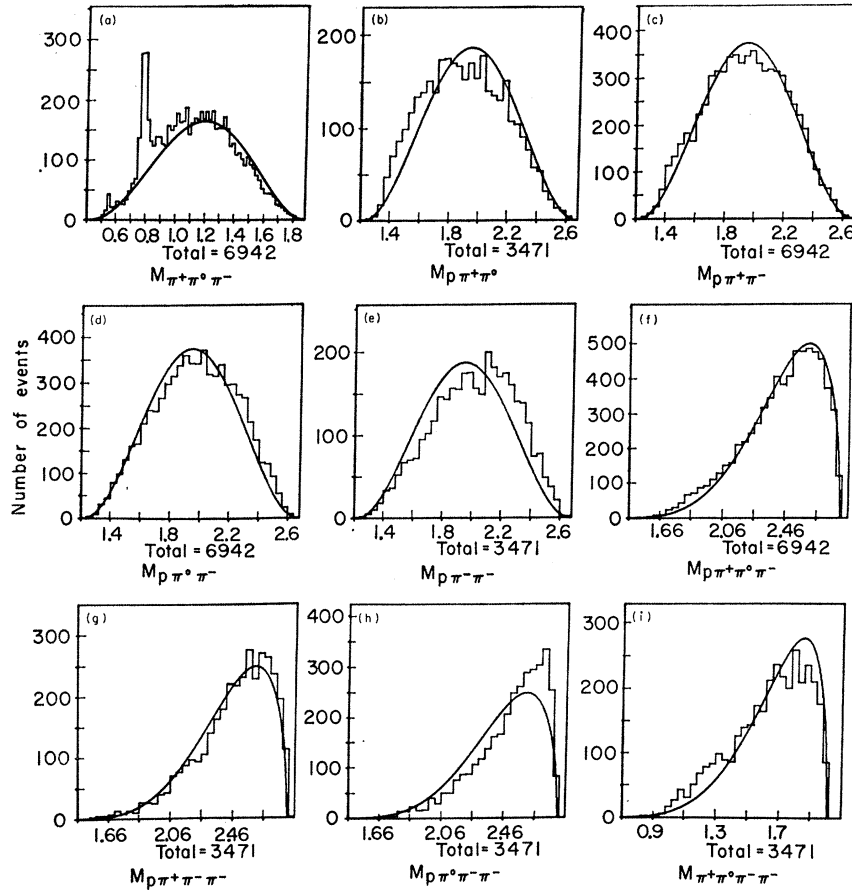


FIG. 32. Same effective-mass distributions as in Fig. 30 for events at 4.2 GeV/c.

shown to be consistent with the hypothesis of kinematic enhancement. The treatment here is similar to that of our earlier work.⁶⁰ This work is based on a larger sample at 3.2 GeV/c, and the total sample is somewhat more refined than the sample on which our earlier work is based.

Throughout this section, we chose the ω region to be in the interval 0.76 to 0.80 GeV. Most of our analysis was done on single- ω events (either neutral pion triplet lies in the ω region—but not both). There are 94 double- ω events (both neutral pion triplets lie in the ω region) in our sample, compared with 1867 single- ω events. For most of our purposes, the interference effect arising from double- ω events is considered to be negligible.

Unlike the $p3\pi$ final state, the $N^{*++}(1238)$ production is weak in the $p4\pi$ final states. In particular, its interference with the $p\pi^-\omega$ final state (and especially the B meson) is negligible for our purposes. To demonstrate this, we show for single- ω events a scatter plot of $M_{p\pi^+}$ against $M_{\pi^-\omega}$ with $\Delta_{p\pi^+} < 1.0$ (GeV/c)² [Fig. 34(a)]; there is little enhancement in the N^{*++} region. This is

further illustrated in Fig. 34(b), a projection onto the $M_{p\pi^+}$ axis in the B region (1.12 to 1.30 GeV). For completeness, we also show in Fig. 34(c) the distribution of $M_{p\pi^0}$ with similar selections. Again, little evidence is seen for the N^{*+} interference.

Therefore, we do not make any cutoffs to suppress $N^{*++}(1238)$ (nor N^{*+}), as we did for the $p3\pi$ final state. In what follows, we demand merely that the $M_{\pi^+\pi^0\pi^-}$ for an event be in the ω region.

1. B Enhancement and $N^{*0}\omega$ Final States

The Chew-Low plot of Δ_{p^2} against $M_{\pi^-\omega}$ for single- ω events shows a cluster of events near the B mass [Fig. 35(a)]. The projected histogram onto the $M_{\pi^-\omega}$ axis [Fig. 35(b)] further illustrates the presence of the B enhancement.

We note that the B enhancement occurs mainly in the region of the low Δ_{p^2} , which suggests a peripheral mechanism for its production. The exchanged particle could either be π^0 or ω [see Fig. 37(a)]. The distributions of Δ_{p^2} for all single- ω events and for events in the B region are shown in Fig. 36. The distributions in the B region show sharp peaks near $\Delta_{p^2} \approx 0$ —a characteristic

⁶⁰ S. U. Chung, M. Neveu-René, Orin I. Dahl, J. Kirz, D. H. Miller, and Z. G. T. Guiragossian, Phys. Rev. Letters 16, 481 (1966).

of π -exchange processes.⁶¹ This would mean that possible spin-parity assignments for the B are $J^P=1^-, 3^-$, etc.⁶² However, the possibility of ω exchange cannot be ruled out, in which case there would be no restriction on the J^P (except 0^+).

Figure 35(c) is a Dalitz plot of $M_{p\pi^-2}$ versus $M_{\pi^-\omega^2}$ for

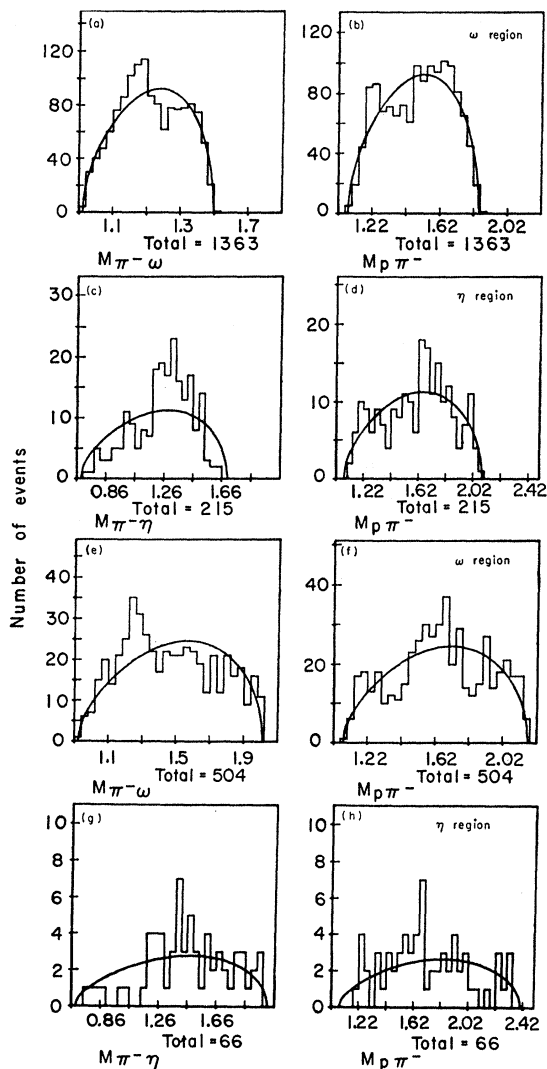


FIG. 33. (a) and (b) The $M_{\pi^-\omega}$ and $M_{p\pi^-}$ spectra for events at 3.2 GeV/c with the remaining three-pion mass in the ω region (0.76–0.80 GeV). (c) and (d) The $M_{\pi^-\eta}$ and $M_{p\pi^-}$ spectra for events at 3.2 GeV/c with the remaining three-pion mass in the η region (0.53–0.57 GeV). (e)–(h) The same effective-mass distributions as in (a)–(d) for events at 4.2 GeV/c.

⁶¹ See, for instance, the Aachen-Berlin-Birmingham-Bonn-Hamburg-London (I. C.)-München Collaboration, Ref. 20; H. O. Cohn, W. M. Bugg, and G. T. Condo, Phys. Letters **15**, 344 (1965); S. Goldhaber, J. L. Brown, I. Butterworth, G. Goldhaber, A. A. Hirata, J. A. Kadyk, and G. H. Trilling, Phys. Rev. Letters **15**, 737 (1965); see also Ref. 56.

⁶² As pointed out in our earlier paper (Ref. 60), these spin-parity sequences would allow the B to decay into $\pi\pi$ or $K\bar{K}$. Although phase-space considerations alone would not inhibit these decay modes, they have not been observed so far: See Refs. 7 and 52.

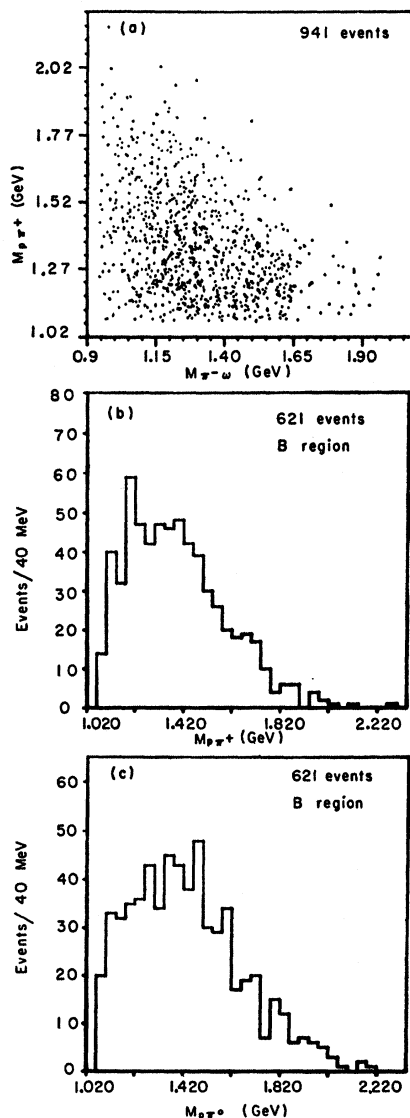


FIG. 34. (a) Scatter plot of $M_{p\pi^+}$ versus $M_{\pi^-\omega}$ for single- ω events at both momenta with $\Delta_{p\pi^+}^2 < 1.0$ (GeV/c)². (b) The $M_{p\pi^+}$ spectrum for ω events at both momenta with $M_{\pi^-\omega}$ in the B interval (1.12–1.30 GeV). (c) The $M_{p\pi^0}$ spectrum for the same events.

single- ω events with $\Delta_{p\pi^+}^2 < 0.35$ (GeV/c)².⁶³ We see that the B enhancement tends to occur in association with nucleon isobars [see also Fig. 40(b)]. In order to further investigate the interference of isobars and the B enhancement, we show in Fig. 38(a) the Chew-Low plot of $\Delta_{p\pi^+}^2$ versus $M_{p\pi^-}$ for single- ω events and the projected histogram in Fig. 38(b). It is evident that the isobars are produced in this final state with low $\Delta_{p\pi^+}^2$, which suggests a peripheral process [see Fig. 37(b)].

On the other hand, Fig. 38(c) shows that the B enhancement is produced mainly with $\Delta_{p\pi^+}^2 < 1.0$

⁶³ We take only one point per event, i.e., the combination $M_{p\pi^+}$ with $M_{\pi^+\pi^0}$ in the ω region.

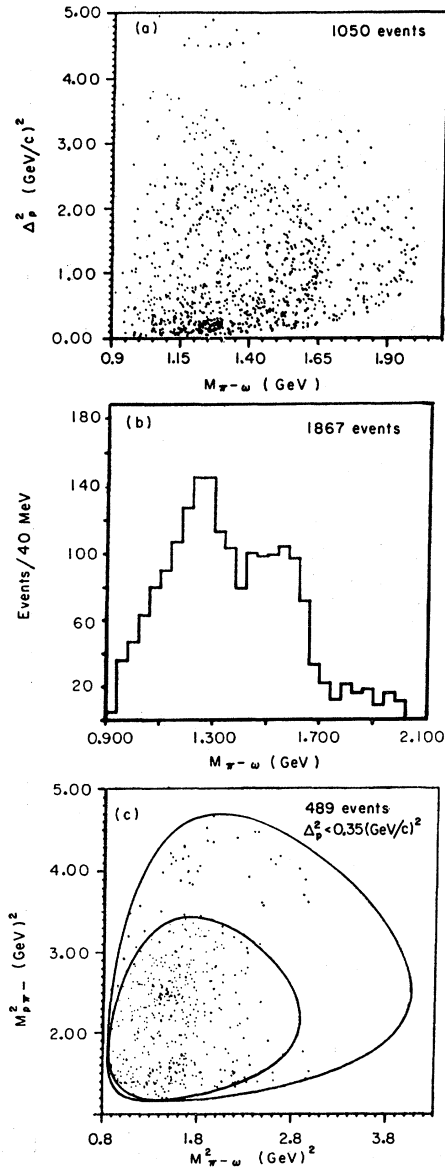


FIG. 35. (a) Scatter plot of Δp^2 versus $M_{\pi^-\omega}$ and (b) the $M_{\pi^-\omega}$ projection for single- ω events at both momenta (see Ref. 21). (c) Dalitz plot of $M_{p\pi^-}^2$ versus $M_{\pi^-\omega}^2$ with the further selection $\Delta p^2 < 0.35$ (GeV/c)².

(GeV/c)², which is also the region where most of the isobar events are concentrated, as is clear from Fig. 38(a) (see also Fig. 40). The extent to which isobars and the B enhancement interfere is further illustrated in Fig. 38(d), the Dalitz plot of the $p\pi^-\omega$ final state with $\Delta p\pi^2 < 1.0$ (GeV/c)². For completeness, we present in Fig. 39 the distributions in $\Delta p\pi^2$ for all single- ω events and also for events with $M_{\pi^-\omega}$ in the B region.

Consequently, if the B enhancement is a genuine resonant state, π^-p interactions at 3 to 4 GeV/c do not provide a suitable final state in which to determine its quantum numbers. Nevertheless, a simple study of the

internal correlations for the B decay is given in Sec. VB4.

2. Interpretation of the B as a Kinematic Enhancement

Since final states pB^- and $N^*\omega$ seem to be so closely associated with each other, one is naturally led to ask: Is it possible to interpret the B enhancement as a kinematic consequence of the final state $N^*\omega$ rather than a resonant state? We shall show in this section that this is indeed the case in our data. However, this kinematic interpretation is meaningful only if the observation of the B is limited to $\pi^\pm p$ interactions. Recently Baltay *et al.*⁶⁴ reported an enhancement at the B mass in the $\pi\omega$ system from $p\bar{p}$ annihilations. It would appear that the B as is observed in our data is perhaps a superposition of a genuine resonant state and a kinematic enhancement.

In extending a suggestion made by Deck,⁴³ Maor and O'Halloran⁴⁴ pointed out that virtual dissociation of the incident pion, $\pi^\pm \rightarrow \omega + \rho^\pm$, followed by the strongly asymmetric inelastic process, $\rho^\pm + p \rightarrow \pi^\pm + p$, should result in a broad enhancement in the region $M_{\pi^+\omega} \approx 1200$ MeV. In this section, we show that such a model accounts naturally for the essential features of the B enhancement as observed in our data.

To this end, we study in detail the decay correlations of the process $\pi^-p \rightarrow N^*\omega$, limiting ourselves to single- ω events with $\Delta p\pi^2 < 1.0$ (GeV/c)². We emphasize that this is the region where we observe *both* the B enhancement and the isobars (see Fig. 40).

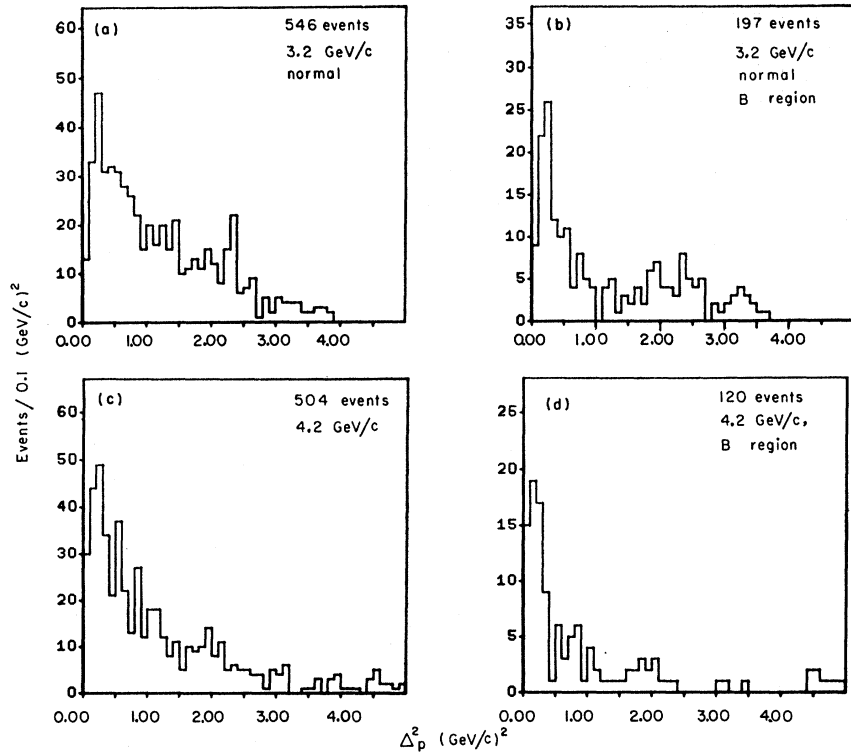
Figure 41 shows the angular distributions for the upper and lower vertex of the exchange process [see Fig. 37(b)]. The angles corresponding to this diagram are defined as follows: In the ω rest frame, $\theta(\omega)$ and $\phi(\omega)$ are, respectively, the polar and azimuthal angles of the normal to the ω -decay plane with the z axis along the incident beam and the y axis along the production normal.⁶⁵ In the $p\pi^-$ rest frame, $\theta(p\pi^-)$ and $\phi(p\pi^-)$ are, respectively, the polar and azimuthal angles of the outgoing proton, in a coordinate system with the z axis along the incident proton and the y axis along the production normal.

If the exchanged particle is the ρ , the Treiman-Yang angles $\phi(\omega)$ and $\phi(p\pi^-)$ need not be isotropically distributed; Figures 41(b) and 41(d) show that the distributions are indeed not isotropic. The hypothesis of the ρ -exchange process can be tested for the process $\pi^-p \rightarrow N^*(1238)\omega$. Figure 42 shows the same angular

⁶⁴ C. Baltay, J. C. Severiens, N. Yeh, and Z. Zanello, Phys. Rev. Letters **18**, 93 (1967).

⁶⁵ In case of the three-body decay of a resonance, the parity conservation in the production process leads to the symmetry property $I(\theta, \phi) = I(\pi - \theta, \pi - \phi)$, where $I(\theta, \phi)$ is the angular distribution of the normal to the decay plane of the resonance. If $I(\theta, \phi)$ is integrated over the angle θ , one obtains $I'(\phi) = I'(\pi - \phi)$, where $I'(\phi)$ is the angular distribution in ϕ . Hence, the proper angular interval for the ϕ distribution is from -90 to $+90$ deg. This result can be shown easily by using Eq. (11) in Ref. 84 and Eq. (A5) in Appendix A.

FIG. 36. The Δ_p^2 distributions for single- ω events (see Ref. 21): (a) 3.2-GeV/c data; (b) the B region ($1.12 < M_{\pi-\omega} \leq 1.30$ GeV) at 3.2 GeV/c; (c) 4.2-GeV/c data; (d) the B region at 4.2 GeV/c.



distributions for the $N^{*0}(1238)$ region. The solid curves which provide a reasonable fit to our data are those obtained by Aderholz *et al.*⁶⁶ in their analysis of the reaction $\pi^+p \rightarrow N^{*++}(1238)\omega$ at 4.0 BeV/c; the curves are also in good agreement with Svensson's calculations⁶⁷ based on the ρ -exchange model with absorptive corrections. Theoretical calculations are not available for higher-mass isobar regions; however, it seems reasonable that the ρ -exchange process leading to $N^{*0}(1238)$ will also produce $N^{*0}(1518)$ and $N^{*0}(1688)$.

The distribution in $\cos\theta(p\pi^-)$ [Fig. 41(c)] shows a strong peaking near $\cos\theta(p\pi^-) \approx +1$. In order to investigate this peak, we show a scatter plot of $M_{p\pi^-}$ versus $\cos\theta(p\pi^-)$ in Fig. 43(a). We see that most of the peaking near $\cos\theta(p\pi^-) \approx +1$ comes from the $M_{p\pi^-}$ region above $N^{*0}(1238)$. The same scatter plot for events in the B region [Fig. 43(b)] shows that most of the B enhancement is associated with the peak at $\cos\theta(p\pi^-) \approx +1$. Conversely, the distribution in $M_{\pi-\omega}$ shows a striking enhancement at the B mass, when only those events with $\cos\theta(p\pi^-) > 0.6$ are plotted [the shaded area in Fig. 40(a)].

For a more detailed analysis, we divide the $M_{p\pi^-}$ spectrum into five intervals; for each of these intervals, the distribution in $\cos\theta(p\pi^-)$ is shown in Fig. 44. The

shaded regions in this figure were obtained in the following manner. The $M_{\pi-\omega}$ distributions for events in each $M_{p\pi^-}$ mass interval were plotted separately for $\cos\theta(p\pi^-) = 0.6$ to 0.8 and 0.8 to 1.0 (not shown), and the number of B events was estimated; these events are shown as shaded areas in Fig. 44. It is apparent that the B enhancement and the bulk of the asymmetry in $\cos\theta(p\pi^-)$ result from the *same* events. Consequently, the nearly flat distribution in $\cos\theta(p\pi^-)$ in the $N^{*0}(1238)$ region [Fig. 44(a)] should not give rise to a strong B enhancement. This is borne out in the $M_{p\pi^-}$ distribution for events in the B region, which shows a relatively reduced $N^{*0}(1238)$ peak [see shaded area in Fig. 40(b)].

It is instructive at this point to compare the A_1 and B enhancements. We have shown that both of them are associated with the peak at $\cos\theta(p\pi^-) \approx +1$. For the A_1 ,

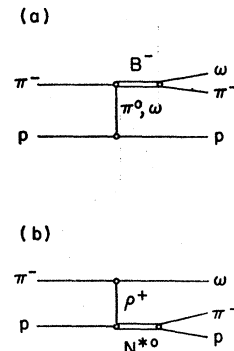


FIG. 37. (a) The π^- (and/or ω) exchange diagram and (b) the ρ -exchange diagram for the process $\pi^-p \rightarrow p\pi^-\omega$.

⁶⁶ M. Aderholz *et al.*, Aachen-Berlin-Birmingham-Bonn-Hamburg-London (I. C.)-München Collaboration, Nuovo Cimento **35**, 659 (1965).

⁶⁷ B. E. Y. Svensson, Nuovo Cimento **37**, 714 (1965).

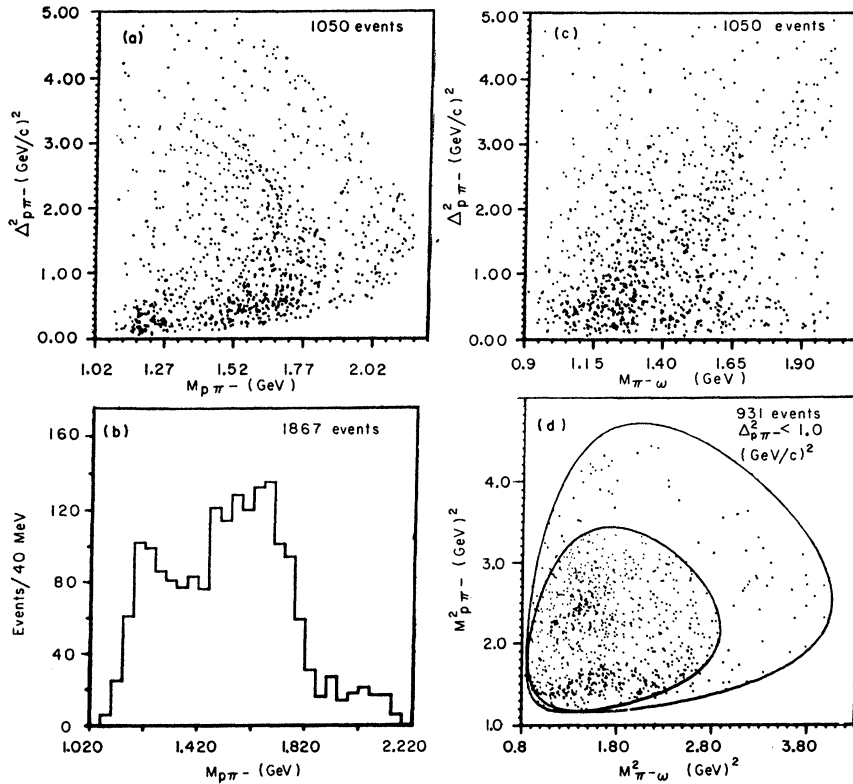


FIG. 38. (a) Scatter plot of $\Delta_{p\pi^-}^2$ versus $M_{p\pi^-}$ and (b) the $M_{p\pi^-}$ projection for single- ω events at both momenta; (c) scatter plot of $\Delta_{p\pi^-}^2$ versus $M_{\pi^-\omega}$ for the same events (see Ref. 21); (d) Dalitz plot of $M_{p\pi^-}^2$ versus $M_{\pi^-\omega}^2$ with the further selection $\Delta_{p\pi^-}^2 < 1.0$ (GeV/c)².

we have compared the $\cos\theta(p\pi^-)$ distribution with the differential cross section for the elastic π^-p scattering and thus inferred that the A_1 is a consequence of the

diffractive π^-p scattering. Unfortunately, the same cannot be done for the B enhancement. The virtual process $\rho^-p \rightarrow \pi^-p$ in the isobar regions is below the

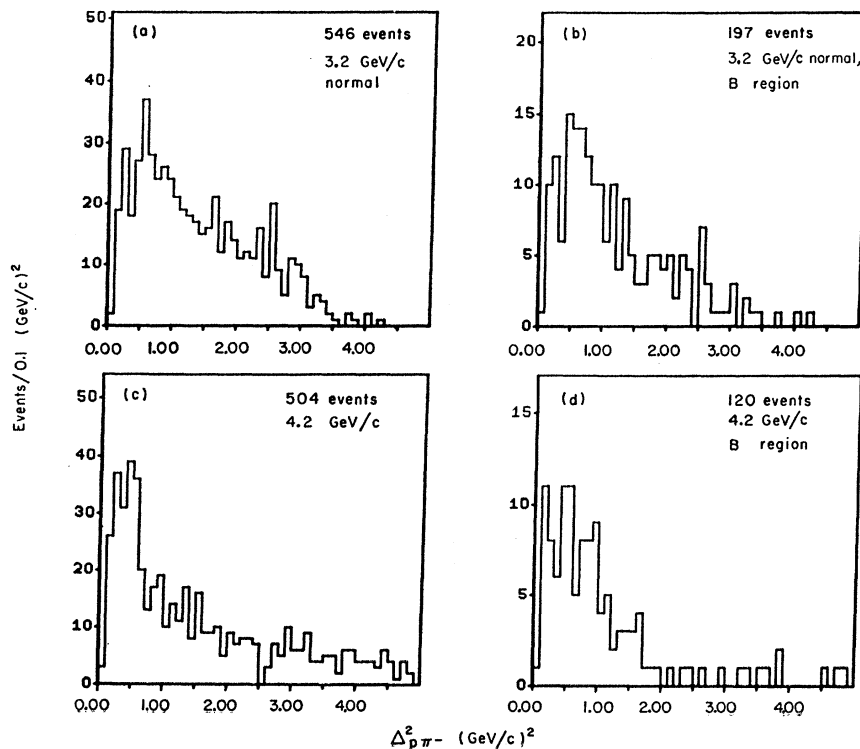
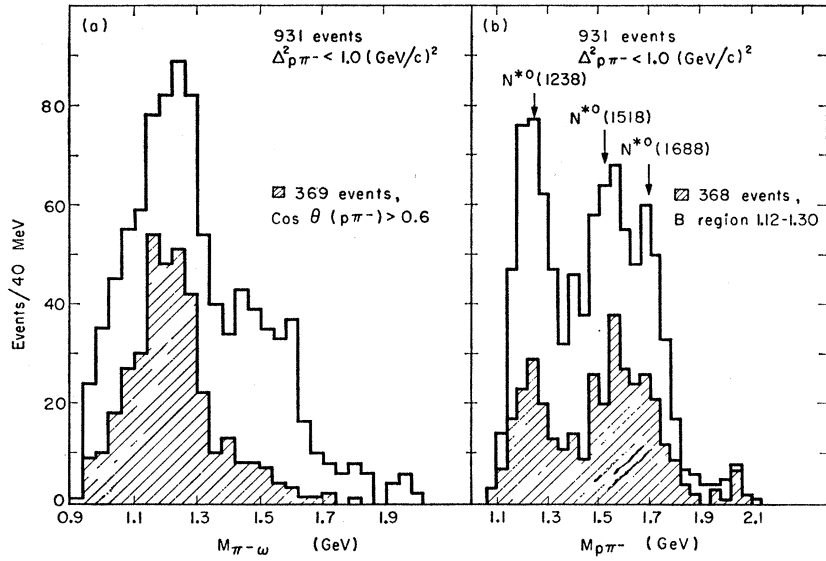


FIG. 39. Distributions in $\Delta_{p\pi^-}^2$ for single- ω events (see Ref. 21): (a) 3.2- GeV/c data; (b) the B region ($1.12 \text{ GeV} \leq M_{\pi^-\omega} \leq 1.30 \text{ GeV}$) at 3.2 GeV/c ; (c) 4.2 GeV/c data; (d) the B region at 4.2 GeV/c .

FIG. 40. (a) The $M_{\pi-\omega}$ spectrum for single- ω events at both momenta with $\Delta_{p\pi^-}^2 < 1.0$ (GeV/c)²; the shaded region indicates events with $\cos\theta(p\pi^-) > 0.6$. (b) The $M_{p\pi^-}$ spectrum for the same events; the shaded region indicates events in the B region (1.12 to 1.30 GeV).



threshold for ρ production.⁶⁸ We have instead taken the following two approaches.

As a first method, we have fitted the $\cos\theta(p\pi^-)$

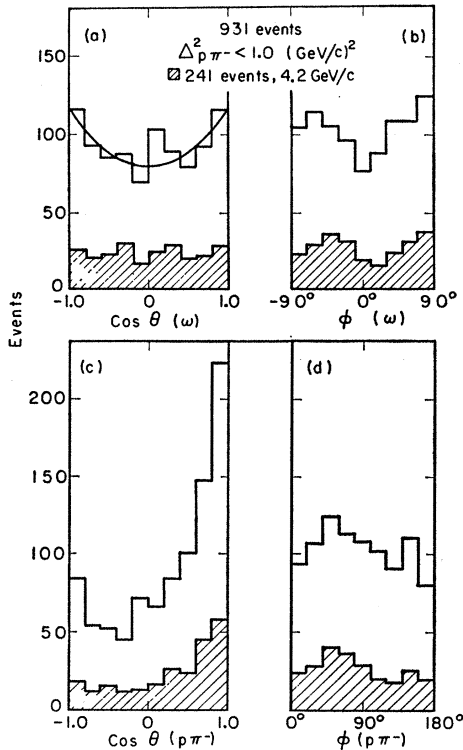


FIG. 41. Angular correlations at the meson and isobar vertices for the ρ -exchange process (see Sec. VB2); single- ω events at both momenta with $\Delta_{p\pi^-}^2 < 1.0$ (GeV/c)² have been used. The shaded histograms are for events at 4.2 GeV/c alone. The curve in (a) is the best fit to the data obtained by the least-squares method [the fitted coefficients for the polynomial in Eq. (2) are: $a_0 = 91.70 \pm 3.03$, $a_1 = -0.09 \pm 5.50$, and $a_2 = 24.06 \pm 7.27$].

⁶⁸ However, the interval of the highest-mass $M_{p\pi^-}$ can be

distribution in each isobar region with the Legendre polynomial series [Eq. (2)] by the least-squares method. The result is shown as solid curves in Figs. 44(a), 44(d), and the fitted coefficients a_i are shown in Table VI. Our data require up to the second-order polynomial for $N^{*0}(1238)$ region, third order for $N^{*0}(1518)$, and fourth order for $N^{*0}(1688)$; these results are consistent with the spin-parity states known

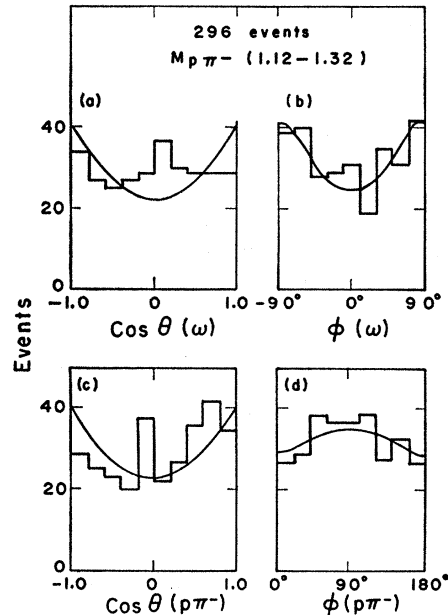


FIG. 42. Same angular correlations as in Fig. 41 for events with $M_{p\pi^-}$ in the $N^{*0}(1238)$ region. See Sec. VB2 for the explanation of the curves.

compared with experiment. The reverse reaction $\pi^- p \rightarrow \rho^- p$ at the $\pi^- p$ c.m. energy of 1.8 GeV shows a strong peak at $\cos\theta \approx +1$: See E. Pickup, D. K. Robinson, and E. O. Salant, Phys. Rev. Letters 7, 192 (1962).

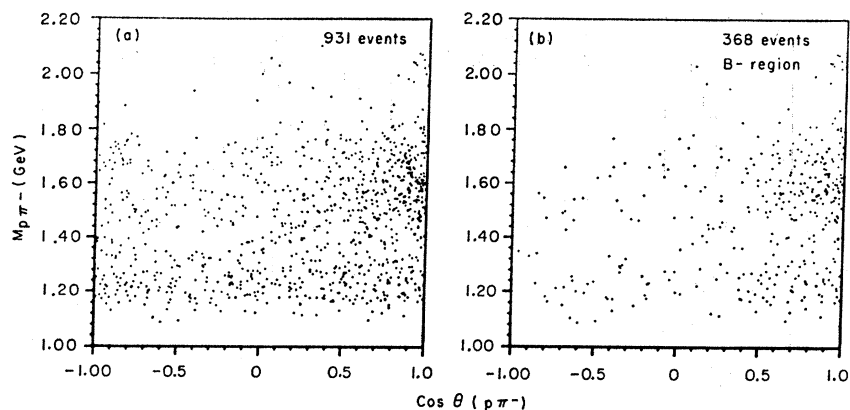


FIG. 43. (a) Scatter plot of $M_{p\pi^-}$ versus $\cos\theta(p\pi^-)$ for single- ω events at both momenta with $\Delta_{p\pi^-}^2 < 1.0$ (GeV/c^2); (b) the same scatter plot in the B region (1.12 to 1.30 GeV).

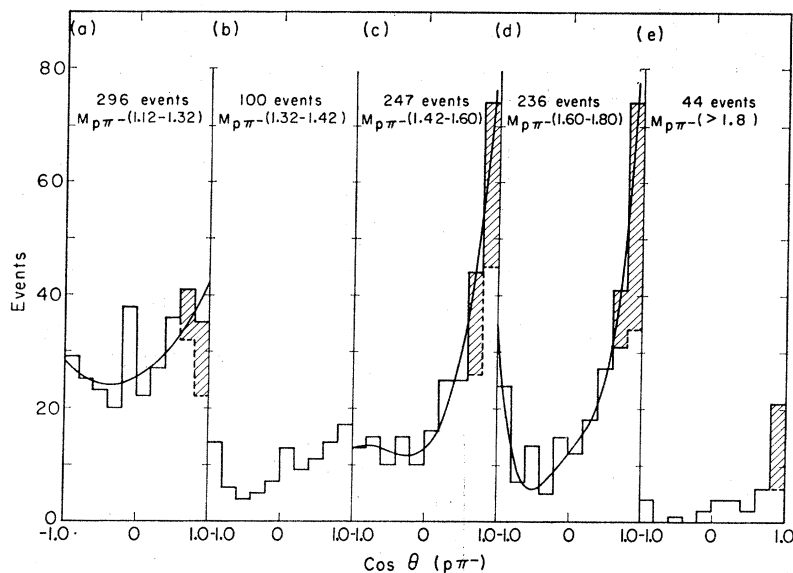


FIG. 44. Distributions in $\cos\theta(p\pi^-)$ for various $M_{p\pi^-}$ intervals (in GeV). See Sec. VB2 for explanations of solid curves and shaded areas. Only single- ω events at both momenta with $\Delta_{p\pi^-}^2 < 1.0$ (GeV/c^2) are plotted.

to exist in these regions.⁶⁹ In general, one would not expect to get these results if the asymmetry in $\cos\theta(p\pi^-)$ were entirely the reflection of a genuine resonant state.

Our second method is to compare our data with the virtual process $\rho N \rightarrow \pi p$ that might occur in a different final state. For this purpose, we investigate the reaction $\pi^- n \rightarrow p \pi^- \pi^-$ from our deuterium data at 3.2 GeV/c.⁷⁰ The Δ_p^2 and $M_{p\pi^-}$ distributions in Figs. 45(a) and 45(b) show evidence of isobar productions through a peripheral mechanism, which is presumably a ρ^0 -exchange process [see insert in Fig. 45(a).] The $\cos\theta(p\pi^-)$ distributions for this reaction are shown in Figs. 45(c)–45(g). We see that these distributions are rather similar to those in Fig. 44. Especially, the peak at $\cos\theta(p\pi^-) \approx +1$ is seen in both reactions, although

⁶⁹ Recent analyses have indicated that both the $N^*(1518)$ and $N^*(1688)$ are probably superpositions of several closely spaced resonances: Sec. P. Bareyre, C. Bricman, A. Stirling, and G. Villet, Phys. Letters 18, 342 (1965).

⁷⁰ See Ref. 38. For this reaction, we have applied a cutoff of 0.2 GeV/c on the momentum (in the laboratory system) of the spectator proton, to ensure a reasonably pure sample of the reaction $\pi^- n \rightarrow p \pi^- \pi^-$.

we do not in general expect identical angular distributions for the two reactions.⁷¹

Judging from the arguments we have presented, it appears likely that the strongly peaked $\cos\theta(p\pi^-)$ distribution is intrinsic to the process $\rho^- p \rightarrow \pi^- p$ and is not a reflection of a resonance in the $M_{\pi^- \omega}$ spectrum. We therefore conclude that the observed correlations are consistent with the model for the B enhancement, as suggested by Maor and O'Halloran.⁴⁴ The low Δ_p^2 distribution in the B region (noted in the previous section) is accounted for by the strongly peaked $\cos\theta(p\pi^-)$ distribution resulting from the process $\rho^- p \rightarrow \pi^- p$. In particular, the model provides a natural explanation for the strong tendency of the B enhancement in our data to be associated with the isobar production. However, as was the case in the A_1 enhancement, the possibility of a genuine resonant state

⁷¹ The presence of ω in the $p\pi^- \omega$ final state affects in general the spin states of the exchange ρ^- differently from that of π^- in the final state $p\pi^- \pi^-$, so that the angular distributions for the reactions $\rho^- p \rightarrow \pi^- p$ and $\rho^0 n \rightarrow \pi^- p$ may be different. However, both reactions proceed through the same N^{*0} intermediate states.

TABLE VI. Least-squares fits to the $\cos\theta(p\pi^-)$ distribution.^a

$M_{p\pi^-}$ (GeV)	a_0	a_1	a_2	a_3	a_4	n^b	χ^2	Confidence level (%)
1.12-1.32	28.74 ± 1.69	7.17 ± 3.06	6.49 ± 3.94			7	8.61	28.2
1.42-1.60	24.23 ± 1.56	25.86 ± 3.18	23.37 ± 3.87	9.70 ± 4.29		6	4.67	58.7
1.60-1.80	22.85 ± 1.51	25.10 ± 3.22	30.59 ± 4.26	6.33 ± 4.49	12.01 ± 5.10	5	7.52	18.5

^a Fitted to the Legendre-polynomial series [see Eq. (2)]. (Coefficients are normalized to the total number of events.)
^b n means number of degrees of freedom.

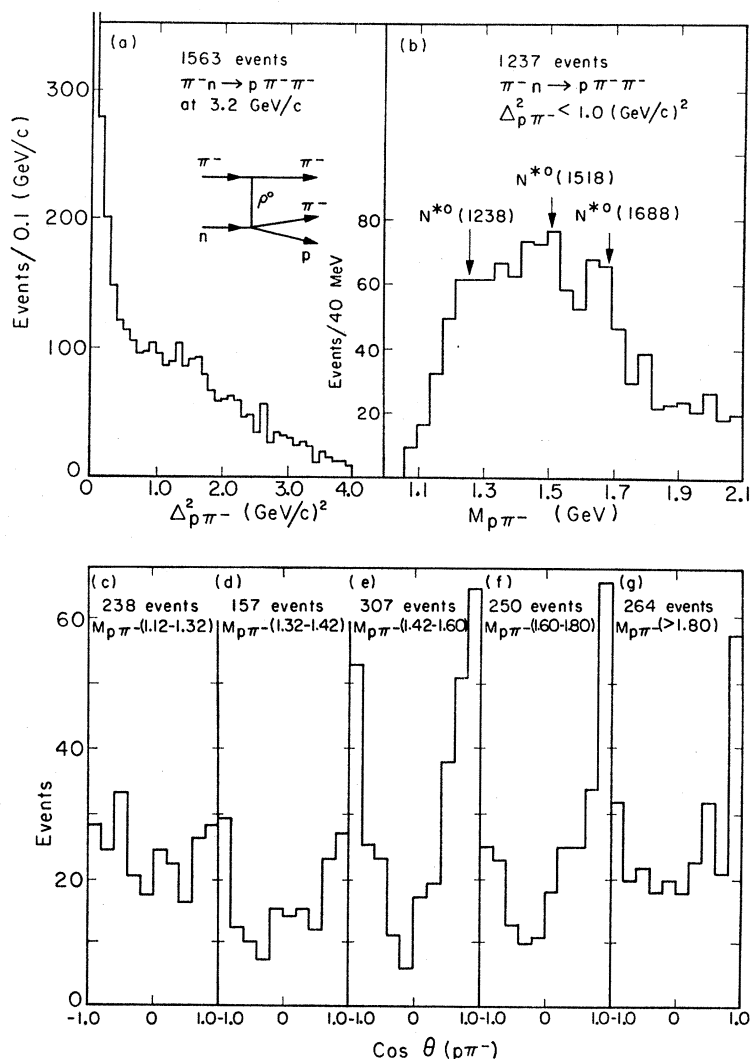


FIG. 45. (a) The $\Delta_{p\pi^-}^2$ distribution (two points per event) for the reaction $\pi^- n \rightarrow p \pi^- \pi^-$ taken from the deuterium data at 3.2 GeV/c (see Ref. 70); (b) the $M_{p\pi^-}$ distribution ($\Delta_{p\pi_1}^2 \leq \Delta_{p\pi_2}^2$) for events with $\Delta_{p\pi_1}^2 < 1.0$ (GeV/c)²; (c)-(g) the $\cos\theta(p\pi_1^-)$ distribution for various $M_{p\pi_1^-}$ intervals (in GeV).

superimposed on a background due to the $N^{*0}\omega$ process cannot be ruled out.

3. Possible Anomaly of the ω 's Associated with the B

Since the J^P of ω is 1^- , the decay distribution in the ω Dalitz plot should be peaked in the center and vanish on the periphery.⁷² Therefore, by selecting events in the

central part of the ω Dalitz plot, we should be able to reduce the relative amount of background associated with the ω peak. For this purpose, we first define a quantity r by

$$r = |\Re \mathfrak{M}|^2 / |\Re \mathfrak{M}|_{\max}^2, \quad (5)$$

where \Re is the matrix element for the ω decay. The central region is then defined by the condition $r > 0.7$, and the peripheral region by $r < 0.7$. The value of r was chosen so that in the absence of background, equal numbers of ω should be contained in the two regions. In Appendix B we give the analytic expression of the

⁷² B. C. Maglič, L. W. Alvarez, A. H. Rosenfeld, and M. L. Stevenson, Phys. Rev. Letters 7, 178 (1961); M. L. Stevenson, L. W. Alvarez, B. C. Maglič, and A. H. Rosenfeld, Phys. Rev. 125, 687 (1962).

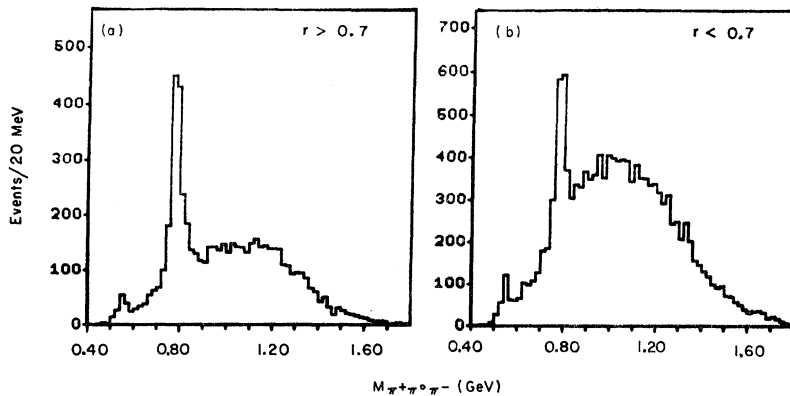


FIG. 46. The $M_{\pi^+\pi^0\pi^-}$ spectra for (a) the central ($r > 0.7$), and (b) the peripheral ($r < 0.7$) regions of the 3π Dalitz plot. Events at both momenta were used in these figures.

contour on the ω Dalitz plot for a given value of r , as well as a brief description of the Dalitz plot.

Recently, Goldhaber *et al.*⁷³ reported possible anomalous behavior of ω mesons associated with the B enhancement. They observed a clear B enhancement for events in the peripheral region of the ω Dalitz plot; within statistics, no enhancement was apparent for the central region. In addition, the Dalitz plot density for ω 's associated with the B enhancement differed significantly from theoretical prediction for a meson with $J^P = 1^-$.

In order to investigate the possible anomaly of ω in

our data, we first show in Figs. 46(a) and 46(b) the $M_{\pi^+\pi^0\pi^-}$ distributions for $r > 0.7$ and $r < 0.7$, respectively. As is expected, we observe a markedly reduced background in the ω region for $r > 0.7$ in Fig. 46(a). The number of ω events above background in Figs. 46(a) and 46(b) is consistent with each other within statistics, as is expected.

In Figs. 47(a) and 47(b) we give the ω Dalitz plot for single- ω events and for double- ω events. The peaking in the center of the Dalitz plot is apparent for single- ω events, but not for double- ω events. This is because double- ω events are constrained to lie within the lower left part of the Dalitz plot [see Fig. 47(b)]. For this reason, in what follows we treat single- and double- ω events separately.

The radial density distributions are given in Figs. 47(c) and 47(d) for single- ω events inside and outside the B region. The background has been estimated from the $M_{\pi^+\pi^0\pi^-}$ spectrum plotted separately for each interval of r . Agreement with the theoretical curve is good in both cases (the confidence levels inside and outside the B regions are 74 and 37%, respectively).

The $M_{\pi^-\omega}$ distribution for single- ω events for the central ($r > 0.7$) and peripheral ($r < 0.7$) regions of the ω Dalitz plot are shown in Figs. 48(a) and 48(b). Within statistics, the number of B events above background for the central region (92 ± 21) is consistent with the number in the peripheral region (83 ± 22). The $M_{\pi^-\omega}$ distributions for double- ω events are shown as shaded areas in Fig. 48. Although these distributions are peaked somewhat below the B peak, it is clear that the inclusion of these double- ω events tends to favor the peripheral region.⁷⁴

Therefore, we conclude that the ω events observed in our data are consistent with a meson with $J^P = 1^-$ for both inside and outside the B region.

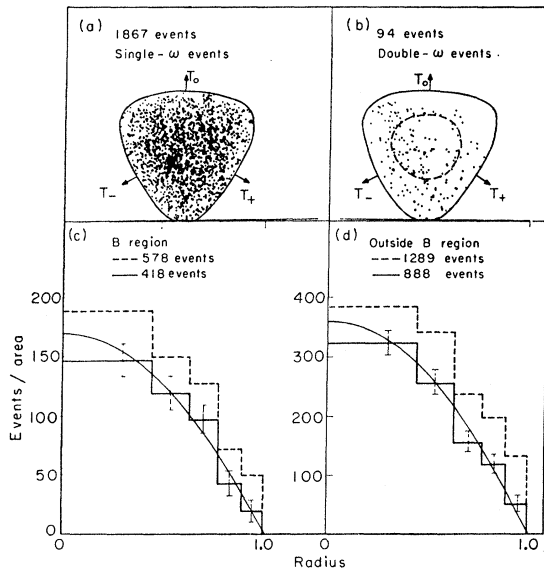


FIG. 47. (a) The ω Dalitz plot for single- ω events at both momenta and (b) for double- ω events. (c) Radial-density distributions of ω decay (single- ω events) for the B region (1.12 to 1.30 GeV) and (d) outside the B region. The dashed-line histograms represent the total number of events in each category; the solid histograms correspond to events with background subtracted (see Sec. VB3). Curves fitted to the solid-line histograms are those expected for the decay of a $J^P = 1^-$ meson.

⁷³ G. Goldhaber, S. Goldhaber, J. A. Kadyk, and B. C. Shen, Phys. Rev. Letters **15**, 118 (1965).

⁷⁴ In a recent compilation of $\pi^\pm\omega$ data, not including ours, the anomaly discussed in Ref. 73 is less pronounced. Although double- ω events were included, the number of B events in the central and peripheral regions were compatible within two standard deviations [G. Goldhaber (private communication)].

FIG. 48. The $M_{\pi-\omega}$ spectra for (a) the central ($r > 0.7$) and (b) the peripheral ($r < 0.7$) regions of the single- ω Dalitz plot (3.2- and 4.2-GeV/ c data combined). The shaded areas are for double- ω events.

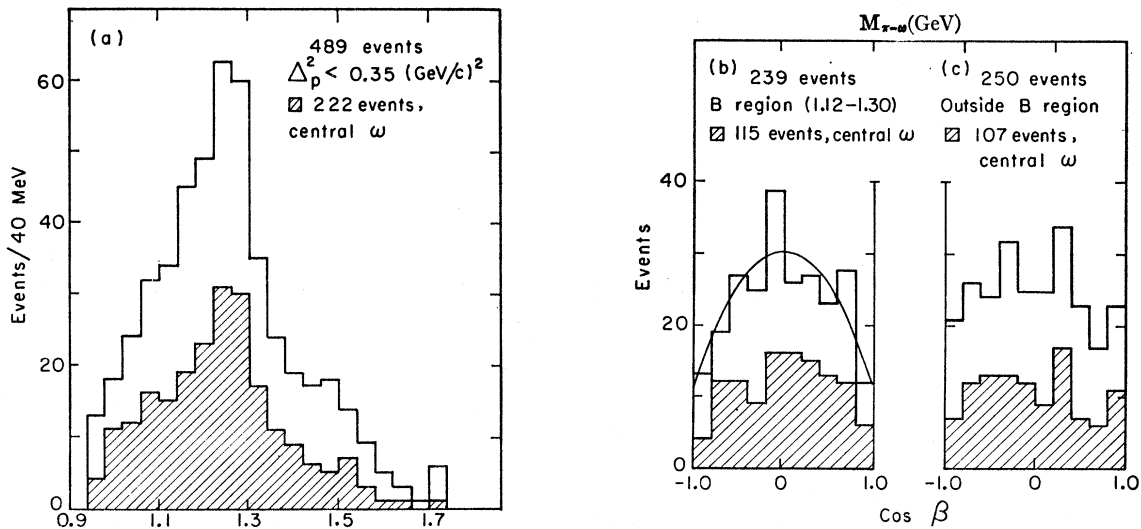
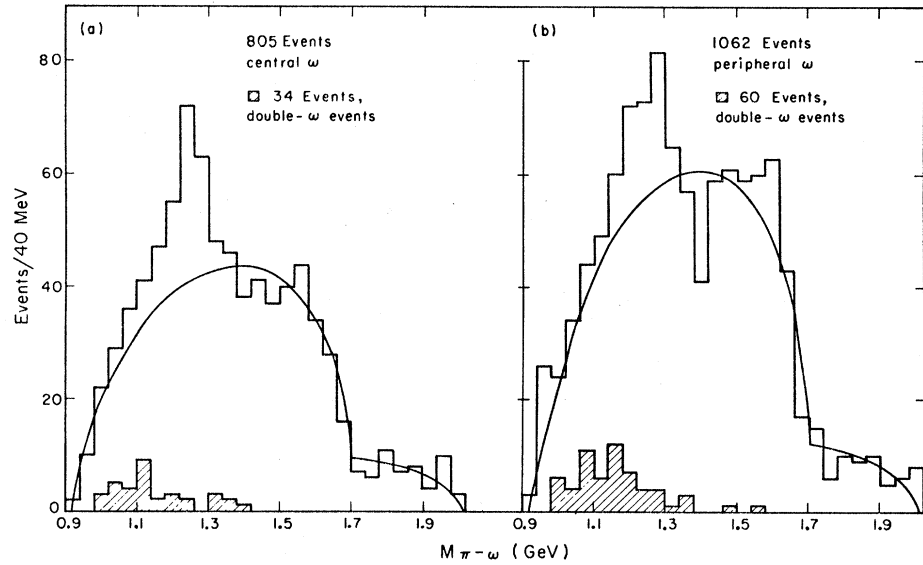


FIG. 49. (a) The $M_{\pi-\omega}$ spectrum for single- ω events at both momenta with $\Delta_p^2 < 0.35$ (GeV/ c)²; (b) the distributions in $\cos\beta$ for the B region (in GeV) and (c) outside the B region. The shaded histograms are for events in the central region ($r > 0.7$) of the ω Dalitz plot. See Sec. VB4 for explanation of the curve in (b).

4. Spin-Parity Analysis of the B enhancement

In this section, we briefly discuss a simple spin-parity analysis on the B enhancement, assuming that it is a genuine resonance.⁷⁵

For this purpose, we first introduce an angle ($\pi-\beta$) which is defined as the angle between the normal to the ω -decay plane and the "bachelor" π^- (not in ω) evaluated in the ω rest frame. Theoretical distributions in $\cos\beta$ for various J^P assignments are given in Appendix C.

In order to increase the signal-to-background ratio for the B , we take single- ω events with $\Delta_p^2 < 0.35$

(GeV/ c)². The $M_{\pi-\omega}$ spectrum for these events, as well as for those events in the central region of the ω Dalitz plot, are shown in Fig. 49(a). Figures 49(b) and 49(c) give the distributions in $\cos\beta$ for both inside and outside the B region.

We see that the distribution in the B region shows approximately a $\sin^2\beta$ distribution, but the distribution outside the B region is relatively isotropic. The curve in Fig. 49(b) is that of $\sin^2\beta$ normalized to the number of events above a uniform background assumed to be about 46%.

If we took this result at face value, we would conclude that the likely spin-parity series is $J^P = 1^-, 2^+$, etc. However, this result cannot be taken seriously, because, as we have shown, the B region is highly contaminated with the channel $N^*\omega$. Furthermore, a J^P assignment

⁷⁵ An attempt to determine the J^P for the B has been described by D. D. Carmony, R. L. Lander, C. Rindfleisch, N-H. Xuong, and P. M. Yager, Phys. Rev. Letters 12, 254 (1964).

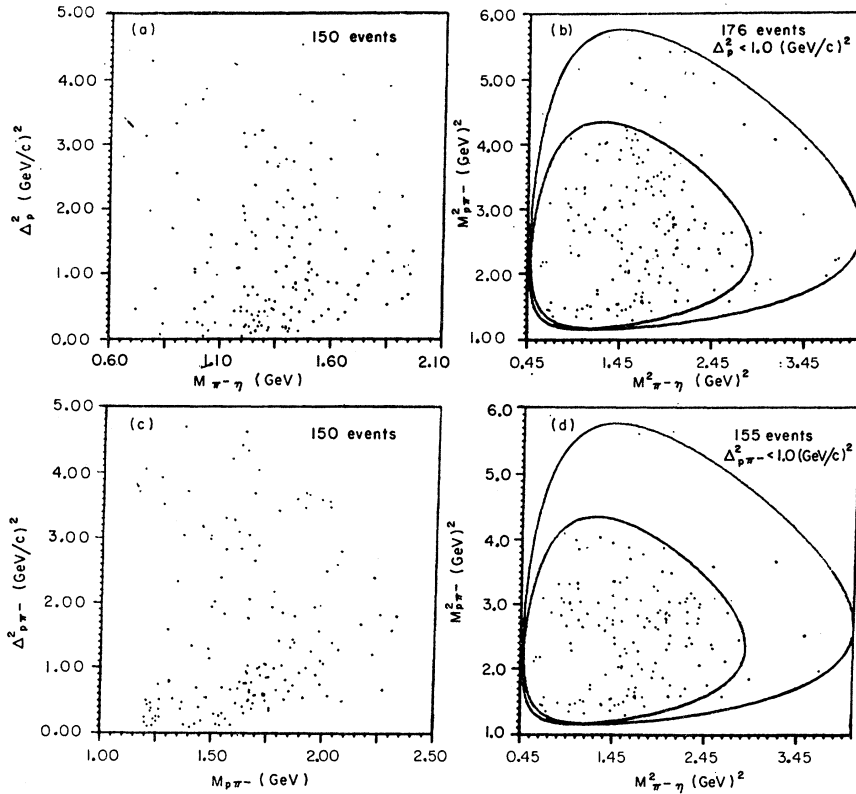


FIG. 50. Scatter plots for events at both momenta in the final state $p\pi^-\eta$ ($0.53 \text{ GeV} \leq M_{\pi^+\pi^0\pi^-} \leq 0.57 \text{ GeV}$): (a) Δ_p^2 versus $M_{\pi^-\eta}$ and (c) $\Delta_{p\pi^-}^2$ versus $M_{p\pi^-}$ (see Ref. 21); Dalitz plots with (b) $\Delta_p^2 < 1.0 \text{ (GeV/c)}^2$ and (d) $\Delta_{p\pi^-}^2 < 1.0 \text{ (GeV/c)}^2$.

of 1^- would mean that the B should decay into $\pi\pi$ and $K\bar{K}$, and these decay modes have not been observed so far.⁶²

C. Reaction $\pi^-p \rightarrow p\pi^-\eta$

As noted earlier, there is evidence of η production in our data [Figs. 30(a) and 32(a)]. In order to study the mechanism for the η production, we give in Fig. 50(a) the Chew-Low plot of Δ_p^2 versus $M_{\pi^-\eta}$. We see evidence for A_2 production in the region of low Δ_p^2 , suggesting a peripheral mechanism for its production [see Fig. 51(a)]. On the other hand, the Chew-Low plot of $\Delta_{p\pi^-}^2$ versus $M_{p\pi^-}$ [Fig. 50(c)] shows evidence for the $N^{*0}(1238)$ and $N^{*0}(1688)$ production, again in the region of low $\Delta_{p\pi^-}^2$. This evidence would suggest that

the isobars are produced through a peripheral mechanism which is presumably an A_2 -exchange process⁷⁶ [see Fig. 51(b)].

The situation here is analogous to the final states $p\pi^-\rho^0$ and $p\pi^-\omega$; there seem to be two competing channels leading to the final state $p\pi^-\eta$. In order to indicate the extent of A_2 and N^{*0} interference, we show in Figs. 50(b) and 50(d) the Dalitz plot of $M_{p\pi^-}^2$ versus $M_{\pi^-\eta}^2$ for events with $\Delta_p^2 < 1.0 \text{ (GeV/c)}^2$ and also for events with $\Delta_{p\pi^-}^2 < 1.0 \text{ (GeV/c)}^2$. However, our sample of η events is not large enough for any detailed analysis.

Figure 52(a) shows the $\Delta_{p\pi^-}^2$ distribution for η events. The peaking at low $\Delta_{p\pi^-}^2$ attests to the peripheral character of the η production. We show in Fig. 52(b) the $M_{p\pi^-}$ spectrum for events with $\Delta_{p\pi^-}^2 < 1.0 \text{ (GeV/c)}^2$. Note that the $N^{*0}(1518)$ production is relatively low. We recall that the production of this isobar is stronger in the final state $p\pi^-\rho^0$ and $p\pi^-\omega$.

Figure 52(c) gives the $M_{\pi^-\eta}$ distribution for events with $\Delta_p^2 < 1.0 \text{ (GeV/c)}^2$. Although A_2 production is evident, there is little evidence for A_1 production. The same distribution for events with $\Delta_{p\pi^-}^2 < 1.0 \text{ (GeV/c)}^2$ is shown in Fig. 52(d); evidence for the A_2 is not so strong. This is, of course, to be expected, as the selection of events with a cut in $\Delta_{p\pi^-}^2$ would enhance the $N^{*0}\eta$ channel. However, this does demonstrate that the

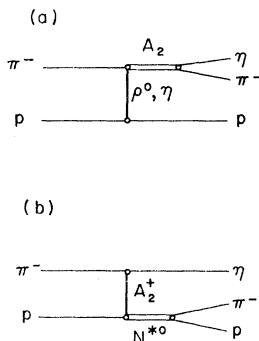


FIG. 51. (a) The $\rho^0(\eta^?)$ -exchange and (b) the A_2 -exchange diagrams for the process $\pi^-p \rightarrow p\pi^-\eta$.

⁷⁶ The quantum numbers of the η are such that the only known particle which can be exchanged is the A_2 meson.

enhancement we observe in the A_2 region is not related to the final state $N^*0\eta$.

VI. $n\pi^+\pi^+\pi^-\pi^-$ FINAL STATE

We present in Figs. 53–56 all the effective-mass distributions obtainable from this final state. The curves drawn in each histogram are the phase-space curves normalized to the total number of combinations.

From these figures, we find that no resonance is produced strongly in this channel, except for some evidence for $N^*(1238)$ production in $M_{\pi\pi^-}$ and ρ^0 in $M_{\pi^+\pi^-}$. The cross sections for N^* and ρ^0 are estimated to be 150 and 65 μb , respectively, at 3.2 GeV/c, and 170 and 70 μb at 4.2 GeV/c. Errors in these values are about 30%.

We have also looked for the 4π decay mode of f^0 (see Ref. 77); no evidence is seen at 3.2 GeV/c, but there may be some evidence of f^0 at 4.2 GeV/c [see Fig. 56(h)]. Rough estimates on its cross sections are 0 ± 20 μb at 3.2 GeV/c, and 30 ± 15 μb at 4.2 GeV/c.

There is no evidence in our data for the 4π decay mode of ρ^0 [see Figs. 54(h) and 56(h)]. We give 2 μb as the upper limit for the cross section of the process

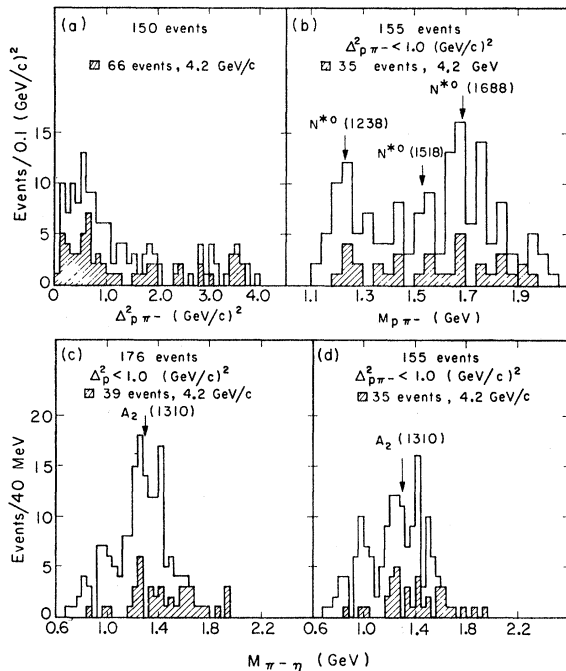


FIG. 52. (a) The $\Delta_{p\pi^-}^2$ and (b) $M_{p\pi^-}$ distributions for η events at both momenta (see Ref. 21). The $M_{\pi\pi^-}$ spectra for η events at both momenta with (c) $\Delta_{p\pi^-}^2 < 1.0$ (GeV/c) 2 and (d) $\Delta_{p\pi^-}^2 < 1.0$ (GeV/c) 2 . The shaded histograms are for events at 4.2 GeV/c alone.

⁷⁷ The branching ratios for decays of the f^0 as well as the A_2 have been described by S. U. Chung, O. I. Dahl, L. M. Hardy, R. I. Hess, L. D. Jacobs, J. Kirz, and D. H. Miller, Phys. Rev. Letters **15**, 325 (1965). The f^0 and the A_2 , together with the recently discovered resonances $f'(1500)$ and $K^*(1400)$, are believed to represent a nonet of 2^+ mesons.

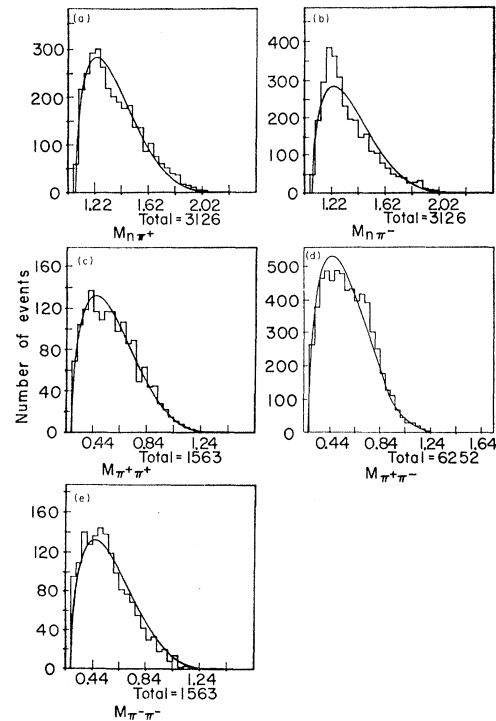


FIG. 53. Two-body effective-mass distributions from the $n4\pi$ final state at 3.2 GeV/c. The horizontal scales are in GeV, and the vertical scales are for the number of combinations per 40 MeV. The total number of combinations is given for each histogram after the heading "Total." The phase-space curves drawn in each histogram are normalized to the total number of combinations.

$\pi^-p \rightarrow n\rho^0(\rho^0 \rightarrow 2\pi^+2\pi^-)$ at both 3.2 and 4.2 GeV/c. At 3.2 BeV/c, Jacobs⁷ finds that the cross section for $\pi^-p \rightarrow n\rho^0(\rho^0 \rightarrow \pi^+\pi^-)$ is 1.1 ± 0.1 mb. Consequently, the branching ratio $\rho \rightarrow 2\pi^+2\pi^-/\rho \rightarrow \pi^+\pi^-$ is smaller than 2×10^{-3} .

VII. $p\pi^+\pi^-\pi^-MM$ FINAL STATE

In this section, we discuss briefly the final state $p\pi^+\pi^-\pi^-+MM$, where MM stands for the mass of unobserved neutral systems (in this case $MM \geq 2m_{\pi^0}$).

This final state of course cannot be fitted; in particular, it cannot be distinguished from the final state $4\pi MM$, except by the ionization density for those events with low-momentum protons. For this reason, we have selected for our analysis only those events with $\Delta_{p\pi^-}^2 < 1.0$ (GeV/c) 2 .

We examined all the effective-mass plots obtainable from charged particles in the final state, but saw little evidence for resonance production. We show in Fig. 57(a) the distribution in MM, the effective mass of the missing neutrals. Here we observe evidence for the neutral decay mode of η . A rough estimate of its cross section is 6 ± 3 μb at 3.2 GeV/c and 26 ± 10 μb at 4.2 GeV/c.⁷⁸

⁷⁸ We have assumed for this calculation that essentially all the η meson is produced with $\Delta_{p\pi^-}^2 < 1.0$ (GeV/c) 2 .

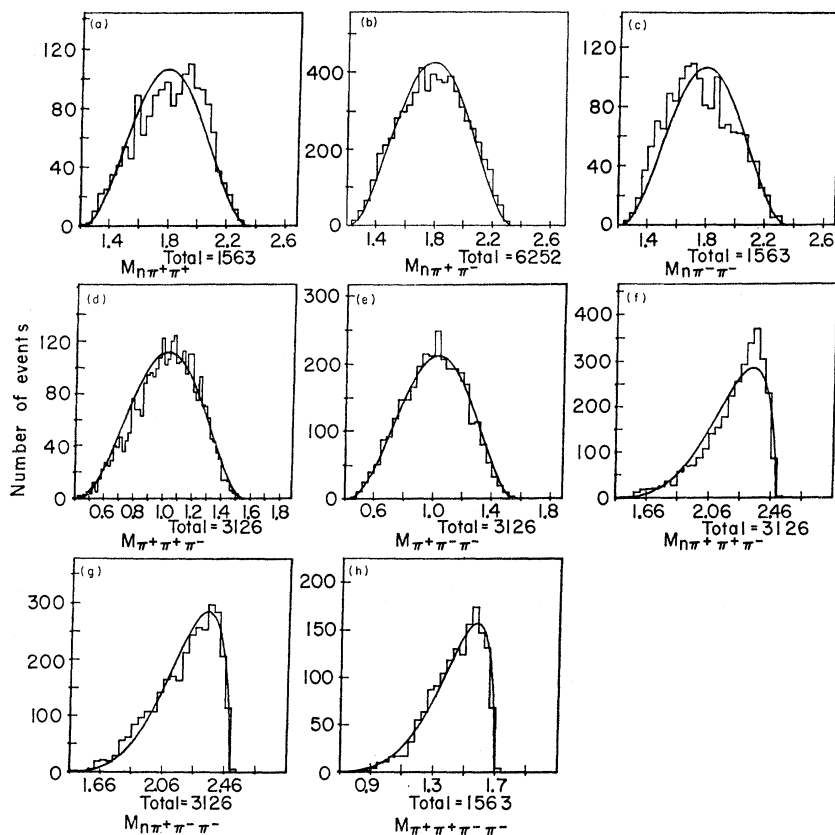


FIG. 54. Three- and four-body effective-mass distributions from the $n4\pi$ final state at 3.2 GeV/c.

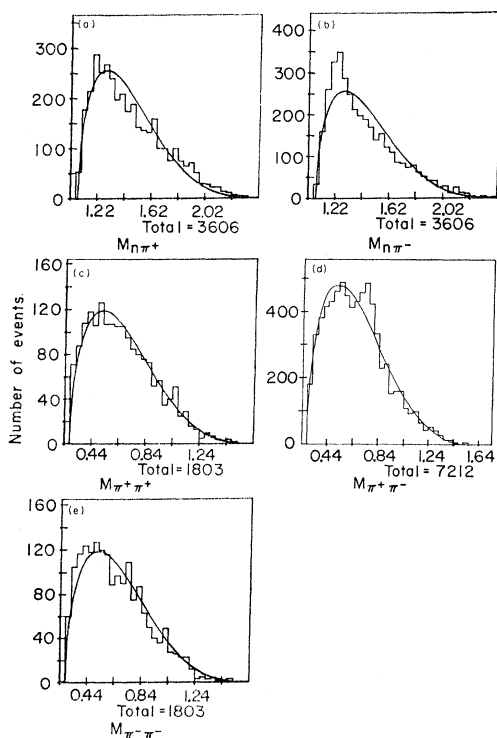


FIG. 55. Same distributions as in Fig. 53 for events at 4.2 GeV/c.

The apparent width of η in the MM spectrum is roughly 80 ± 20 MeV. The large experimental width reflects the poor resolution inherent in this final state; this is not surprising, however, if we recall that the $p3\pi$ MM final state cannot be fitted. One may compare this value with the typical resolution of about 15 MeV for $M_{\pi^+\pi^-}$ in the $p3\pi$ final state (4C fit) and with the resolution of about 25 MeV for $M_{\pi^+\pi^0\pi^-}$ (near the mass of ω) in the $p4\pi$ final state (1C) fit.

Recently, Kienzle *et al.*⁷⁹ reported a negatively charged resonance $X^-(962)$ with a width of about 15 MeV, produced in a reaction $\pi^-p \rightarrow pX^-$ at the pion incident momenta ranging from 3.0 to 5.0 GeV/c. The meson was found to decay into the final states $(\pi^-\pi^+\text{neutrals})$ and $(\pi^+\pi^-\pi^-\text{neutrals})$. It was suggested that this may be a charged mode of the $X^0(960)$ (generally considered to be an isoscalar).⁸⁰

Assuming that their peak indeed represents a decay mode of a charged $X^0(960)$, we have looked for its decay

⁷⁹ W. Kienzle, B. C. Maglič, B. Levrat, F. Lefébvre, D. Freytag, and H. R. Blieden, *Phys. Letters* **19**, 438 (1965); see also J. Oostens, P. Chavanon, M. Crozon, and J. Tocqueville, *ibid.* **22**, 708 (1966).

⁸⁰ G. R. Kalbfleisch, O. I. Dahl, and A. Rittenberg, *Phys. Rev. Letters* **13**, 349 (1964); M. Goldberg, M. Gundzik, J. Leitner, M. Primer, P. L. Connolly, E. L. Hart, K. W. Lai, G. W. London, N. P. Samios, and S. S. Yamamoto, *ibid.* **13**, 249 (1964); P. M. Dauber, W. E. Slater, L. T. Smith, D. H. Stork, and H. K. Ticho, *ibid.* **13**, 449 (1964).

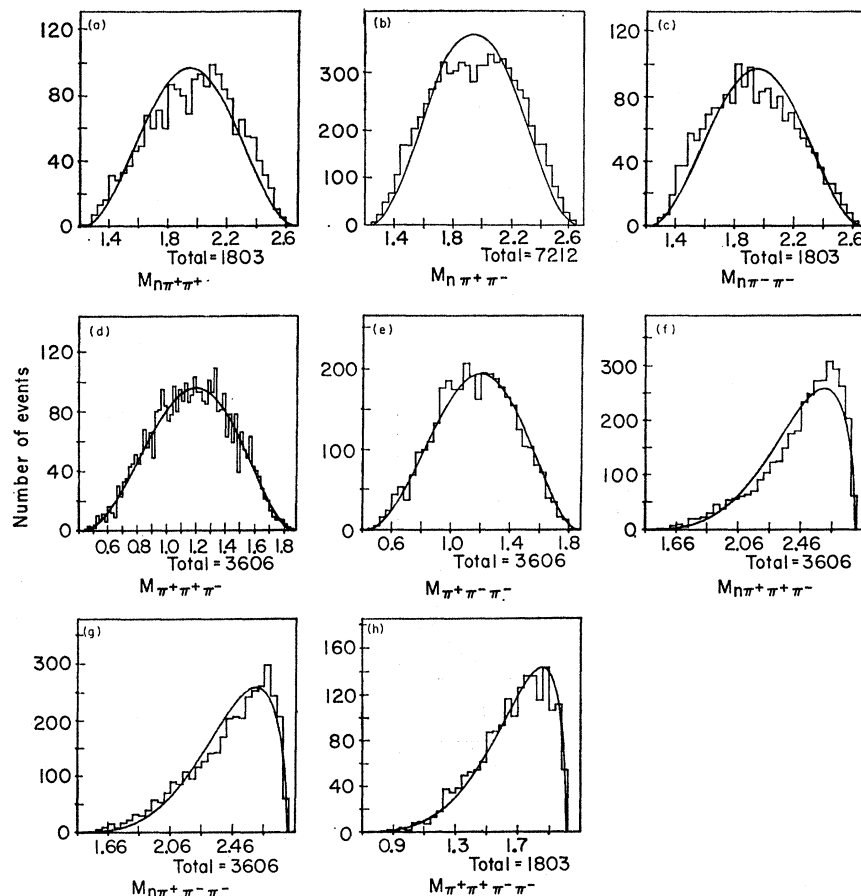


FIG. 56. Same distributions as in Fig. 54 for events at 4.2 GeV/c.

into $\pi^-\pi^0\eta$ ($\eta \rightarrow \pi^+\pi^-\pi^0$) in our data. Using a cross section of $4.6 \pm 1.5 \mu\text{b}$ for the above decay chain,⁸¹ we expect to see about 30 ± 10 events in the $M_{\pi^+\pi^-\pi^-\text{MM}}$ distribution [see Fig. 57(b)]; but we see no events at all in this region. We thus conclude that we do not have evidence for the $X^-(962)$ production in our data.

However, if $X^-(962)$ is an object which has different quantum numbers from $X^0(960)$, it can decay into $\pi^-\eta$. The distribution in $M_{\pi^-\eta}$ only at 3.2 GeV/c [see Fig. 33(c)] shows an enhancement near the region of 960 MeV, although the evidence is not striking, due to poor statistics. We quote $8 \pm 4 \mu\text{b}$ as the cross section for $X^-(962) \rightarrow \pi^-\eta$ (including the neutral decay mode of η).

By restricting the MM to the η region (0.5 to 0.6 GeV), we have searched for evidence of $X^0(960)$ decay. Figure 57(c) shows the $M_{\pi^+\pi^-\eta}$ distribution in our data; we see some evidence for $X^0(960)$. Its cross section is estimated to be about $2 \pm 2 \mu\text{b}$ at 3.2 GeV/c, $4 \pm 3 \mu\text{b}$ at 4.2 GeV/c.

We have also searched for the decay mode of the A_2

into $\pi^\pm\eta$ ($\eta \rightarrow \text{MM}$) in the $M_{\pi^\pm\eta}$ distributions, but saw no evidence for it, because of possibly large background under the η peak in the MM distribution. In addition, we have looked for the possible decay mode of the A_2 into $\pi^-X^0(960)$, but found little evidence for it either.

VIII. SUMMARY AND CONCLUSIONS

In all the reactions studied here, we have seen that the peripheral processes are mainly responsible for the production of resonant states. In particular, we have observed that the resonances $N^{*++}(1238)$ and ρ^0 are produced mainly via peripheral processes in the $p\pi^+\pi^-\pi^-$ final state, and that the A_1 and A_2 enhancements are produced peripherally in the $p\pi^-\rho^0$ channel. In the $p\pi^+\pi^0\pi^-\pi^-$ final state, we have found that peripheral processes are again responsible for the production of η and ω mesons, and that the B enhancement is also produced peripherally in the channel $p\pi^-\omega$.

We have found that the regions of the A_1 and B enhancements are strongly contaminated by the channel of the neutral isobar formation. In addition, we have demonstrated that the diffractive scattering at the isobar vertex may explain the A_1 and B enhancements in our data, consistent with the kinematic model

⁸¹ Assuming that their reported total cross section, $15 \pm 5 \mu\text{b}$, is applicable to our data at 3.2 and 4.2 GeV/c, we have simply corrected the value by 30% for the charged-decay mode ($\pi^+\pi^0\pi^-$) of the η .

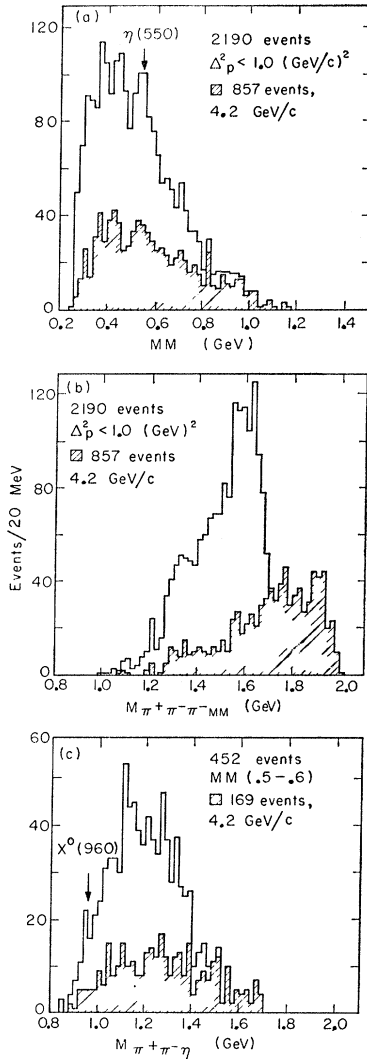


FIG. 57. (a) Distribution in MM for $p3\pi MM$ events at 3.2 and 4.2 GeV/c with $\Delta_p^2 < 1.0$ (GeV/c)²; (b) distribution in $M_{\pi^+\pi^-\pi^-\text{MM}}$ for the same events; (c) distribution in $M_{\pi^+\pi^-\eta}$ for events with MM in the η region (0.50 to 0.60 GeV). The shaded histograms are for events at 4.2 GeV/c alone.

proposed by Deck⁴³ and Maor and O'Halloran.⁴⁴ Consequently, if the A_1 and B are genuine resonant states, we may conclude that the π^-p interactions in the energy range 3 to 4 GeV/c do not provide suitable final states in which to study these resonances.

The A_2 enhancement, unlike the A_1 , has been shown to be consistent only with the hypothesis of a genuine resonant state. Assuming a noninterfering background, we have shown that its spin parity is uniquely assigned to be 2^+ . Thus one may conclude that the A_2 is the same particle as that observed in $K\bar{K}$ effective mass distributions⁵²; the branching ratio $\Gamma(A_2^- \rightarrow K\bar{K})/\Gamma(A_2^- \rightarrow \pi\rho)$ is estimated to be $(5.4 \pm 2.2)\%$.⁷⁷ We have also seen evidence for the $\pi\eta$ decay mode of the A_2 .

We have found that the $n4\pi$ final state is mostly

TABLE VII. Cross sections for resonance production.

Final states	Cross sections (μb)	
	3.2 GeV/c	4.2 GeV/c
$N^{*++}\pi^-\pi^-$	590 ± 70	590 ± 70
$p\pi^-\rho^0$ (including A_1 , and A_2)	480 ± 70	520 ± 70
$\downarrow \pi^+\pi^-$		
$p\pi^-\omega$ (including B)	230 ± 30	185 ± 25
$\downarrow \pi^+\pi^0\pi^-$		
$p\pi^-\eta$ (including A_2)	30 ± 10	21 ± 7
$\downarrow \pi^+\pi^0\pi^-$		
$pA_1^- \rightarrow p\pi^-\rho^0$	140 ± 60	160 ± 60
$\downarrow \pi^+\pi^-$		
$pA_2^- \rightarrow p\pi^-\rho^0$	150 ± 50	175 ± 45
$\downarrow \pi^+\pi^-$		
$pA_2^- \rightarrow p\pi^-\eta$	12 ± 7	5 ± 5
$\downarrow \pi^+\pi^0\pi^-$		
$pB^- \rightarrow p\pi^-\omega$	110 ± 30	67 ± 20
$\downarrow \pi^+\pi^0\pi^-$		

consistent with phase-space predictions, and saw little evidence for resonance production. The final state $p3\pi MM$ revealed very little interesting information, except for evidence for the neutral decay mode of η in the spectrum of MM.

We list in Table VII a summary of the cross sections for resonance production.

ACKNOWLEDGMENTS

We are grateful to the scanning and measuring staff and, in particular, to W. Koellner, whose efforts have been invaluable in the completion of this work. We had the pleasure of collaborating with Dr. L. M. Hardy, Dr. R. I. Hess, and Dr. L. D. Jacobs, who worked on other final states from the π^-p exposure. We thank Dr. M. Neveu-René for her help and collaboration in the analysis of part of this experiment. Finally, we acknowledge with pleasure the encouragement and support we received from Professor L. Alvarez throughout the course of this experiment.

APPENDIX A: ANGULAR DISTRIBUTIONS FOR $A \rightarrow \pi+\rho^0$

Here we list explicitly all the matrix elements assumed for the spin-parity analysis on the A_1 and A_2 .

A general formalism for describing a three-pion system has been developed by Zemach.⁸² Adopting his notation, we write the matrix element for the A decaying via $\pi\rho$ intermediate state as

$$M(\pi_1^-\pi_2^-\pi_3^+) = \alpha_1 M_{1,23} - \alpha_2 M_{2,31}, \quad (\text{A1})$$

where $M_{k,lm}$ is an antisymmetric function in lm , and α_k

⁸² C. Zemach, Phys. Rev. **133**, B1202 (1964).

is the propagator for ρ^0 . It is given by

$$\alpha_k = \frac{\Gamma_\rho^{1/2}}{(M_{lm^2} - M_\rho^2) + iM_\rho\Gamma_\rho} \quad (\text{with } klm, \text{ cyclic}), \quad (\text{A2})$$

where Γ_ρ is the width of ρ^0 .

Let \mathbf{p}_1 , \mathbf{p}_2 , and \mathbf{p}_3 be the momenta of the three pions in the 3π center-of-mass system, with their energies denoted by E_1 , E_2 , and E_3 . Let us further define $\mathbf{q}_k \equiv \mathbf{p}_l \times \mathbf{p}_m$ and $\mathbf{t}_k \equiv \mathbf{p}_l - \mathbf{p}_m$. In terms of these quantities, the matrix element assumed for each J^P and orbital angular momentum (l) is

J^P	$M_{1,23}$
1^-	\mathbf{q}_1
2^+	$\mathbf{p}_1\mathbf{q}_1 + \mathbf{q}_1\mathbf{p}_1$
0^-	$E_2 - E_3$
$1^+ (l=0)$	\mathbf{t}_1 (A3)
$1^+ (l=2)$	$(\mathbf{p}_1 \cdot \mathbf{t}_1)\mathbf{p}_1 - \frac{1}{3}\rho_1^2\mathbf{t}_1$
$2^- (l=1)$	$\frac{1}{2}(\mathbf{p}_1\mathbf{t}_1 + \mathbf{t}_1\mathbf{p}_1) - \frac{1}{3}(\mathbf{p}_1 \cdot \mathbf{t}_1)\tilde{I}$
$2^- (l=3)$	$(\mathbf{p}_1 \cdot \mathbf{t}_1)\mathbf{p}_1\mathbf{p}_1 - \frac{1}{3}\rho_1^2(\mathbf{p}_1 \cdot \mathbf{t}_1)\tilde{I} - \frac{1}{3}\rho_1^2(\mathbf{p}_1\mathbf{t}_1 + \mathbf{t}_1\mathbf{p}_1)$,

where \tilde{I} is a unit dyadic.

We emphasize that the above matrix elements are different from those of Diebold⁵³ for 1^+ and 2^- . The quantity \mathbf{t}_1 used above is evaluated in the 3π rest frame, whereas Diebold used \mathbf{t}_1' , which is evaluated in the ρ^0 rest frame. In a phenomenological approach, both methods may be considered equally valid.⁵³ We have tried both methods for our spin-parity analysis; the results obtained did not depend critically on the method used.

Next we present the production correlations predicted for various J^P assignments. The angle we have chosen for the purpose is z , which is defined as the angle between the normal to the decay plane of the A and the incident beam. The most general distribution for this angle has been given by Berman and Jacob.⁵⁴ Since, in our case, we have two identical particles (two π^- 's), the angular distribution $I(z)$ is proportional to

J^P	$I(z)$
1^-	$\rho_{00} \cos^2 z + \rho_{11} \sin^2 z$
2^+	$\frac{3}{4}\rho_{00} \sin^2 2z + \rho_{11}(\cos^2 z + \cos^2 2z)$ $+ \rho_{22}(1 + \cos^2 z) \sin^2 z$
0^-	constant
1^+	$\rho_{00} \sin^2 z + \rho_{11}(1 + \cos^2 z)$ (A4)
2^-	$a[3\rho_{00} \sin^4 z + 4\rho_{11}(1 + \cos^2 z) \sin^2 z$ $+ \rho_{22}(\sin^4 z + 8 \cos^2 z)] + b[\rho_{00}(1 - 3 \cos^2 z)^2$ $+ 3\rho_{11} \sin^2 2z + 3\rho_{22} \sin^4 z]$,

⁵³ The authors wish to thank A. Goldhaber for helpful discussions on this point.

⁵⁴ See S. M. Berman and M. Jacob, Phys. Rev. **139**, B1023 (1965), Eqs. (23)-(27).

where $\rho_{mm'}$ is the density matrix element for the A . Constants a and b appearing in $I(z)$ for 2^- depend in general on the internal structure of the 3π system. In writing down the distributions in (A4), we have also used a symmetry property on $\rho_{mm'}$; with the production coordinate system as defined in the text, we obtain, for parity-conserving reactions,⁵⁵ the relation

$$\rho_{mm'} = (-)^{m-m'} \rho_{-m-m'}. \quad (\text{A5})$$

If we assume that the A is produced via the ρ^0 -exchange process and that absorptive effects are negligible, the angular momentum conservation at the meson vertex demands that certain matrix elements be identically zero. With this condition, (A4) simplifies to

J^P	$I(z)$
1^-	$\sin^2 z$
2^+	$\cos^2 z + \cos^2 2z$
0^-	constant
1^+	$\sin^2 z - \rho_{11}(1 - 3 \cos^2 z)$ (A6)
2^-	$a[3 \sin^4 z - 2\rho_{11}(1 - 5 \cos^2 z) \sin^2 z]$ $+ b[(1 - 3 \cos^2 z)^2 - 2\rho_{11}(1 - 12 \cos^2 z + 15 \cos^4 z)]$.

APPENDIX B: ω DALITZ PLOT

We describe briefly the ω Dalitz plot and give an expression for the equal-probability contour on this plot. Let the mass of π^\pm be μ and that of π^0 be μ_0 ($\mu \neq \mu_0$). In the ω rest frame, we denote the momenta of π^+ , π^0 , and π^- by \mathbf{p}_+ , \mathbf{p}_0 , and \mathbf{p}_- .

We define the decay matrix element squared of the ω decay as

$$|\mathfrak{M}|^2 = 4|\mathbf{p}_+ \times \mathbf{p}_0|^2 = 4p_+^2 p_0^2 - (p_+^2 + p_0^2 - p_-^2)^2. \quad (\text{B1})$$

The maximum value of $|\mathfrak{M}|^2$ can easily be shown to be

$$|\mathfrak{M}|_{\text{max}}^2 = (W/E_0)(E_0^2 - \mu_0^2)^2. \quad (\text{B2})$$

Here W is the effective mass of the 3π system (mass of ω), and E_0 is the energy of the π^0 at the point where $|\mathfrak{M}|^2$ is at its maximum, which is given by

$$E_0 = (1/6W)\{W^2 - 4\mu^2 + \mu_0^2 + [(W^2 - 4\mu^2 + \mu_0^2)^2 + 12W^2\mu_0^2]^{1/2}\}. \quad (\text{B3})$$

The energy of the π^\pm at the point $|\mathfrak{M}|^2 = |\mathfrak{M}|_{\text{max}}^2$ is then simply given by

$$E = \frac{1}{2}(W - E_0). \quad (\text{B4})$$

Using these quantities, we define the polar-coordinate variables ρ and ϕ (both unitless quantities) by

$$T_0 = (E_0 - \mu_0)(\rho \cos \phi + 1),$$

$$T_+ = (E_0 - \mu_0)\{\rho \cos(\phi - \frac{2}{3}\pi) + [(E - \mu)/(E_0 - \mu_0)]\},$$

$$T_- = (E_0 - \mu_0)\{\rho \cos(\phi + \frac{2}{3}\pi) + [(E - \mu)/(E_0 - \mu_0)]\}, \quad (\text{B5})$$

⁵⁵ K. Gottfried and J. D. Jackson, Nuovo Cimento **33**, 309 (1964).

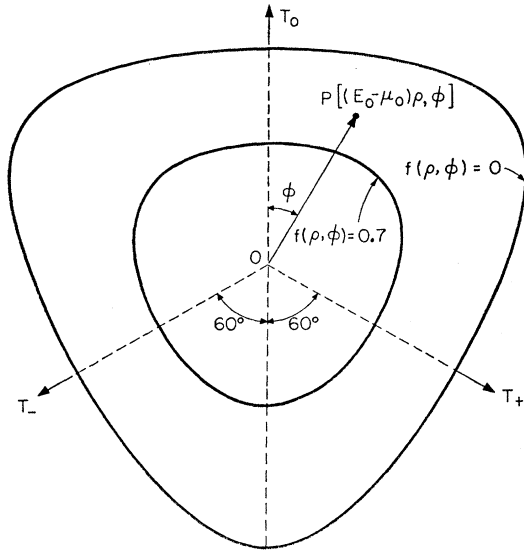


FIG. 58. The ω Dalitz plot ($M_\omega=0.783$ GeV). The inner contour corresponds to $r=0.7$, and the outer contour (boundary) to $r=0$.

where T_0 , T_+ , and T_- are kinetic energies of the three pions, and ρ varies from 0 to 1.

We now choose the origin of the polar-coordinate system to be the point where $|\mathfrak{M}|^2 = |\mathfrak{M}|_{\max}^2$ (see Fig. 58). An arbitrary point P on the ω Dalitz plot is then described by the polar-coordinate variables $[(E_0 - \mu_0)\rho, \phi]$.

Next we define a function $f(\rho, \phi)$ by

$$f(\rho, \phi) = |\mathfrak{M}|^2 / |\mathfrak{M}|_{\max}^2. \quad (\text{B6})$$

The contour on the ω Dalitz plot of the equal probability for the ω decay is then given by

$$f(\rho, \phi) = r, \quad \text{for } 0 \leq r \leq 1. \quad (\text{B7})$$

In particular, we note that the boundary of the ω Dalitz plot is simply given by

$$f(\rho, \phi) = 0. \quad (\text{B8})$$

The explicit expression for $f(\rho, \phi)$ can be derived by substituting (B5) into (B1):

$$f(\rho, \phi) = 1 - (a + b \cos^2 \phi) \rho^2 - c \rho^3 \cos 3\phi, \quad (\text{B9})$$

where

$$\begin{aligned} a &= 3E_0(W^2 - 2WE_0 + \mu_0^2) / W(E_0 + \mu_0)^2, \\ b &= 4E_0[W(3E_0 - W) + \mu^2 - \mu_0^2] / W(E_0 + \mu_0)^2, \\ c &= 2E_0(E_0 - \mu_0) / (E_0 + \mu_0)^2. \end{aligned} \quad (\text{B10})$$

If we put $\mu = \mu_0$, we have $E_0 = \frac{1}{3}W$, so that

$$\begin{aligned} a &= 3(W^2 + 3\mu^2) / (W + 3\mu)^2, \\ b &= 0, \\ c &= 2W(W - 3\mu) / (W + 3\mu)^2. \end{aligned} \quad (\text{B11})$$

With these values, Eq. (B8) reduces to an expression for the boundary given by Lee.⁸⁶

The expression for the boundary (B8) is, of course, independent of the J^P state assumed for the 3π system. In particular, it describes the boundary for the η Dalitz plot with W set equal to the mass of η . Note that (B8) can also describe the boundary of the Dalitz plot for the $\pi^+\pi^-\gamma$ decay mode of the η or $X^0(960)$, if we put $\mu_0 = 0$. In addition, it will also describe the boundary for the $\pi^+\pi^-\eta$ decay mode of the $X^0(960)$, if we set μ_0 equal to the mass of η (in this case, ρ can be larger than 1).

APPENDIX C: ANGULAR DISTRIBUTIONS FOR $B \rightarrow \pi + \omega$

We describe here the angular distributions for the decay $B \rightarrow \pi + \omega$. As defined in Sec. VB, $(\pi - \beta)$ is the angle between the normal to the decay plane and the "bachelor" pion (not in ω) as evaluated in the ω rest frame. In terms of this angle, the angular distribution $I(\beta)$ predicted for each J^P assignment is

J^P	$I(\beta)$
$1^-, 2^+, \dots$	$\sin^2 \beta$
0^-	$\cos^2 \beta$
$1^+ (l=0)$	1
$1^+ (l=2)$	$1 + 3 \cos^2 \beta$
$2^- (l=1)$	$1 + \frac{1}{3} \cos^2 \beta$
$2^- (l=3)$	$1 + 2 \cos^2 \beta$

As is well known, the above results can be derived by using the tensor representation of angular momenta.⁸⁷ It is instructive, however, to derive the above results within the helicity formalism.

In the B rest frame, we denote the density matrix of the B (spin J) by $\rho_{mm'}$, evaluated in a coordinate system fixed by the production variables. In this coordinate system, the momentum of ω is along the direction (θ, ϕ) . In the ω rest frame, the normal to the ω decay plane is along the direction (β, α) in a coordinate system with the z axis along the direction of the ω momentum.

In terms of the helicity amplitude g_λ , the decay amplitude T_m for the B is given by⁸⁸

$$T_m \propto \sum_\lambda g_\lambda D_{m\lambda}^{(J)*}(\phi, \theta, -\phi) D_{\lambda 0}^{(1)*}(\alpha, \beta, -\alpha), \quad (\text{C2})$$

where the magnetic quantum number m refers to the spin states of the B in the production coordinate system and $D_{mm'}^{(J)}$ is the standard rotation matrix element.⁸⁹

⁸⁶ See Eq. (12), T. D. Lee, Phys. Rev. **139**, B1415 (1965); see also G. Källén, *Elementary Particle Physics* (Addison-Wesley Publishing Company, Inc., Reading, Mass., 1964), p. 198.

⁸⁷ See, for instance, C. Zemach, Phys. Rev. **140**, B97 (1965).

⁸⁸ S. M. Berman and M. Jacob, Stanford Linear Accelerator Report No. SLAC-43, 1965 (unpublished); S. U. Chung, Phys. Rev. **138**, B1541 (1965).

⁸⁹ M. E. Rose, *Elementary Theory of Angular Momentum* (John Wiley & Sons, Inc., New York, 1957).

The decay angular distribution is now given by

$$\begin{aligned}
 I(\theta, \phi; \beta, \alpha) &\propto \sum_{m, m'} T_m \rho_{mm'} T_{m'}^* \\
 &\propto \sum_{\lambda, \lambda', m, m'} g_\lambda g_{\lambda'}^* \rho_{mm'} D_{m\lambda}^{(J)*}(\phi, \theta, -\phi) \\
 &\quad \times D_{m'\lambda'}^{(J)}(\phi, \theta, -\phi) D_{\lambda 0}^{(1)*}(\alpha, \beta, -\alpha) \\
 &\quad \times D_{\lambda' 0}^{(1)}(\alpha, \beta, -\alpha). \quad (C3)
 \end{aligned}$$

If we integrate $I(\theta, \phi; \beta, \alpha)$ first over α and then over ϕ and θ , we obtain

$$I(\beta) \propto \sum_\lambda |g_\lambda|^2 [d_{\lambda 0}^{(1)}(\beta)]^2, \quad (C4)$$

where we have used the condition $\text{tr}\rho = 1$. We note that $I(\beta)$ does not contain $\rho_{mm'}$, so that it is independent of the production mechanism of the B .

The helicity amplitude g_λ may be expanded in terms of partial-wave amplitudes⁹⁰:

$$g_\lambda = \sum_l a_l (2l+1)^{1/2} (l01\lambda | J\lambda), \quad (C5)$$

where a_l is the l -wave amplitude and $(j_1 m_1 j_2 m_2 | JM)$ are the Clebsch-Gordan coefficients. Using (C4) and (C5), we can readily calculate all the distributions in (C1).⁹¹ For example, for 2^- ($l=3$), we merely put all a_l 's to zero except a_3 , so that

$$g_\lambda = (\sqrt{7}) a_3 (301\lambda | 2\lambda)$$

and

$$I(\beta) \propto \sum_\lambda (301\lambda | 2\lambda)^2 [d_{\lambda 0}^{(1)}(\beta)]^2 \propto 1 + 2 \cos^2 \beta.$$

APPENDIX D: EXPERIMENTAL DETAILS

1. Beam

The 72-in. bubble chamber was exposed to the π^- beam from the bevatron; the momentum ranged from 1.6 to 4.2 GeV/ c . The beam was originally designed for π^- mesons by Trilling, Goldhaber, Kadyk, and Shen, and later by Murray for the separated K^- beam. The details of the beam are described elsewhere.⁹²

For this experiment on four-prong events, we selected the film exposed at the π^- beam momenta of 3.2 and 4.2 GeV/ c .

2. Scanning and Measuring

For the incident pion momentum at 3.2 GeV/ c , approximately 22 000 four-prong events, i.e., events with four outgoing charged tracks were measured. In about 43% of these, which were scanned and measured at the early stage of this experiment, *all* the four-prong events within the fiducial volume were accepted (the normal sample). For the rest of the pictures, scanners were instructed to "flag" those four-prong events for which one of the positive tracks could be identified as a

TABLE VIII. Summary of measured film.

Sample	*Events/ μb	Number of events measured	Beam momentum (GeV/ c) ^b
3.2 GeV/ c , normal	1.24 \pm 0.04	9100	3.220 \pm 0.035
3.2 GeV/ c , selected		12 400	3.200 \pm 0.020
4.2 GeV/ c	1.56 \pm 0.08	15 300	4.160 \pm 0.015

* Based on the number of events given in Table I. See Sec. D4.

^b See Fig. 59 for the spectrum of beam momentum.

proton, and only such events were measured and processed (the selected sample).

For the pion incident momentum at 4.2 GeV/ c , a total of approximately 15 000 events were measured and *all* four-prong events within the fiducial volume were used.

A summary of the quantity of film used for this experiment is shown in Table VIII. In Fig. 59, we show the spectrum of the beam momentum for the three samples.

All the measurements were done either on the SMP (scanning and measuring projector) or on the Franckenstein.⁴ The measured events were then processed through the standard data-reduction system of the Alvarez group.⁴

After the first measurement, events that were ambiguous and resolvable⁹³ were looked at by physicists and trained scanners for 3.2-GeV/ c normal and 4.2-GeV/ c samples. As for the 3.2-GeV/ c selected sample, if an event fitted the hypothesis (its confidence level was greater than 0.5%) for which the outgoing proton track is the same as that identified by the scanner, the hypothesis was considered to be the correct one for that event. When the computer and the scanner did not agree on a given hypothesis for an event, it was looked at by trained scanners, provided the event was resolvable.

If an event failed to fit any hypothesis (its confidence level was smaller than 0.5%) or did not have enough missing mass to be consistent with a missing-mass (MM) hypothesis, it was automatically remeasured. If it again failed to fit any hypothesis (including MM hypotheses), it was looked at on the scanning table by trained scanners, after which the event was either measured again or discarded if there was a reason to do so (e.g., two-prong event with a Dalitz pair, or strange-particle events "faking" four-prong ones). In this way, an event was measured as many as four times. At the end of this series of measurements, there remained only about 2% failing events.

⁹⁰ See S. U. Chung, Ref. 88, Eq. (A4).

⁹¹ See Ref. 84 for the explicit form of $d_{mm'}^i$ for small values of j .

⁹² Joseph J. Murray *et al.*, Lawrence Radiation Laboratory Report No. UCRL-11426, 1964 (unpublished).

⁹³ An event is considered to be ambiguous if there is more than one hypothesis fitting the event with the confidence level greater than 0.5%. An ambiguous event is considered to be resolvable if the ionization density of one of the tracks is at least 1.4 times the minimum ionization density.

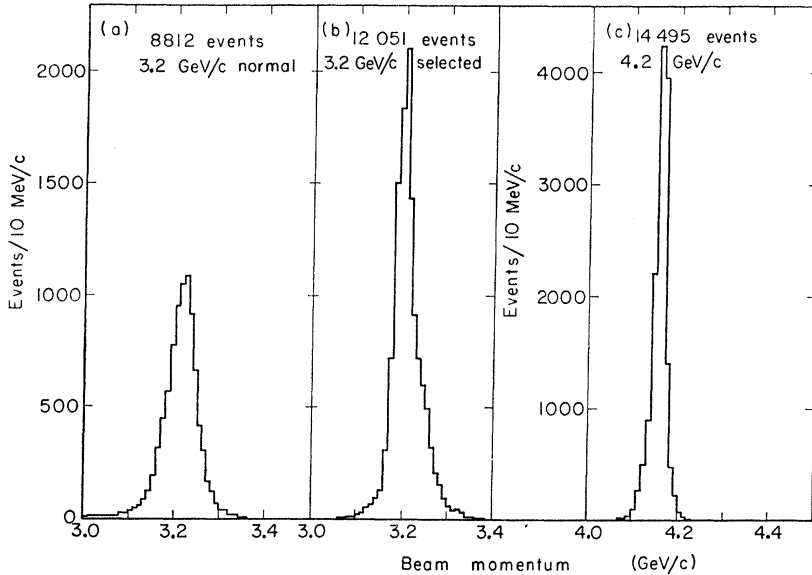


FIG. 59. Beam-momentum spectrum for (a) the 3.2-GeV/c normal, (b) the 3.2-GeV/c selected, and (c) the 4.2-GeV/c sample.

3. Separation of Hypotheses

Types of reactions that have been tried are shown in Sec. II in reactions (1a) through (1e).

Note that the reaction (1a) is a four-constraint (4C) fit, while (1b) and (1c) are one-constraint (1C) fits. The reactions (1d) and (1e) are unfittable hypotheses. An event was tried for (1d) and (1e) only if it failed to fit hypotheses (1a), (1b), or (1c).

After the series of measurements described in Sec. D2, events were distributed among various hypotheses as shown in Table IX. This table shows, for fitted events, the correlation of the best hypothesis with the second-best hypothesis. We see that a great majority of events has a unique assignment to a given hypothesis; ambiguous events amount to less than 10% for all three hypotheses. Also, there is very little ambiguity (less than 2%) in the identification (by the computer) of the proton track. Of course, this is largely because much of the film was looked at by the scanners, and the proton track was uniquely identified on the basis of ionization density.

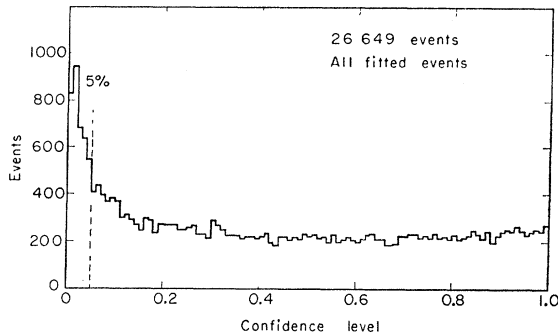


FIG. 60. Distribution in the confidence level for all the fitted events.

In order to investigate the nature of the ambiguous events and further separate the events among different hypotheses, extensive use was made of the confidence level (C.L.) for each hypothesis. Figure 60 shows the distribution of the C.L. for all fitted events.⁹⁴ It is relatively flat, as it should be, except at smaller values of the C.L. The character of the distribution remains essentially the same when events with the different hypotheses (1a), (1b), and (1c) are plotted separately. The excess of events at smaller values of the C.L. is presumably caused by factors such as small-angle scattering and bad measurements. *In addition*, one suspects that it is to a large extent due to the contamination of misassigned hypotheses.

In order to further distinguish the $p4\pi$ final state from the $p3\pi$ final state and the MM final state, we examine the $M_{\pi^+\pi^0\pi^-}$ distribution, where we observe a sharp peak due to the ω -meson production, characteristic of the $p4\pi$ final state.

Figure 61 shows the effective-mass distribution of the neutral-pion triplet from the $p4\pi$ final state, when we select only those events that are ambiguous with the

TABLE IX. Distribution of events among different hypotheses.

Second-best hypotheses	Best hypotheses			Total
	$p\pi^+\pi^-\pi^-$	$p\pi^+\pi^0\pi^-\pi^-$	$n\pi^+\pi^+\pi^-\pi^-$	
$p\pi^+\pi^-\pi^-$	9780	338	11	10 129
$p\pi^+\pi^0\pi^-\pi^-$	825	10 950	567	12 342
$n\pi^+\pi^+\pi^-\pi^-$	15	551	3612	4178
Total	10 620	11 839	4190	26 649

⁹⁴ Because our geometry program consistently assigns too small errors to the measured quantities, abnormally high values of χ^2 result. Therefore, χ^2 has been corrected by an empirical factor before the corresponding confidence level is calculated: The actual values used for the factors are 0.6 and 0.8 for the 4C and 1C fits, respectively.

$p3\pi$ final state and whose C.L. is smaller than 5%. There are very few ω events in this sample compared with the same distribution of all $p4\pi$ final states. In addition, the phase space is grossly distorted. Therefore, we conclude that this sample of $p4\pi$ events is largely composed of $p3\pi$ events. This is easy to understand; the 4C $p3\pi$ final state is much harder to fit than the 1C $p4\pi$ final state, so if an event had an acceptable C.L. for $p3\pi$, it is in reality $p3\pi$, even though it may have higher C.L. for $p4\pi$. It is estimated that about 80% of this sample is in reality $p3\pi$ events. So this sample has been deleted altogether from the $p4\pi$ sample (the deleted sample amounts to less than 3% of the total).

In order to further investigate other possible contaminations in the $p4\pi$ events, we plot in Fig. 62(a) the missing-mass squared (MM^2) for all $p4\pi$ events calculated from the measured (unfitted) quantities. As is expected, there is a huge peak at the mass (squared) of π^0 . Partly on the basis of the shape of this distribution and partly on consideration of the threshold for $2\pi^0$ production, the MM^2 cut was chosen in the range -0.12 to 0.1 (GeV^2). Figure 62(b) shows the distribution of the neutral-pion triplet only for those events whose MM^2 is outside the aforementioned cut and whose C.L. is less than 5%; there are hardly any ω events in the sample. We therefore concluded that this sample certainly does not belong to the $p4\pi$ events, and again we deleted this sample from the $p4\pi$ events (less than 4% of the total). The sample consisting of events with MM^2 outside the cut and with the C.L. greater than 5% showed some ω events, and we decided to keep this sample in the $p4\pi$ events.

Inasmuch as $n4\pi$ events [the reaction (1c)] are 1C fits, one would expect contamination similar to that in the $p4\pi$ events. Unfortunately, however, there is no sharp resonance like ω in the sample. Nevertheless, we chose a MM^2 cut from 0.52 to 1.20 (GeV^2) in a similar fashion. If an event had a MM^2 outside this range and a C.L. less than 5%, it was dropped from the $n4\pi$ sample (this amounted to about 6% of the total sample).

FIG. 62. (a) Spectrum of the square of the missing mass (MM^2) calculated from the measured quantities for all $p4\pi$ events. (b) The $M_{\pi^+\pi^0\pi^-}$ spectrum for events outside the MM^2 cut [dotted lines in (a)] and with C.L. < 5%.

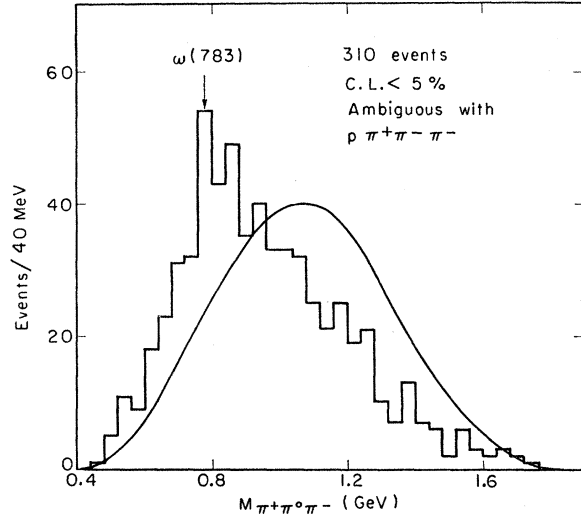
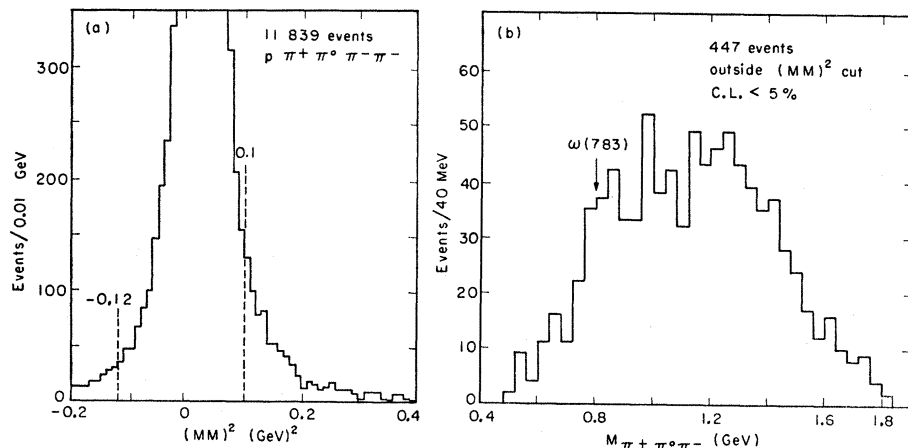


FIG. 61. The $M_{\pi^+\pi^0\pi^-}$ spectrum for $p4\pi$ events ambiguous with the $p3\pi$ hypothesis and with C.L. less than 5%. The phase-space curve is normalized to the total number of combinations.

The $p3\pi$ events constitute a rather pure sample, since it consists of events with a 4C fit. Nonetheless, if an event fell outside the MM^2 cut [chosen to be in the range -0.02 to $+0.02$ (GeV^2)] and had a C.L. less than 5%, it was dropped from the sample (less than 2% of the total sample). The deleted sample showed very little evidence for ρ^0 production, whereas the total $p3\pi$ sample showed strong ρ^0 production.

4. Cross Sections

For the purpose of cross-section calculations, we have decided to count, in a special cross-section scan, the number of four-prong interactions along with the total number of *all* interactions, and then normalize it to the existing precise measurements of the total π^-p cross section taken from counter experiments.⁶ For this purpose, every fifth frame of the entire quantity of film at 3.2 and 4.2 GeV/c was scanned.

We note that small-angle elastic scatterings can easily be missed by scanners. This effect, which is a serious one for two-prong final states, has been studied in detail by Jacobs.⁷ Using the result of his analysis, we have made a correction to the total number of interactions (from the cross-section scan); this correction amounts to about 8% at 3.2 GeV/c, 7% at 4.2 GeV/c.

In order to obtain any reliable cross sections, one must also correct for the scanning efficiency of the scanners. Based on two separate second scans of 15 rolls (about 3000 events) of film each, the scanning efficiency was found to be $(96 \pm 2)\%$ for the first scan.

In addition, for partial-cross-section calculations, we have corrected for the contamination in each category resulting from erroneously assigned hypotheses (see Sec. D3).

The resulting cross sections, after all these corrections have been made, are shown in Table II for both 3.2 and

4.2 GeV/c. Of course, only the 3.2-GeV/c normal sample was used to calculate the cross sections at that momentum.

We point out here that cross sections were calculated from the data that had no cutoff based on the fiducial-volume criterion. For subsequent analysis in Secs. IV through VIII, however, the rigid fiducial-volume criterion was applied. The events failing to satisfy the criterion (about 11% of the total) showed a poor resolution, based on the width⁸ of ω from this sample. This is, of course, because these events are largely from the periphery of the bubble chamber and they tend to have short tracks; this results in poor measurements.

We have also applied a cutoff at $\pm 2^\circ$ for the dip angle of the beam evaluated at the interaction vertex, thereby eliminating about 2% of the total events. The number of events shown in Table I is that obtained after these cutoffs were applied.

New Low-Energy Theorems for Nucleon Compton Scattering*

VIRENDRA SINGH†

Argonne National Laboratory, Argonne, Illinois

and

The Rockefeller University, New York, New York

(Received 30 August 1967)

Two new low-energy theorems for Compton scattering from spin- $\frac{1}{2}$ targets, giving some terms of order ω^2 , are derived using a recently obtained lemma. One of these theorems is a generalization to the spin- $\frac{1}{2}$ case of a similar theorem for the spin-0 case. The other theorem involves "magnetic moment radius," i.e., $[dG_M(t)/dt]_{t=0}$, which does not occur in any of the low-energy theorems obtained earlier.

I. INTRODUCTION

WE report here two new low-energy theorems for nucleon Compton scattering, giving coefficients of the $\omega^2(1-\cos\theta)$ terms, where ω is the incident lab photon energy and θ the lab angle of scattering, in two of the amplitudes. It is obvious that the possibility of writing down such theorems depends on being able to deal with excited-state contributions to $T_{00}^{\alpha\beta}(p', k'; p, k)$, where

$$i(2\pi)^4 \delta^4(p' + k' - p - k) \frac{1}{(2\pi)^3} (m^2/E_{p'}E_p)^{1/2}$$

$$\times T_{\mu\nu}^{\alpha\beta}(p', k'; p, k) = \int d^4x d^4y e^{i(k' \cdot x - k \cdot y)}$$

$$\times \langle p' | [T\{J_\mu^\alpha(x), J_\nu^\beta(y)\} - i\rho_{\mu\nu}^{\alpha\beta}(x)\delta^4(x-y)] | p \rangle, \quad (1)$$

and $p, k, E_p(p', k', E_{p'})$ are, respectively, initial (final) nucleon and photon four-momenta and nucleon energy. The "charge labels" for final and initial photons are denoted by α and β , respectively. The general form of

the excited-state contributions was discussed recently using current conservation and was used to derive a new low-energy theorem for pion Compton scattering.¹ The use of this information for the Compton scattering from systems with spin $S \geq 1$ leads to a number of new theorems; in particular, for the spin-1 case one obtains a "quadrupole moment" theorem.²

2. LOW-ENERGY THEOREMS

Let us write the nucleon Compton scattering in the lab frame ($\mathbf{p}=0$) as

$$\begin{aligned} \epsilon_m' T_{mn}^{\alpha\beta}(\omega', \mathbf{k}'; \omega, \mathbf{k}) \epsilon_n = & \epsilon_m' U_{mn}^{\alpha\beta}(\omega', \mathbf{k}'; \omega, \mathbf{k}) \epsilon_n \\ & + \boldsymbol{\epsilon}' \cdot \boldsymbol{\epsilon} E_1^{\alpha\beta} + \frac{1}{2} [\boldsymbol{\sigma} \cdot \boldsymbol{\epsilon}' \boldsymbol{\sigma} \cdot \boldsymbol{\epsilon}] E_2^{\alpha\beta} \\ & + (\boldsymbol{\epsilon}' \cdot \mathbf{k} \boldsymbol{\epsilon} \cdot \mathbf{k}' - \mathbf{k}' \cdot \mathbf{k} \boldsymbol{\epsilon}' \cdot \boldsymbol{\epsilon}) E_3^{\alpha\beta} \\ & + \frac{1}{2} ([\boldsymbol{\sigma} \cdot \mathbf{k}', \boldsymbol{\sigma} \cdot \mathbf{k}] \boldsymbol{\epsilon}' \cdot \boldsymbol{\epsilon} - \mathbf{k}' \cdot \mathbf{k} [\boldsymbol{\sigma} \cdot \boldsymbol{\epsilon}', \boldsymbol{\sigma} \cdot \boldsymbol{\epsilon}]) E_4^{\alpha\beta} \\ & + \frac{1}{2} ([\boldsymbol{\sigma} \cdot \boldsymbol{\epsilon}', \boldsymbol{\sigma} \cdot \mathbf{k}] \boldsymbol{\epsilon} \cdot \mathbf{k}' - \boldsymbol{\epsilon}' \cdot \mathbf{k} [\boldsymbol{\sigma} \cdot \boldsymbol{\epsilon}, \boldsymbol{\sigma} \cdot \mathbf{k}'] \\ & \quad - 2\mathbf{k}' \cdot \mathbf{k} [\boldsymbol{\sigma} \cdot \boldsymbol{\epsilon}', \boldsymbol{\sigma} \cdot \boldsymbol{\epsilon}]) E_5^{\alpha\beta} \\ & + \frac{1}{2} ([\boldsymbol{\sigma} \cdot \boldsymbol{\epsilon}', \boldsymbol{\sigma} \cdot \mathbf{k}] \boldsymbol{\epsilon} \cdot \mathbf{k}' + \boldsymbol{\epsilon}' \cdot \mathbf{k} [\boldsymbol{\sigma} \cdot \boldsymbol{\epsilon}, \boldsymbol{\sigma} \cdot \mathbf{k}']) E_6^{\alpha\beta} \\ & + \frac{1}{2} ([\boldsymbol{\sigma} \cdot \boldsymbol{\epsilon}', \boldsymbol{\sigma} \cdot \mathbf{k}'] \boldsymbol{\epsilon} \cdot \mathbf{k}' - \boldsymbol{\epsilon}' \cdot \mathbf{k} [\boldsymbol{\sigma} \cdot \boldsymbol{\epsilon}, \boldsymbol{\sigma} \cdot \mathbf{k}]) E_7^{\alpha\beta} \\ & + \frac{1}{2} ([\boldsymbol{\sigma} \cdot \boldsymbol{\epsilon}', \boldsymbol{\sigma} \cdot \mathbf{k}'] \boldsymbol{\epsilon} \cdot \mathbf{k}' + \boldsymbol{\epsilon}' \cdot \mathbf{k} [\boldsymbol{\sigma} \cdot \boldsymbol{\epsilon}, \boldsymbol{\sigma} \cdot \mathbf{k}]) E_8^{\alpha\beta}, \end{aligned} \quad (2)$$

* Work performed under the auspices of the U. S. Atomic Energy Commission.

† On leave from (and address after Sept. 1, 1967) Tata Institute of Fundamental Research, Bombay, India.

¹ V. Singh, Phys. Rev. Letters **19**, 730 (1967).

² A. Pais, Phys. Rev. Letters **19**, 544 (1967).